Novel *in vitro* and *in vivo* models of Kaposi's sarcoma for investigation of viral maintenance and validation of antiviral compounds

Von der Fakultät für Lebenswissenschaften

der Technischen Universität Carolo-Wilhelmina zu Braunschweig

zur Erlangung des Grades einer

Doktorin der Naturwissenschaften

(Dr. rer. nat.)

genehmigte

D i s s e r t a t i o n

von Tatyana Dubich
aus Rivne / Ukraine

1. Referent: Prof. Dr. Reinhard Köster
2. Referentin: Prof. Dr. Dagmar Wirth
eingereicht am: 09.07.2018
mündliche Prüfung (Disputation) am: 28.09.2018

Druckjahr 2018

Vorveröffentlichungen der Dissertation

Teilergebnisse aus dieser Arbeit wurden mit Genehmigung der Fakultät für Lebenswissenschaften, vertreten durch den Mentor der Arbeit, in folgenden Beiträgen vorab veröffentlicht:

Publikationen

Dubich, T. & Wirth, D.: Function or Expansion: How to Investigate Cells of Human Blood Vessels. Front. Young Minds. 6:25. DOI 10.3389/frym.2018.00025

Dubich, T., Lieske, A., Santag, S., Beauclair, G., Rückert, J., Herrmann, J., Gorges, J., Büsche, G., Kazmaier, U., Hauser, H., Stadler, M., Schulz, T. F., Wirth, D.: A combined *in vitro* and *in vivo* system for the investigation of KSHV and for validation of small molecule inhibitors against Kaposi's sarcoma. Submitted

Lipps, Ch., Badar, M., Butueva, M., Dubich, T., Singh, I. V., Rau, S., Weber, A., Kracht, M., Köster, M., May, T., Schulz, T. F., Hauser, H., Wirth, D.: Proliferation status defines functional properties of endothelial cells. Cell. Mol. Life Sci. 2017 Apr;74(7):1319-1333. DOI 10.1007/s00018-016-2417-5

Tagungsbeiträge

Dubich, T., Lipps, Ch., May, T., Stadler, M., Schulz, T.F., Wirth, D.: Novel predictive 3D cultivation models for validating small molecules against KSHV infection (Oral presentation), DECHEMA: 3D cell culture 2018, Freiburg, Germany (2018)

Dubich., T., Lipps, Ch., Butueva, M., May, T., Stadler, M., Schulz, T. F., Wirth, D.: Analysing mechanisms of KSHV latency and intervention using novel in vitro and in vivo models (Oral presentation, Poster) 20th International Workshop on Kaposi's Sarcoma Herpes Virus (KSHV) and Related Agents, Berlin, Germany, (2017)

Dubich., T., Lipps, Ch., Butueva, M., May, T., Stadler, M., Schulz, T. F., Wirth, D.: Analyzing mechanisms of KSHV latency and intervention using novel in vitro and in vivo models (Oral presentation) 6th European Congress of Virology, Hamburg, Germany (2016)

Dubich., T., Lipps, Ch., Butueva, M., May, T., Wirth, D.: Conditionally immortalized human endothelial cells for the investigation of KSHV latency and intervention in novel in vitro and in vivo models" (Oral presentation) 3D Cell culture 2016: How close "in vivo" can we get? Models, Application & Translation, DECHEMA, Freiburg, Germany (2016)

Dubich., T., Lipps, Ch., Butueva, M., May, T., Stadler, M., Schulz, T. F., Wirth, D.: Analysis of mechanisms of KSHV latency and intervention using novel in vitro and in vivo models (Oral presentation) 8th International PhD and ESR Symposium by the Helmholtz International Graduate school for Infection research, Braunschweig, Germany (2015)

Posterbeiträge *

Dubich., T., Lipps, Ch., Butueva, M., May, T., Stadler, M., Schulz, T. F., Wirth, D.: Novel predictive 3D cultivation models for validation small molecules against HHV-8 infection (Poster) N2 Science Communication conference, Berlin (2017)

Dubich., T., Lipps, Ch., Butueva, M., May, T., Stadler, M., Schulz, T. F., Wirth, D.: Analysis of mechanisms of KSHV latency and intervention using novel in vitro and in vivo models" (Poster) 6th Summer School on Infection Research, Buchenau, Germany (2016)

Dubich., T., Lipps, Ch., Butueva, M., May, T., Stadler, M., Schulz, T. F., Wirth, D.: Analysis of mechanisms of Kaposi's sarcoma associated virus latency and intervention using novel in vitro and in vivo models (Poster) HZI International Graduate School retreat, Braunschweig, Germany (2014)

Table of Contents

Summary

Kaposi's sarcoma-associated herpesvirus (KSHV) is the etiological agent of Kaposi's sarcoma (KS), a tumor of endothelial origin predominantly affecting immunosuppressed individuals. Up to date, vaccines and targeted therapies are not available. Screening and identification of antiviral compounds are compromised by the lack of scalable cell culture systems reflecting properties of virus transformed cells in patients. Further, the strict specificity of the virus for humans limits the development of *in vivo* models.

In this study conditionally immortalized human endothelial HuARLT cells were validated as a system to study KSHV-induced pathogenesis and testing of novel antiviral drugs. Systematic analysis of cellular marker expression as well as cellular functions in 2D and 3D cell culture conditions showed that HuARLT cells closely mimic KSHV infection of primary cells. A humanized mouse model for KSHV based on the cell line develop lesions which histologically resemble KS. Importantly, invasive properties and tumor formation were completely reverted by purging cells from KSHV confirming for the first time that tumor formation is primarily dependent on viral infection, rather than being a consequence of irreversible transformation of the infected cells.

The cell line was used to investigate the molecular mechanisms of KSHV maintenance in endothelial cells. This study proved that lack of cell proliferation is not sufficient to maintain the episomal virus, as was believed before. Rather, it demonstrated that 3D culture conditions (in vitro or in vivo) are required for efficient viral maintenance. Transcriptome analysis and pharmacological studies showed that increased activity of the PI3K/mTOR pathway governs viral maintenance in 3D cell culture, likely due to increased viral reactivation and favorable conditions for viral transmission. At the same time, inhibitor studies indicate that the DNA damage response associated MRN complex restricts viral maintenance in 2D, but not 3D cell culture. MRN-dependent episome degradation might thus be a second mechanism contributing to the differential viral maintenance in 2D and 3D cell culture conditions.

A subset of 26 compounds from a natural compound library was screened for reducing the episomal viral copy number and the tumorigenic properties of KSHV-infected cells in 2D and 3D in vitro cell culture systems. Selected compounds were subsequently tested for the ability to reduce the tumor size in xenotransplanted mice. Based on the assay three drug candidates, namely pretubulysin D, epothilone B and chondramid B showed significant tumor reduction, with comparable or even higher efficiencies than rapamycin, a drug that was proposed for treatment of Kaposi's sarcoma.

Thus, this study shows that the combined use of antiviral and antitumor assays based on the same cell system is indicative for tumor reduction in vivo and therefore allows faithful selection of novel drug candidates against Kaposi's sarcoma.

1. Introduction

Kaposi's sarcoma (KS) is a skin tumor which was named after a Hungarian dermatologist who in 1872 first described cases of "idiopatic multiple pigmented sarcoma of the skin". It was an extraordinary observation at the time and for many years the tumor was considered to be a rare disease of elderly men of Mediterranean origin[1]. In 1981, Alvin Friedman-Kein reported of an aggressive form of the disease in human immunodeficiency virus (HIV) infected men[2], which eventually was classified as HIV-associated (epidemic) Kaposi's sarcoma. With the advent of HIV the incidence of KS with bad prognosis dramatically increased and the tumor was recognized as one of the AIDS-defining malignances. In 1994, Chang and Moore isolated the etiological agent, a new human herpesvirus, called Kaposi's sarcoma associated herpesvirus (KSHV), or human herpesvirus 8[3]. Later, the virus was also associated with two lymphoproliferative disorders: primary effusion lymphoma and multicentric Castleman's disease. The International Agency for Research on Cancer classifies KSHV as a class I carcinogen[4].

1.1 Structure and biology of Kaposi's sarcoma associated herpesvirus

1.1.1 Virus structure

Based on phylogenetic analysis, KSHV is classified as a genus *Rhadinovirus* of the *gamma-2 herpesvirus* subfamily in the family *Herpesviridae*[5]. Morphologically KSHV resembles herpes simplex virus 1 and human cytomegalovirus. Viral particles are 100-150 nm with a lipid envelope surrounding the tegument and the capsid. The envelope is represented by a lipid bilayer incorporating the viral glycoproteins ORF4, gB, gH/gL, gM/gN, and gpK8.1[6]. 3D analysis of the capsid revealed that it is composed of hexamers and pentamers formed by the major capsid protein (ORF25) and the small capsid protein (ORF65)[7,8] (Fig. 1.1 A and B).

KSHV has a double-stranded genome, which is approximately 165 kB long and consists of a single, continuous unique region flanked on either side by a terminal repeat (TR) region. The unique region is 140,5 kB long and encodes 87 predicted ORFs which include genes for structural proteins, replication enzymes as well as genes for untranslated RNAs and miRNAs (Fig. 1.1 C). The terminal repeat region consists of a variable number of repeats with high G:C content[9]. It contains two binding sites for the latent nuclear antigen (LANA) and the latent origin of replication. By binding to multiple TRs LANA tethers the circular viral episome to the host chromosome by binding nucleosomes through the folded region of histones H2A-H2B and ensures transmission of the episome to daughter cells during mitosis[10,11].

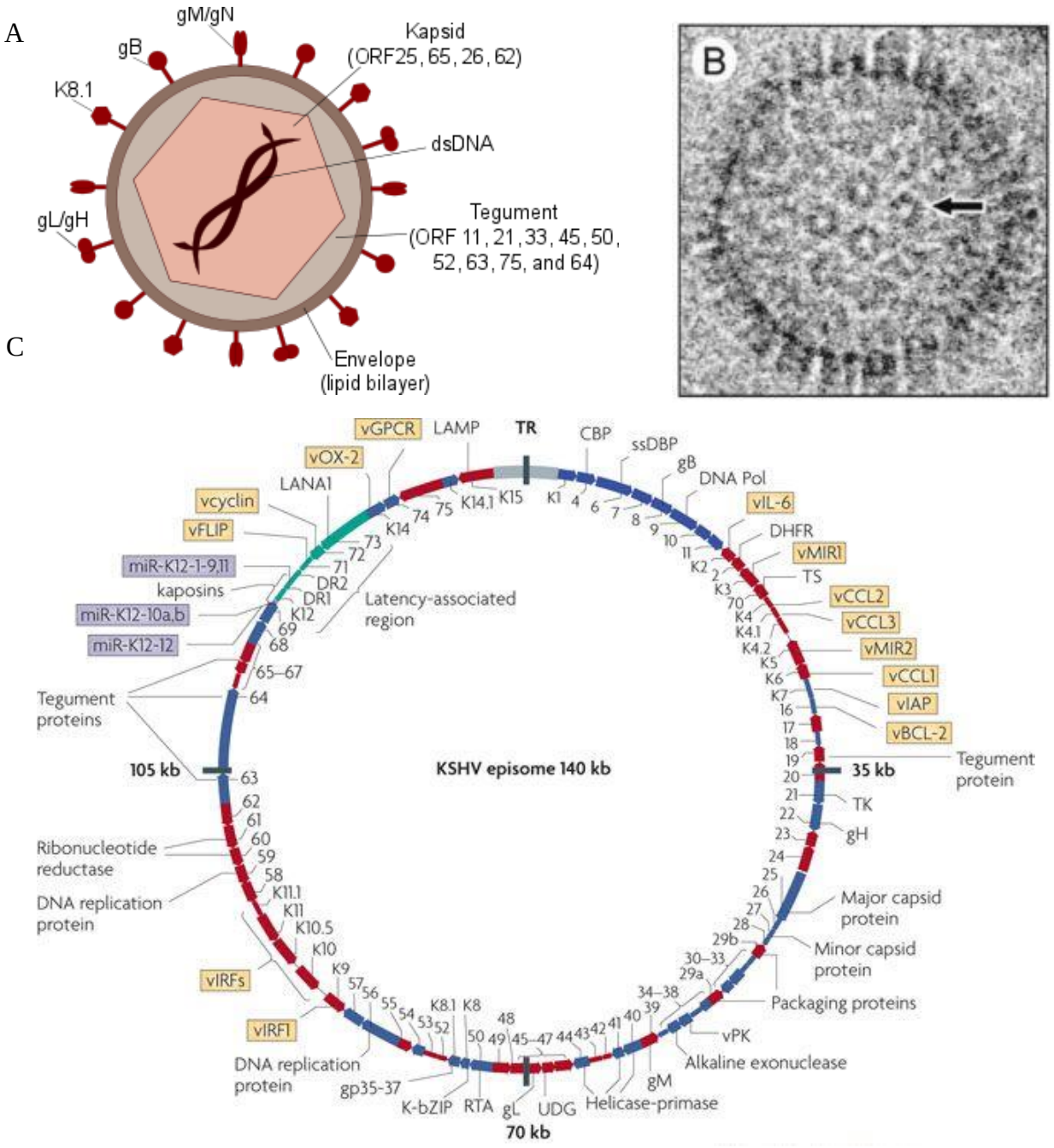

Figure 1. 1 Structure of KSHV.
A) Schematic representation of the viral capsid. B) the enlarged view on the virus capsid (reprinted from[7] with a permit from *American Society for Microbiology*. Copyright © 2000, *American Society for Microbiology*). Capsomers are indicated with an arrow. C) The structure of the KSHV episome. Kaposi's sarcoma-associated herpesvirus (KSHV) encodes 87 open reading frames (ORFs) and at least 17 microRNAs (purple boxes). Putative latent transcripts are indicated in green. Viral lytic genes are indicated in blue, cellular orthologs are highlighted with yellow boxes. (The figure is reprinted from[12] with a permit from *Springer Nature*, licence Nr. 4380940529605. Copyright 2010 by *Springer Nature*)

1.1.2 Hosts and viral tropism

Humans are the natural hosts of KSHV. Except humans, only common marmosets, New World Primates, are susceptible for KSHV. In these animals, the infection reflects the course and pathology

observed in human, including the formation of skin KS-like lesions[13]. In humans the KSHV genome and its transcripts were detected in endothelial cells, B cells, macrophages, dendritic cells, oropharynx, prostatic epithelium, and keratinocytes[6].

1.1.3 Virus entry and early events

KSHV recognizes two categories of cellular receptors, binding and entry receptors. The interaction between binding receptors, ubiquitously expressed cellular heparan sulfate (HS), and viral glycoproteins enables viral attachment and concentration on target cells. The interaction between cellular HS and viral glycoproteins promotes conformational changes and allows the access to adjacent cellular receptors. The entry receptors are cell-type specific and vary according to cell type and include cellular integrins, CD98, DS-SIGN, Eph2A (Table 1.1)[14,15].

Table 1.1 Binding, entry receptors and mode of entry of KSHV in various target cells (adapted from [14,15])

Target cells	Binding receptors	Entry receptors	Mode of entry
Endothelial cells	HS	Integrins α3β1, αVβ3, αVβ5, CD98, Eph2A	Macropinocytosis
B cells, macrophages, dendritic cells	DC-SIGN	DC-SIGN	Clathrin-mediated endocytosis
Monocytes	HS, DC-SIGN	DC-SIGN, Integrins α3β1, αVβ3, αVβ5	
Fibroblasts	HS	Integrins α3β1, αVβ3, αVβ5, CD98, Eph2A	Clathrin-mediated endocytosis

KSHV utilizes diverse endocytic pathways for entry into the target cells. Macropinocytosis is the major route of infection in endothelial cells[16], whereas the clathrin-mediated endocytosis is utilized to enter B-cells and fibroblasts[17]. Enveloped viral particles are detected in cellular cytoplasm at 5 minutes post infection and reach the nuclear periphery within 15 minutes p.i[16]. KSHV infection induces aggregation and thickening of microtubules. Virus capsid colocalizes with microtubules in a PI3K- and Rho-GTPase dependent manner. Rho-GTPase is involved in acetylation and aggregation of microtubules, which is crucial for the delivery of the viral genome to the nucleus[18].

KSHV penetrates the host cells and delivers its DNA as early as 15 minutes after infection with a peak at 90 minutes[18–20]. Following delivery to the nucleus, rapid circularization of the DNA occurs

and within the host nucleus the virus exists in the episomal form. Viral gene expression starts as early as 30 minutes after the infection. Transcriptome analysis of human PBMC, CD14+ and endothelial cells revealed that a number of viral transcripts, including polyadenylated nuclear (PAN) RNA, ORF58/59, kaposin B, K2, K4, K6, ORF11, ORF17, ORF45, ORF27, ORF37, ORF57, ORF64, ORF65, ORF73, and T0.7 accumulate in the infected cells at 4 hours post infection. The majority of viral transcripts, however, get decreased at 24 hours p.i. whereas, the expression of ORF73 (LANA) becomes predominant[21].

1.1.4 Latent KSHV infection

Like the other members of the γ-herpesvirus family, KSHV exhibits two different phases of infection: a persistent latent infection and a transient lytic reactivation that are distinguished by the viral gene expression patterns (see Figure 1.2. for a summary). During the predominant latent stage of the infection, the viral genome is maintained as a circular episome within the host cell nucleus with highly restricted protein expression and no production of virus particles.

Latent viral transcripts are derived from a single genomic region, the so called latency locus, and include LANA, vCyclin, viral FLICE-inhibitory protein (vFLIP), Kaposins, as well as 18 miRNAs. These transcripts promote cell growth, evasion of apoptosis as well as proangiogenic and inflammatory signals[12]. During the latent stage of infection, LANA does not only tether KSHV episome to the cellular chromosome thereby ensuring viral maintenance[11], but also regulates the expression of ORF50[22–24], the key protein required for lytic reactivation.

Viral latent proteins directly contribute to KSHV-induced tumorigenesis. LANA interferes with several anti-tumorigenic pathways, including p53[25,26], RB-E2F[27], and TGFβ[28] as well as contributes to virus-induced angiogenesis by stabilizing HIF1α[29]. vFLIP is responsible for spindle cell transformation of endothelial cells in vitro[30]. It activates NF-κB by direct binding to inhibitor of κB kinase ɣ[31], which leads to suppression of apoptosis by activation of BCL-2 and BCL-X[32]. Kaposin A induces tumorigenic transformation of the cells and leads to formation of high-grade, highly vascular, undifferentiated sarcomas upon subcutaneous injection of Kaposin-transfected cells to athymic nu/nu mice[33]. Transgenic mice expressing LANA, vFLIP, or Kaposin A develop lymphoproliferative malignancies, indicating that the viral transcripts induce lymphatic cell proliferation. However, the induced tumors fail to exhibit the typical morphological features, suggesting that the latent viral genes alone are not sufficient to transform the cells[12].

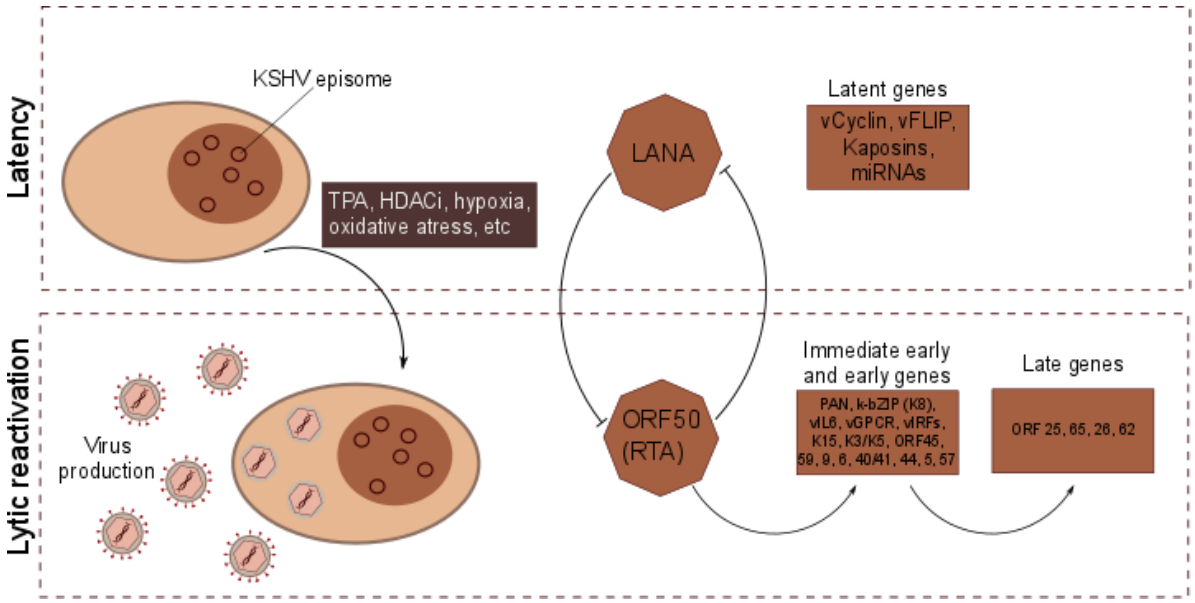

Figure 1. 2 KSHV biphasic life cycle and the genes expressed during latency and lytic reactivation.
Reactivation can occur when the promoter of ORF50 is activated, resulting in the expression of replication and transcription activator (RTA), the main regulator for the viral lytic replication program. Early lytic genes include those encoding viral proteins required for DNA replication or viral gene expression, whereas late lytic genes are those encoding viral structural proteins, such as envelope and capsid proteins, that are required for assembly of viral particles (virions).

1.1.5 Lytic reactivation

The latent phase is reversible and certain environmental and physiological factors including oxidative stress[34,35], hypoxia[29,36], inflammatory cytokines[37], co-infection[38,39], and histone deacetylase inhibition[40,41] may periodically reactivate the virus. Unlike latent replication, lytic replication is initiated from another origin of replication[42], relying on specific KSHV-encoded transcription factors. Lytic reactivation proceeds via a rolling circle mechanism and leads to rapid multiplication of viral genome. Viral lytic reactivation results in the production of the virus particles which are released by cell lysis. It requires the activation of another virus-encoded set of ORFs in a temporally regulated cascade.

Depending on the time of induction the lytic genes can be classified to the immediate early, early, and late lytic genes[37]. Immediate early genes require no previous viral gene expression and encode viral proteins that are directly involved in gene transcription as well as cellular modifications for viral replication. They include ORF50 (replication and transcription activator, RTA), ORF45, K4.2/K4.1/K4, ORF48, ORF29b, K3, ORF70, PAN, and k-bZIP[43]. ORF50-encoded RTA is a key regulator for lytic reactivation from the latency and its expression is both necessary and sufficient for viral reactivation. Ectopic expression of RTA in latently infected B-lymphocytes results in completion of the cascade leading to KSHV lytic replication[44–46]. k-bZIP is not required for lytic reactivation, however, it is needed for viral DNA replication, as k-bZIP together with RTA binds the lytic Ori promoter and initiates viral replication[47].

RTA induces the expression of early viral genes. Early genes are expressed 10-24 hours post-induction and include genes comprising the viral replication machinery as well as genes evading innate immune response. The genes encoding for viral structural proteins (capsid proteins, tegument protein, envelope glycoproteins, and relevant auxiliary factors) are initiated 48 hours post induction, and they are referred to as late genes. Expression of this final fraction of viral genes results in the assembly of viral particles and release of the virus from the infected cell[43].

Although the classic view on KSHV clearly divides its life cycle into two separate states with distinct gene expression patterns, recently, an independent transcriptional program has been described in KSHV infected lymphatic endothelial cells (LECs). It comprises the expression of several lytic genes, including ORF45, but lacks the full lytic program and does not result in the production of viral particles. The study indicated that this unique transcription program confers a selective sensitivity of infected cells to Rapamycin, observed in KSHV-infected LECs, but not blood endothelial cells[48]. This suggests that besides classically defined lytic and latent programs, the virus is able to establish also an intermediate state in LECs, referred to as relaxed latency[49].

1.2 Kaposi's sarcoma – a virus induced tumor of endothelial origin

1.2.1 Epidemiological aspects of Kaposi's Sarcoma

Unlike other herpesviruses with equally high seroprevalence around the globe, KSHV prevalence has a geographical distribution. It is generally low (less then 10%) in Northern Europe, the USA and Asia, elevated in the Mediterranean region (10-30%) and high in sub-Saharan Africa (25-85%)[4]. KSHV is primarily transmitted via saliva. The virus can be transmitted between family members as well as sexually transmitted and transmitted via blood transfusion and injecting drug use[4,50].

Kaposi's sarcoma is divided into 4 epidemiological forms: 1) classic KS affecting elderly men in Mediterranean region, 2) endemic KS observed Central and eastern Africa, 3) iatrogenic KS, developing after organ transplantation, 4) epidemic, or AIDS-KS[12]. The histological features of the four epidemiological forms of KS are indistinguishable[12,51]. Although infection with KSHV is a prerequisite to development of Kaposi's sarcoma, the infection only is not sufficient and requires cofactors. The most important cofactor is immunosuppression. When KS incidence in the general population is 0.3:100,000[52], it is highly increased in patients with HIV from 1:20, climbing up to 1:3 in HIV-infected homosexual men before introduction of highly active antiretroviral therapy (HAART)[12,53]. Transplant KS appears to be more common in kidney transplant patients and has been estimated to occur in approximately 0.6-5.3% of solid organ transplants depending on the region[54]. It is the second most common cancer after prostate cancer in men in Uganda, where incidence rate is up to 30:100,000[55].

1.2.2 KS histogenesis

Clinically the lesions have been classified to four stages: patch, plaque, nodule, and tumor. The lesions comprise the spindle cells, (tumor cells), immature blood vessels, and abundant inflammatory infiltrate. Viral DNA and transcripts can be detected in spindle cells at different stages of the tumor development[56–58]. Early lesions (plaques) have no evident tumor mass. They represent well-defined non-ulcerated lesions with slight lymphocytic infiltrate. At this stage, the tumor contains only 10% of KSHV infected spindle-like cells, which line poorly structured vascular spaces and interspaced with extravasated red blood cells. As the tumor progresses, infiltrative tumor lesions contain than 90% KSHV-infected cells. Spindle-like cells form slit-like vascular spaces and bizarre vascular channels with evident extravasation of red blood cells and microscopic evidence of ulceration[59,60].

Spindle-like cells express markers of vascular endothelium, such as CD31, CD34, and factor VIII as well as markers of lymphatic endothelium including VEGFR3, LYVE1, D2-40 and markers of hematopoetic progenitor cells (CD117)[59–65]. A small proportion of spindle cells also express markers of dendritic cells (Factor XIII), macrophages (CD68), and α smooth muscle cells (αSMA)[66,67]. The diversity of the markers expressed sparkled the debate about the origin of the tumor and indicate polyclonality. It is unclear, whether the lesions descent from differentiated blood endothelial cells, lymphatic endothelial cells or circulating precursor cells. In the last years, a body of evidence indicated the ability of KSHV to transdifferentiate infected cells, which could at least partially explain the heterogeneity of the lesions.

Immunohistochemistry analysis of KS lesions showed that most of the spindle cells and endothelial cells express LANA. Similarly, in situ hybridization studies showed that the vast majority of spindle cells comprising KS lesions expressed T0.7/Kaposin in a cytoplasmic distribution with a predicted membrane proclivity. In contrast, only small proportion of the cells (1-10%) of Kaposin-positive cells express PAN, as an indicator of lytic reactivation. Taken together, the studies indicate that latency is a predominant stage of the infection within KS lesions[68].

1.2.3 Endothelial fate reprogramming by KSHV

Transcriptome analysis of nodular KS with more them 80% of spindle cells showed that the cells within the lesions more closely resemble endothelial cells than other cell types. More detailed analysis showed that the gene expression pattern is more similar to lymphatic endothelial cells (LECs) than to blood endothelial cells (BECs)[69]. Infection of primary BECs with KSHV leads to induction of more than 70% LEC-specific genes, as was shown by transcriptome and RT-qPCR analysis in both primary human dermal microvascular endothelial cells (HDMECs) as well as in the immortalized HDMECs[70,71]. Interestingly, infection of primary LECs leads to the upregulation of several BECs-specific markers, bringing the phenotype closer to the one of the blood vascular endothelium[69].

The reprogramming is likely due to virus-induced changes in cell fate-specifying transcription factors, such as PROX1, a master regulator of lymphatic development, and MAF. Induction of PROX1 expression requires activation of the JAK2/STAT3 and the PI3K/Akt pathway through gp130 and can be reverted by pharmaceutical inhibitors of the pathway[72]. Expression of viral IL-6 alone, but not the expression of other viral genes is sufficient to mimic this process in telomerase-immortalized HDMECs[73]. Kaposin B is shown to increase cellular cytokine production by activating p38/MK2 and thereby increasing stability of cytokine's mRNA[74]. Utilizing the same mechanism Kaposin B stabilizes PROX1 and induces the expression of it's downstream targets[75]. The other studies indicate that activation of IL3 receptor alpha (IL3Rα) in BECs leads to upregulation of PROX1, whereas activation of Notch/Hey1 signaling in KSHV-infected LECs leads to repression of PROX1[76].

Although MAF was not previously linked to LEC/BEC differentiation, a study identified MAF as a transcriptional repressor, preventing expression of BEC-specific genes, thereby maintaining the differentiation status of LECs. Expression of KSHV-encoded miRNAs silence MAF in infected LECs thereby promoting expression of BEC-specific genes[77].

1.2.4 Endothelial-to-mesenchymal transition upon KSHV infection

Endothelial-to-mesenchymal transition (EndMT) plays a vital role during cardiovascular system development[78,79]. In adults it is linked to several cardiovascular diseases, such as pulmonary hypertension[80], vascular malformations[81], myocardial infarction[82], and contributes to tumor environment and cancer progression.[83]. EndMT involves a progressive loss of endothelial markers and appearance of mesenchymal markers, such as αSMA, vimentin, platelet-derived growth factor receptor (PDGFR). These changes are accompanied by a transition from polarized to a motile and invasive phenotype.

Recently it was shown that upon KSHV infection primary dermal microvascular endothelial cells reduce expression of endothelial-specific markers , such as CD31, VE-Cadherin and CD31, and upregulate mesenchymal markers, such as Vimentin, aSMA and PDGFRβ. Transcriptome analysis of the cells showed upregulated expression of the genes linked to cell motility and cytoskeleton rearrangement. The cell undergo as well virus-induced functional changes, such as increased motility and loss contact inhibition[84,85]. Similarly, KSHV infection of lymphatic endothelial cells leads to increased expression of mesenchymal markers and increased invasiveness of the cells in 3D cell culture[86]. Taken together, these observations indicate that the cells acquired mesenchymal-like properties during infection. This transformation is induced by activation of Notch pathway and associated with expression of viral genes vGPCR and vFLIP[86].

KSHV-induced EndMT may help to explain the heterogeneity of the cell types found in the KS lesions and allows to speculate that the cells with a mesenchymal expression profile can be derived from KSHV-infected endothelial cells.

1.3 Molecular mechanisms of KSHV-induced tumorigenesis

1.3.1 The PI3K-Akt-mTOR pathway

Mutations in PI3K are found in one third of human cancers and 40% of breast cancers and are linked with cellular transformation and tumor progression. Triggering of receptor tyrosine kinases or G-protein coupled receptors facilitate the recruitment of class I PI3Ks which phosphorylate phosphatidylinositol-(4,5) bisphosphate (PIP2) to phosphatidylinositol (3,4,5)-trisphosphate (PIP3). Accumulation of the latter allows phosphorylation of Akt, the main effector of the cascade which regulates several pathways, including inhibition of apoptosis, stimulation of mTORC1-dependent cell growth, and modulation of cellular metabolism.

PI3K/Akt signalling is activated as early as 5 minutes post KSHV infection and inhibition of the pathway with LY294002 or wortmannin blocks virus entry. The studies indicated that PI3K phosphorylation is required for the activation of Rho-GTPases which play a role in endosomal formation and viral trafficking to the nucleus.

Several viral proteins, including K1, vGPCR and vIL6, have been shown to induce PI3K activation to promote tumorigenesis and angiogenesis of the infected cells. In addition, activation of PI3K pathway has been shown to govern the survival advantage to the infected cells in serum starvation conditions. The downstream target of PI3K, mTOR is activated in lymphatic endothelial cells and its inhibition by rapamycin has been shown to reduce tumor progression in transplant recipients. Interestingly, PI3K activation is required for reactivation of the virus from latency and efficient virion production.

In summary, these studies indicate that PI3K is one of the central pathways required for KSHV induced tumorigenesis as well as viral dissemination.

1.3.2 NF-κB pathway

Nuclear factor-κB (NF-κB) plays a central role in the regulation of diverse biological processes, including immune responses, development, cell proliferation and survival. Deregulated NF-κB has been linked to a variety of human diseases, particularly cancers.

Similarly to PI3K, NF-κB is activated 5 minutes p.i. and persist at later time points. Although inhibition with small molecules does not affect viral entry, it blocks viral gene expression. The other studies indicate that the pathway contributes to latent maintenance of the virus, since activation of NF-κB blocks lytic reactivation of KSHV.

Activated NF-κB confers a survival advantage to the infected cells and inhibition of the pathway with a small molecule leads to apoptosis of the infected cells as well as inhibits the expression of several antiapoptotic genes. Treatment of the mice with Bay11-7082, a selective pharmacologic inhibitor of NF-κB, prevents or delays tumor growth in murine mouse models for B-cell lymphomas.

1.3.3 DNA damage response and its role in virus-induced tumorigenesis

The DNA damage response (DDR) is a cellular response to DNA damage, accidentally occurring either during cell division or induced by different agents. The DDR includes the detection of DNA damage and finally leads to either repair of damaged DNA or cell cycle arrest and apoptosis. It secures genome integrity and ensures the transmission of intact genomes to daughter cells during cell division. The inability of the cells to adequately respond to the damage results in various clinical conditions, including cancer. Genome instability and a high mutation rate are considered to be enabling characteristics for cancer development, therefore DNA damage response genes are considered to be tumor suppressor genes[87].

Double-strand breaks are recognized by the MRN complex (comprising Mre11, Rad50 and NBS1), which mediates recruitment and activation of ATM kinase[88,89]. ATM, in turn, phosphorylates a number of downstream targets that include serine 139 of H2AX. Phosphorylated H2AX attracts MDC1 protein, which form the H2AX-MDC1-ATM complex flanking a damaged region, amplifying the DNA damage signal and initiating repair[90]. ssDNA, in turn, is recognized by RPA, which recruits ATR kinase to the damage site and induces its activation by facilitating ATR-ATRIP complex formation[91]. Phosphorylation of H2AX plays a central role in DDR.

In addition to ATM-dependent phosphorylation at Ser139, H2AX is constitutively phosphorylated at Tyr142 by WSTF[92]. The Phosphorylation status of Tyr142, regulated by Eya phosphatases during DNA damage response, determines the decision for DNA repair or cell apoptosis pathways[93].

Double strand DNA damage repair is mainly carried out by two key pathways: non-homologous end joining and homologous recombination. Non-homologous end joining is the prevalent pathway, which is active during the whole cell cycle. The DNA ends are recognized by Ku70/80 heterodimer recruiting DNA-PK to the site of damage, which facilitates the joining of the DNA strands. Homologous recombination occurs in S and G2 phases of cell cycle and is orchestrated by the MRN complex, recruiting BRCA1 and CtIP to the site of damage[94–96].

There is accumulating evidence that in addition to their conventional role in DNA damage response the sensors of DNA damage also serve as cytosolic DNA sensors and trigger innate immune response and therefore can be viewed as a part of intrinsic intracellular defense against viruses. In particular, detection of viral DNA by Rad50, Mre11, IRF16, or DNA-PK induces type-1 interferon and NF-Kb pathways and trigger the production of downstream cytokines[97–103]. Several oncogenic viruses, such as human papilloma virus, Epstein-Barr virus, and adenovirus, induce DDR and manipulate them to their advantage[104–107].

KSHV triggers DDR on various stages of infection. Although ATM-dependent phosphorylation of H2AX determines establishment and maintenance of KSHV latency[108], recognition of viral DNA by the MRN complex restricts KSHV replication[109]. KSHV evolved to manipulate DDR to its advantage

and the evasion of DDR by the virus is one of the molecular mechanisms of KSHV-induced tumorigenesis.

1.3.4. KSHV-induced angiogenesis

Tumor progression and metastasis rely on angiogenesis and lymphangiogenesis, since the tumor growth is highly dependent on the supply of oxygen, nutrients and host-derived regulators. Vascularization of malignant tumors involves several mechanisms, among which are directed capillary ingrowth (endothelial sprouting), remodeling of existing vessels, recruiting of circulating endothelial progenitor cells, and vasculogenic mimicry[110]. The letter refers to a process during which tumor cells acquire the ability to form vessel-like networks in three-dimensional conditions. Vasculogenic mimicry has been described for a various aggressive carcinomas associated with poor prognosis[111].

KS is an angiogenic tumor characterized by newly formed, leaky, poorly organized vessels[112]. KSHV induces angiogenesis in the infected endothelial cells by VEGF-dependent and VEGF-independent mechanisms[49] (Fig. 1.3). VEGF has been detected in KS tissue[85] as well as in plasma of KS patients[86] and its expression is induced by overexpression of several lytic proteins, such as vGPCR[115], K1[116], vIL6, and K15, in endothelial cells. The virus proteins can induce VEGF expression directly or activate VEGF signaling via PI3K/Akt/mTOR[117], Erk and p38 signaling[118,119]. Although the proteins involved in activation of VEGF-dependent angiogenesis are expressed during lytic reactivation and therefore only present in minority of spindle cells, they initiate a paracrine loop inducing angiogenesis in the neighboring cells[118].

vGPCR and vIL6 induce Notch signaling as well as Ang2 expression via the MAPK pathway[120], thereby leading to angiogenesis in a VEGF-independent manner. In addition, the viral K15 protein stimulates the phosphorylation of phospholipase Cγ1 activating VEGF downstream pathways even in absence of VEGF or its receptor, thereby inducing tube formation in primary VECs[121]. Viral latent proteins LANA and vFLIP contribute to angiogenesis by Ezh2-dependent regulation of ephrinB2, a regulator of angiogenic growth[122].

In contrast to tumorigenesis induced by other oncogenic viruses, which primarily affect cellular cell cycle and apoptosis, KSHV-induced tumorigenesis is characterized by altered differentiation and function of endothelial cells. Angiogenesis induced by KSHV in both autocrine and paracrine manner is the core of KS and therefore is an attractive target for novel therapeutic strategies.

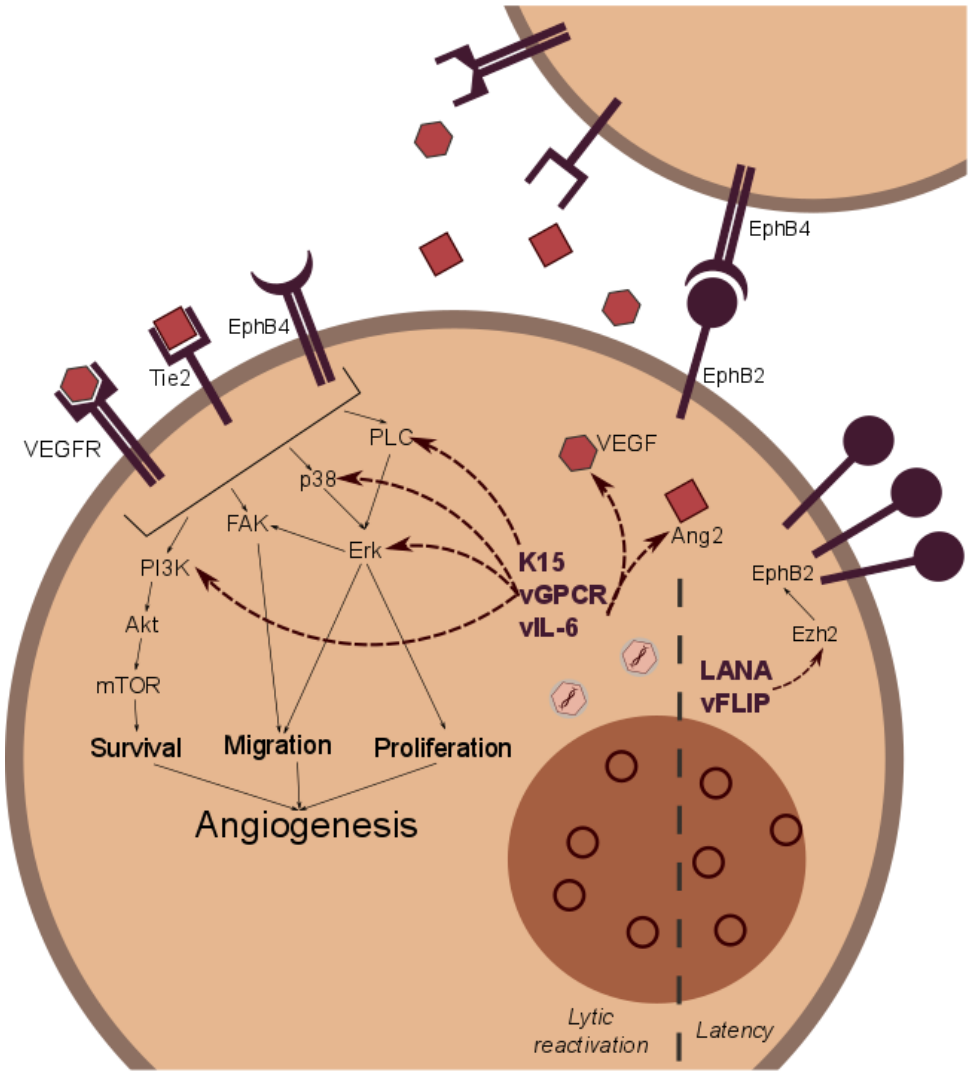

Figure 1. 3 Schematic representation of KSHV-induced angiogenesis in endothelial cells (based on literature data).

1.4 Existing treatment options and prognosis

Up to now, there are no standard therapeutic guidelines for the management of Kaposi's sarcoma, and the therapeutic strategy of each case depends on tumor location, the variant of KS, the rate of progression, the severity of the symptoms and the immune competence of the patient[123–125].

Therapeutic approaches for treatment of KS could be classified to local and systemic approaches. Local approaches include surgical excision, cryotherapy, radiotherapy, laser therapy and local administration of chemotherapeutic drugs[123].

Key component of treatment of HIV-associated KS is the highly active antiretroviral therapy (HAART), which reduces HIV viremia and reconstitutes immune system[126]. Some studies indicate that in addition to their antiretroviral activity, HIV protease inhibitors have antitumor and antiangiogenic properties[127,128] and are able to directly inhibit KSHV thymidine kinase[129], thereby

blocking KS growth. Although implementation of HAART reduced the risk of AIDS-KS, this tumor can still occur in patients with low viral load and T-cell count above 300 cell/mm^3, which is above the level typically associated with susceptibility to opportunistic diseases[130,131]. Even after the development of HAART only 50% of patients with advanced stages of AIDS-KS achieve complete resolution[132].

Although early lesions of AIDS-KS are responsive to HAART, management of more advanced lesions requires systemic treatment[123]. The current first-line systemic treatment includes liposomal antracyclines, including daunorubicin and doxorubicin. Although the response rate to the drugs in combination with HAART reaches 76%, the response is 3 to 6 months delayed. The adverse effects include myelosuppression, opportunistic infections, stomatitis, and infusion reactions[133]. Second-line systemic drugs approved for KS include paclitaxel and etoposide. Although the response to these drugs reaches 71%, the adverse effects are more severe compared to first-line treatment, which makes them less favorable treatment options. The first- and second-line agents are expensive and not readily available in developing countries, where KS incidence is the highest[123]. When the agents are not available, systemic treatment includes cytotoxic therapy (bleomycin, vincristine) alone or in combination with HAART. This treatment has numerous adverse effects and the response range varies from 25-88%[134,135].

Inhibitors of viral DNA polymerase, which were initially developed for other herpesviruses, such as ganciclovir, cidofovir, and foscanet were shown to reduce viral load of KSHV[136] and reduce the risk of KS in HIV-positive patients up to 62%[137,138]. Although the efficacy of the treatment is limited, it can be used to prevent new lesions[123].

Treatment of iatrogenic KS often requires reduction or elimination of immunosuppressive therapy, which may lead to draft rejection in 50% of the patients[125]. Rapamycin, a natural product from actinobacteria, has emerged as a therapeutic compound of benefit for transplantation-associated KS and was shown to have antiangiogenic effects in a murine tumor model[139]. Several studies also suggest a selective sensitivity of KSHV-infected cells to rapamycin, as its molecular target mTOR is crucial for the survival of KSHV-infected cells and viral pathogenesis[48,140,141]. This is in line with the observation that after renal transplantation in KSHV-infected patients the replacement of standard immunosuppressive drugs with rapamycin resulted in a reduction of Kaposi's sarcoma lesions[142].

Inhibitors of angiogenesis[143], VEGF[144–146], tyrosine kinase[50,147], and matrix metalloproteinases[148] which are related to KSHV pathogenesis, have been discussed lately and now are investigated in preclinical and Phase I-III clinical studies[12,124].

1.5 Models to study KSHV infection

The lack of a specific antiviral therapy as well as limited results that can be achieved by existing treatment options dictates the need for novel therapeutics. Although a set of cell-free high throughput screen were developed to find inhibitors of herpesviral latent proteins[149,150] or proteins needed for viral replication[151,152], the hit compounds found in those assays have to be validates in cell culture and in vivo models before.

1.5.1 Cell culture systems to investigate infection of endothelial cells

Although up to 90% of spindle cells are infected with the virus[51], the cells isolated from KS lesions[153–155], as well as newly KSHV-infected human umbilical vein endothelial cells (HUVECs)[156], fail to efficiently retain viral episomes in classic cell culture conditions. In addition, primary cells are of limited availability, have high batch-to-batch and donor-to-donor variation and therefore are of limited use for drug screening.

Several B cell culture models were proposed as a system for screening and validation of novel herpesviral drugs, either targeting KSHV maintenance in latently-infected cells[157] or viability of KSHV-infected cells[158]. However, there are only few cell culture systems available for investigation viral pathogenesis in endothelial cells and drug validation against KS.

Studies show that telomerase-immortalized endothelial cells are susceptible for KSHV infection, however, similarly to the primary cells they tend to lose viral genomes upon cultivation. Intriguingly, upon long-term culture of the cells single clones that are able to retain viral copies, so called TIVE-LTC, were isolated. The cells showed increased capacity to form colonies in soft agar and survival upon serum-deprivation, indicating tumorigenic transformation. However, similar to other adherent cell types[8], the cells show limited potential for lytic reactivation[161]. Although the cell line allows investigation of the virus in endothelial cells and closely mimics infection of primary endothelial cells, several aspects of the infection differ from those described for primary cells. In particular, the cells fail to establish spindle-like morphology in vitro upon KSHV infection[161]. In addition they induce the expression of VEGF upon long term infection[162], which is not observed upon infection of primary endothelial cells[49,163].

Infection of SKL cells, the uninfected cells derived from a gingival KS lesion of an HIV-negative renal transplant recipient, with rKSHV.219 results in a stable, latently infected cell population. In order to overcome the restricted reactivation rate, the cells were transduced with doxycycline-inducible RTA transgene. The resulting cell line allows the specific viral reactivation upon addition of doxycycline and enables studying viral reactivation without addition of TRA or HDAC inhibitors, disturbing host cell biology[160]. Despite of the fact that SLK is generally believed to be a cell line of endothelial origin, recent studies show that it is indistinguishable from the human renal carcinoma cell

line Caki-1[164].This data show that SKL is not a cell line of endothelial origin and therefore is of limited relevance to study KS.

In summary, although existing cell culture models can mimic various aspects of KSHV infection, there is still a need for a novel cell culture model which would closely resemble the features of primary cells in vitro.

1.5.2 3D cell culture systems in cancer research

Unlike classical monolayer (2D) culture, 3D cell culture allows mirroring in vivo situation by incorporating physiologically relevant gradients, such as oxygen, nutrients, and metabolites[165]. These conditions are shown to be beneficial for improving the in vitro phenotype of various cell types. For example, global gene expression profiling showed upregulation of hepatocyte-specific markers and increased hepatic functions in 3D cell culture conditions of immortalized hepatocytes[166]. Studies showed that some anticancer therapeutics lose their activity in 3D cell culture and in vivo compared to the activity observed in a monolayer culture[167]. This highlights that investigation of tumor cells in 3D cell culture conditions allows better understanding of tumor physiology and serves to the faithful preselection of novel antitumor drugs.

Embedding of HUVEC cells, cultured on microcarrier beads, into a fibrin gel was described as a reliable system to study angiogenesis[168]. Embedding of the cells into 3D gel increases the expression of the genes needed for angiogenesis increased[169]. Moreover, 3D cell culture assay was used to study invasive potential of various endothelial cell lines and used a system to test novel antiangiogenic agents[170,171].

3D cell culture of KSHV-infected lymphatic endothelial cells showed higher expression of EndMT markers and therefore reflect KSHV-induced cellular transformation better than 2D cell culture[86]. Culture of KSHV-infected B cells in 3D spheroid culture showed a beneficial effect on viral maintenance and lytic reactivation[172]. This suggests that 3D cell culture conditions may better reflect KSHV-induced tumorigenesis and therefore represent a better system for validation of novel antitumor drugs.

1.5.3 Animal models for Kaposi's sarcoma

The strict human-specificity of KSHV challenges the development of in vivo models. One approach to complement the lack of in vivo system is an investigation of genetically close herpesviruses tropic to other species, for example herpesvirus saimiri infecting primates and some rabbits[173], rhesus monkey rhadinovirus[174,175], and murine herpesvirus 68 (MHV68)[176]. Despite genetic similarity to KSHV and similarity in the induced B-cell pathologies[177–180], the viruses fail to establish endothelial-cell tumors and therefore are not suitable to investigate Kaposi's sarcoma. Similarly, humanized

immunodeficient mice, although susceptible to KSHV and establish infection of B-cells and macrophages, fail to establish KS-like lesions[181–183].

Chimeric MHV68 allows studying function of individual viral genes in vivo[184]. By replacing G-protein coupled receptor of MHV68 with the KSHV analog the scientists could achieve formation of KS-like lesions of endothelial origin in immunocompetent BALB/c mice[185].

Another approach to tackle this challenge is xenograft transplantation of the cells carrying KSHV genome into immunodeficient mice. Transplantation of either murine endothelial precursor cells (mECK36)[186] or human HEK cells[187] carrying a bacterial artificial chromosome (BAC) encoding the full length KSHV genome leads to an increased tumor potential of the cells. Similarly, KSHV infection of TIME cells induces tumorigenic transformation of the cells[161]. Both TIVE-LTC and mECK36 cells form KS-like lesions consisting of spindle-like cells.

1.5.4 Conditionally immortalized human endothelial cells as a model for KSHV infection

The limited number and patient-to patient heterogeneity of primary cells restrict their use in drug development. Researchers often use immortalized cell lines to overcome these limitations. The cell lines are usually derived from tumor tissues, upon spontaneous immortalization or upon transduction of immortalizing genes. However, immortalized cell often lose primary-like properties and poorly represent in vivo phenotype.

It has been shown that the use of cell-type-specific immortalization regiments results in rapid immortalization of various cell types while preserving their properties. In particular, this approach allowed establishment of a series of endothelial and hepatic cell lines with primary-like phenotype and functionality[166]. However, prolonged constitutive expression of immortalizing genes can lead to a premalignant phenotype[188]. Inducible expression of immortalizing genes overcomes this limitation by offering strict control of cell proliferation[189].

A number of synthetic gene regulation systems were developed that allow quantitative control of gene expression upon administration of exogenous effector molecules. The bacteria-derived Tet promoter is the most commonly used inducible system[190]. The system consists of two elements: Tet-promoter and its transactivator proteins. Tet-promoter is composed of seven tet operator (TetO) DNA sequences from E. Coli and the minimal hCMV immediate early promoter. Transactivator proteins (rtTA) induce gene expression by binding to TetO sites only in presence of doxycycline while in the absence of doxycycline gene expression is shut off[191]. In addition, bidirectional tet-promoters were developed, which contain two minimal CMV regions flanking 7 TetO. These promoters allow simultaneous expression of two genes[192].

Conditional immortalization of primary HUVEC cells by transduction of the cells with lentiviral vector carrying immortalizing genes (SV40 large T antigen and the catalytic fragment of human

telomerase hTert) as well as the transcriptional transactivator rtTa driven by bidirectional tet-promoter resulted in growth controlled endothelial cell line, HuARLT[193]. The cell line preserves relevant phenotypic characteristics of primary endothelial cell, such as expression of majority of endothelial markers, uptake of macromolecules, and efficient tube formation in matrigel assay[193,194]. Moreover, HuARLT cell form a network of hCD31 positive vessels upon transplantation into immunocompromised mice. The formed vessel are filled with mouse erythrocytes, which indicates that they are functional and connected with mouse vasculature[194].

Moreover, previous studies indicate that the cell line is susceptible to infection with bacterial and viral pathogens targeting endothelial cells, such as human cytomegalovirus. The cell line supports the early and late phase of viral replication as well as the release infectious progeny virus at titers comparable to primary HUVECs, thus representing the full replication cycle of hCMV in endothelial cells[195]. The cells are permissive for KSHV infection. Similar to primary cells, HuARLT cells establish spindle-like morphology and undergo a series of transcriptional changes, reflecting EndMT[194]. Taken together, these properties allow the usage of the HuARLT cell line as an alterative to primary cells to investigate endothelial properties upon infection both in vitro and in vivo.

1.5.5. Recombinant KSHV.219 as a system to study latent-to-lytic switch

The inability of endothelial cells to retain the virus can be experimentally circumvented by the use of a recombinant virus, carrying a selection marker. The rKSHV.219 virus carries the GFP gene under the control of the constitutive EF1α promoter as well as an RSV-driven puromycin acetyl transferase as well as the viral PAN-promoter driven RFP, enabling detection of lytically reactivated cells (Fig. 1.4). The virus allows for selection and monitoring of the infected cells and significantly expands a toolbox for understanding KSHV latent-to-lytic switch[196].

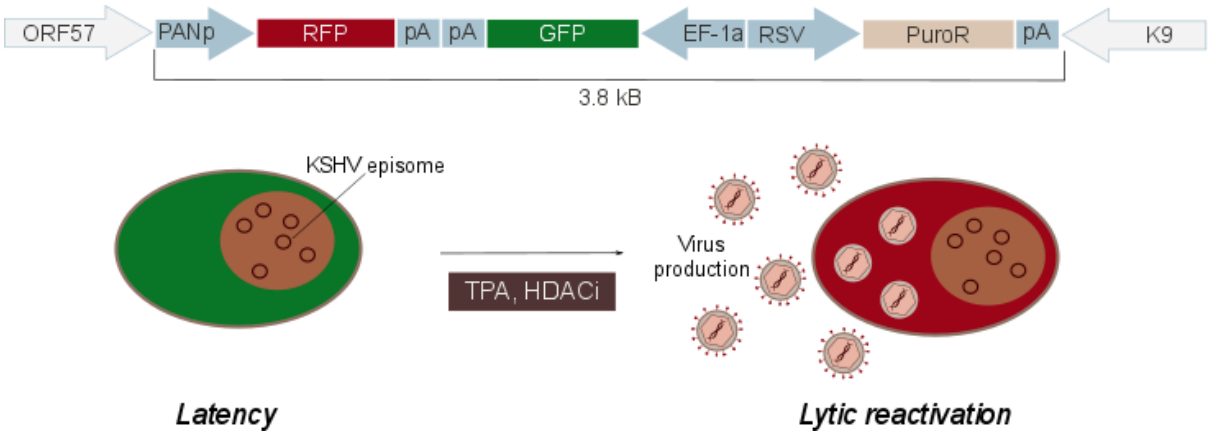

Figure 1. 4 Schematic diagram showing the structure, the integration site of BFP/RFP/PuroR construct in rKSHV.219 (adapted from[196]) and the schematic diagram of latent-to-lytic switch in KSHV.219-infected cells.

1.6 The aim of the study

KS is the most common neoplasm in untreated AIDS patients and in men in sub-Saharan Africa, as well as one of the most common malignancies in patients after organ transplantation with limited treatment options and poor outcome. Although the etiological agent has been identified to be KSHV, a herpesvirus, the investigation of the viral pathogenesis and identification of potential antiviral compounds are compromised by the lack of scalable and robust in vitro models that reflect the virus-induced changes observed in vivo. Moreover, due to the restricted host tropism of KSHV, small animal models have not been available so far.

The aim of this study was to develop predictive in vitro and in vivo models to investigate the consequences of KSHV infection. To this end, a recently developed conditionally immortalized endothelial cell line should be explored upon infection with recombinant rKSHV.219. The capacity of the cell line to mimic KSHV-induced cell transformation and tumorigenesis should be investigated in standard 2D, physiologically relevant 3D cell culture conditions, as well as upon xenograft transplantation in vivo.

Overall the study aimed at contributing to the understanding of molecular mechanisms of viral maintenance as well as the identification of novel antivirals, which can be used as targeted therapy for KS.

2. Materials and methods

2.1. Materials

2.1.1 Equipment

Table 2. 1 Summary of laboratory equipment used in the study

Name	Company
NanoDrop ND-1000 spectrophotometer	PeqLab
TriStar² LB 942 Modular Multimode Microplate Reader	Berthold Technologies
LightCycler 480 II	Roche
FACSCalibur™ analyzer	Becton-Dickinson
BD™ LSR II analyzer	Becton-Dickinson
Guava EasyCount	Millipore
Zeiss LSM META	Zeiss
CO_2 incubators for cell culture C200	Labotect
Sterile work bench MaxiSafe 2020	Unity Lab Service
Nikon TMS Inverted Microscope	Nikon
Axio Observer A1 Inverted microscope	Axio
AxioCam MRc	Axio
Axiovert 135TV	Zeiss
White light source HYP 120	
Agilent Technologies 2100 Bioanalyzer	Agilent Technologies
Illumina HiSeq2500	Illumina

2.1.2 Consumables

Table 2. 2 The list of consumables

Name	Company	Catalogue Number
AggreWell™400	Stemcell Technologies	27945
Cell culture plates	Nunc Multidish/Nunclon	
Falcon tubes (15, 50 ml)	Greiner bio-one	188271, 227261
SafeSeal tubes (1,5 ml)	Sarstedt	72.706
LightCycler 480 Multiwell Plates 96	Roche	04 729 692 001
Cell strainer EasyStrainer 40 µm	Greiner bio-one	542040
Syringes, 1ml	Omnifix®, Braun	9161406V
Disposable hypodermic needle Sterican 100, 20G	Braun	4657519

2.1.3 Chemicals

Table 2. 3 Summary of the chemicals and kits used in the study

Compounds	Company	Catalogue number
12-O-Tetradecanoylphorbol 13-acetate (TPA)	Sigma	P1585-1MG
5-dodecanoylaminofluorescein di-beta-D-galactopyranoside (C_{12}FDG)	Molecular probes	D2893
5-fluoro-2'-deoxyuridine (FuDR)	Sigma	F0503
Agarose LE	Biozym	840004
Albumin from bovine serum (BSA)	Sigma	A3294-100G
AlexaFluor™ 488 acetylated low dencity Lipoprotein From Human Plasma	Invitrogen	L2338
Bafilomycin A1 from Streptomyces griceus	Sigma	B1793-10UG
BAY11-7085	Cayman Chemical	14795
DAPT	Cayman Chemical	13197
Doxycycline hyclate	Biochemica	24390-14-5
Dynabeads® mRNA DIRECT™ Micro Purification Kit	Thermo Fisher	61006
Fetal Bovine Serum (FCS)	Sigma	F7524
FGF	PeproTech	100-18B-250
Fibrin	Calbiochem	341576
FK506	Abcam	Ab120223
FluoroshieldTM	Sigma	F6057-20ML
Gelatin	Sigma	G1393-100ML
Glycarrhizic acid (GA)	abcam	Ab143127
Guava ViaCount®	EMD Millipore	4000-0040
GW5074	Cayman Chemical	10010368
IsoFlo (Isofluran)	Zoetis	TU061220
Ku55933	Cayman Chemical	16336
LY294002	Cayman Chemical	70920

Manumycin	BioViotica	BVT-91-M001
Matrigel high protein (HC), growth factor reduced	Becton Dickinson	354263
Matrigel, growth factor reduced	Becton Dickinson	354230
Methylcellulose	Sigma	M0512
Mirin	Cayman Chemical	13208
MLS000544460	Calbiochem	5.31085.0001
Nu7441	Cayman Chemical	14881
Phosphonoformic acid trisodium salt hexahydrate (PhA)	MP biomedicals, LLC	195426
Proteinase K	Qiagen	19133
Puromycin dihydrochloride from Streptomyces alboniger	Sigma	P7255-1G
Rapamycin	Cayman Chemical	13343
Reverse-Aid First Strand cDNA Synthesis Kit	Fisher Scientific	K1622
RNAeasy mini kit	Quiagen	74106
Saponin Quillaja sp.	Sigma	S4521
ScriptSeq v2 RNA-Seq Library Preparation Kit	Epicentre	SSV21106
SsoFast™ EvaGreen® Supermix	Biorad	1725204
Thrombin	Merck Millipore	605190-100U
Triton® X-100 molecular biology grade	Serva	39795.02
TruSeq SBS Kit v3-HS	Illumina	FC-401-3002
U126	Calbiochem	662005-1MG
VEGF	Randox	RCPG246
WST cell counting kit 8	Sigma	96992-500TESTS-F

2.1.4 Media and buffers

Table 2. 4 Media and buffers used in the study

Name	Company	Catalogue number
Endothelial growth media	Lonza	CC-3124
Endothelial Cell Growth Medium (Ready-to-use)	Promocel	C-22010
Hanks' Balanced Salt Solution	Tebu-Bio	088HBSS-500

Table 2. 5 Buffer formulations

Buffer	Composition
PBS	NaCl 140 mM KCl 27 mM Na_2HPO_4 7,2 mM pH 6.8-7.0
FACS buffer	PBS 2% FCS
Modified Bradley's Buffer	Tris 1.21 g/l NaCl 0.58 g/l EDTA 2mM SDS 0,5% pH 7,5 Proteinase K 30 mAU/ml

2.1.5 Antibodies

Table 2. 6 List of antibodies and applications. IF – immunofluorescence, IHC – immunohistochemistry.

Epitope	Conjugate	Dilution	Host	Company	Catalogue Nr	Application
LANA	Unconj.	1:100	Mouse	Leica	NCL-HHV8-LNA	IF
		1:30				IHC
CD141	Unconj.	1:40	Mouse	Serotech	MCA641T	IHC
CD34	Unconj	1:100	Mouse	BD Pharmingen	555746	FACS, IHC
GFP	HR	1:10	Rabbit	Santa Cruz Biotechnology	sc-8334	IHC
Vimentin	Unconj.	1:100	Mouse	Dako	M0725	IHC, FACS, IF
Ki67	Unconj.	1:100	Rabbit	NeoMarkers	RM-9106-PCS	IF
CD31	Unconj.	1:100	Mouse	BD Pharmingen	555444	IF
CD146	Unconj.	1:100	Mouse	BioLegend	134701	FACS
CD 144 (VE-Cadherin)	Unconj	1:100	Mouse	BioLegend	348501	FACS, IF

ZO-1	Unconj	1:100	Mouse	BD Transduction Laboratories	610966	IF
mouse	Cy3	1:1000	Goat	Dianova	115-165-068	IF, FACS
mouse	APC	1:1000	Goat	Biolegend	405308	FACS
rabbit	Cy3	1:200	Goat	Dianova	111-166-045	IF, FACS

2.1.6 Primers

Table 2. 7 List of primers used. All the primers used in the assay were synthesized by Eurofins genomics.

Name		Sequence	Number
ACTB	Forward	TCACCCACACTGTGCCCATCTACGA	P5440
	Reverse	CAGCGGAACCGCTCATTGCCAATGG	P5441
Akt	Forward	TGAAGGTGCCATCATTCTTG	P5422
	Reverse	ATGAGCGACGTGGCTATTGT	P5423
C1ORF43	Forward	AAGGAGCTGGGGCTCATACT	P5629
	Reverse	GTGAATGTCGTGCTGGTGAT	P5630
CD31	Forward	GGAAACCATGCAATGAAACCAA	P5464
	Reverse	GTCCTTCTTTCCTAGATCTTTGTGA	P5465
cRaf	Forward	TGAATCCAAAACCATTGCTG	P5426
	Reverse	GAACGACAGGACGTTGGG	P5427
Eya1	Forward	TCCAACAGACCATACCCACA	P5589
	Reverse	AATCCTGTCTGTCCAGGTGA	P5590
Eya2	Forward	ACACAATGGACCTTCCACAC	P5591
	Reverse	TGGTCACAATCCTTCCCGTA	P5592
Eya3	Forward	TACTTCCGGTTCCTAGCGAT	P5593
	Reverse	GTAAAAGCCCCACAACAGGA	P5594
Eya4	Forward	GTTTAGGAGGTGCTTTCCCC	P5595
	Reverse	TTGCTGCCTGTTCTTCTTCT	P5596
GFP	Forward	AGCTGCCCGTGCCCTGGCCC	P3429
	Reverse	TGTACTCCAGCTTGTGCCCC	P3430
H2AX	Forward	ACAACAAGAAGACGCGAATC	P5597
	Reverse	CTCTTAGTACTCCTGGGAGGC	P5598
Hes1	Forward	TACTTCCCCAGCACACTTGG	P5448
	Reverse	CGGACATTCTGGAAATGACA	P5449
Hey1	Forward	CGAAATCCCAAACTCCGATA	P5450
	Reverse	TGGATCACCTGAAAATGCTG	P5451
Jag1	Forward	GTCCATGCAGAACGTGAACG	P5446

	Reverse	GCGGGACTGATACTCCTTGA	P5447
Jak2	Forward	CCATTCCCATGCAGAGTCTT	P5430
	Reverse	CAGGCAACAGGAACAAGATG	P5431
Kaposin	Forward	GGATAGAGGCTTAACGGTGTTT	P5609
	Reverse	CAGACAAACGAGTGGTGGTATC	P5610
k-bZIP	Forward	GGTCTGTGAAACGGTCATTGA	P5601
	Reverse	TCTATGTAGTCGCCTCTTGGA	P5602
LANA	Forward	TTGGATCTCGTCTTCCATCC	P5442
	Reverse	ACCAGACGATGACCCACAAC	P5443
MEK	Forward	GGGAGCTCTCTGAGGATGG	P5428
	Reverse	CGGAGGATCGACCTCAAC	P5429
MMP2	Forward	TCTCCTGACATTGACCTTGGC	P5621
	Reverse	CAAGGTGCTGGCTGAGTAGATC	P5622
MMP10	Forward	GCATCTTGCATTCCTTGTGCT	P5623
	Reverse	TTTTGCTGCCCCACTCAGA	P5624
mTOR	Forward	TCCGGCTGCTGTAGCTTATTA	P5424
	Reverse	CGAGCATATGCCAAAGCACT	P5425
Notch1	Forward	GAGGCGTGGCAGACTATGC	P5444
	Reverse	CTTGTACTCCGTCAGCGTGA	P5445
ORF33	Forward	CGACCTGACCAATTGCACTA	P5615
	Reverse	ATGTTAGATAGACCCGGCGA	P5616
ORF45	Forward	GCGGCTTAAGTTTGGTTGTC	P5613
	Reverse	ACATCGGACTCTGATAGCGA	P5614
ORF50	Forward	CACAAAAATGGCGCAAGATGA	P5603
	Reverse	TGGTAGAGTTGGGCCTTCAGTT	P5604
PAN	Forward	TGCATTGGATTCAATCTCCAGGCCA	P5599
	Reverse	GTAGTGCACCACTGTTCTGATACAC	P5600
PI3K	Forward	TGCTATGCCTGCTCTGTAGTGGT	P5420
	Reverse	GTGTGACATTGAGGGAGTCGTTG	P5421
PROX1	Forward	ATCCTAATTTATTTGATGAAGGTG	P5472
	Reverse	TGCACATACATTCAGTTTAAGAGG	P5473
RPS6KB1	Forward	TTCATATGGTCCAACTCCCC	P5438
	Reverse	AGGACATGGCAGGAGTGTTT	P5439
Tie-1	Forward	CACGACCATGACGGCGAAT	P5625
	Reverse	CGGCAGCCTGATATGCCTG	P5626

Tie-2	Forward	AGTAGDCATATTCACCATCAACCG	P5627
	Reverse	TGCCAAGCCTCATAGTGATTAACG	P5628
TLR2	Forward	CCACTGACAAGTTTCAGGCA	P5434
	Reverse	TCATTTGGCATCATTGGAAA	P5435
TLR4	Forward	AACTCTGGATGGGGTTTCCT	P5436
	Reverse	GTGAGACCAGAAAGCTGGGA	P5437
vCyclin	Forward	AGCTGCGCCACGAAGCAGTCA	P5607
	Reverse	CAGGTTCTCCCATCGACGA	P5608
VE-cadherin	Forward	TCCTCTGCATCCTCACTATCACA	P5619
	Reverse	GTAAGTGACCAACTGCTCGTGAAT	P5620
VEGFR1	Forward	TGGGACAGTAGAAAGGGCTT	P5466
	Reverse	GGTCCACTCCTTACACGACAA	P5467
VEGFR2	Forward	CATCACATCCACTGGTATTGG	P5468
	Reverse	GCCAAGCTTGTACCATGTGAG	P5469
VEGFR3	Forward	CCCACGCAGACATCAAGACG	P5470
	Reverse	TCGAGAACTCCACGATCACC	P5471
vFLIP	Forward	GCGGGCACAATGAGTTATTT	P5611
	Reverse	GGCGATAGTGTTGGGAGTGT	P5612
vIL-6	Forward	AAAACACGCACCGCTTGACCTG	P5605
	Reverse	TTCACTGCTGGTATCTGGAACG	P5606
vIRF2	Forward	CGGAATGGCTCACGGACTTTAT	P5617
	Reverse	AGACATCCTTCACATCCCTTGT	P5618

2.2 Methods

2.2.1 Cell culture

Human conditionally immortalized endothelial cells HuARLTs were described before[193]. rKSHV-HuARLT cells[194] were derived upon infection of HuARLTs with recombinant KSHV.219 carrying the constitutively expressed GFP and puromycin selection genes as well as RFP under control of a viral lytic promoter[196].

The cells were cultivated on plates coated with 0.5% gelatin in endothelial growth medium in a humidified normoxic atmosphere with 5% CO_2 in the presence of 2 µg/ml doxycycline. Maintenance cultures of rKSHV-HuARLT cells additionally contained 5 µg/ml puromycin, while all the experiments were performed in the absence of the selection drug.

When needed, the cells were counted using Guava ViaCount staining solution according to the manufacturers protocol. In brief, the cells were diluted 1:10 in the staining solution, incubated for 5 minutes at rom temperature prior to evaluation of cell viability and cell counting on Guava analyzer.

2.2.2 Cell viability and determination of drug concentrations

To assess cell viability upon treatment with standard drugs, rKSHV-HuARLT cells and HuARLT cells were seeded in 96-well plates (5000 cells/well) and incubated with the compounds in the indicated concentrations. The maximal concentration of solvent did not exceed 0.5% of the total volume. Cell viability was measured using the WST-based Cell Counting Kit 8 according to the manufacturer's instructions. In brief, cells were incubated with 100 µl of fresh media and 10 µl of the WST-8 solution at 37° C for 2-4 hours followed by absorbance measurement at 450 nm using TriStar² LB 942 Modular Multimode Microplate Reader. To calculate cell viability, the background values were subtracted and the data was normalized to DMSO-treated control values.

2.2.3 Natural compound library and selection of the drug concentration

The natural compounds used in this study have been compiled at the Helmholtz Center for Infection Research and the Helmholtz Institute for Pharmaceutical Research Saarland in a ready-to-screen library that is available for screenings to evaluate their utility in various biological assays. The chemical synthesis of pretubulysin D was described before[197]. For assays on endothelial cells only derivatives from active compound classes were selected that are feasible for *in vivo* studies due to availability and overall better characterization in terms of biological effects in other *in vitro* and *in vivo* experiments.

To determine the appropriate concentration for the drugs, at least 4 concentrations per compound with 3 replicates were tested for cell viability. The drug concentration that resulted in at least 80% viability is summarized in Table 2.7 and was used for further experiments.

Table 2. 8 Final concentration of the novel compounds used in the study.

Compound	Concentration
Glycyrrhinic acid (GA)	25 µM
Phosphonoformic acid (PhA)	100 µM
Carolacton	20 nM
Chondramid B	25 nM
Chondramid C	25 nM
Disorazol A5	10 nM
Eliamid	50 nM
Epothilon B	1 nM
Epothilon E	20 nM
Hyaboron	50 nM
Icumazol B2	20 nM
Myxalamid PI	1 µM

Myxochelin A	20 nM
Myxothiazol A	1 µM
Pellasoren A	1 nM
Phenoxan	500 nM
Pretubulysin D	1 nM
Saframycin Mx 1	20 nM
Soraphen A	500 nM
Soraphen B	500 nM
Stigmatellin A	2,5 µM
Stigmatellin F	20 nM
Stigmatellin G	20 nM
Thiangazol A	500 nM
Trichangion	4 µM
Tubulysin A	25 nM
Tubulysin G	1 nM
Tubulysin X	25 nM
Tubulysin Y	10 nM

2.2.4 Spheroid production

4000 rKSHV-HuARLT cells per well were seeded on a 0.5% agarose-coated 96-well plate and cultivated at 37° C in a humidified normoxic atmosphere with 5% CO_2. After 24- or 48 hours, the formed aggregates (spheroids) were harvested and embedded either in a fibrin gel (for spheroid sprouting assays) or in a Matrigel matrix (for copy number analysis).

2.2.5 Viral copy number analysis

2D cultures: rKSHV-HuARLT cells were seeded on a 12-well plate (1×10^5 cell/well) and treated with the test compounds in absence of doxycycline and puromycin for 14 days.

3D cultures: for every well 6 to 8 spheroids were mixed with 0.7 mg/ml fibrin, 0.4% methylcellulose and 0.5 U/ml thrombin in EGM medium. Growth-factor reduced Matrigel was added to the spheroid mixture in a ratio of 1:1. 100 µl of the gels were cast onto a 96-well plate and allowed to solidify for 30 min at 37° C. 100 µl of EGM supplemented with selected compounds was added on top of the gels.

After 14 days of treatment, DNA was isolated from cells cultured under 2D or 3D culture according to a protocol described before[198]. Briefly, the cells were lysed using modified Bradley's buffer with Proteinase K at 55° C overnight. Cellular DNA was precipitated in 75 mM sodium acetate in 96% ethanol solution. The pellet was washed with 70% ethanol, dried and suspended in nuclease-free water. qPCR was performed at 58° C annealing temperature using SsoFast™ EvaGreen® Supermix in a LightCycler 480 II. The data were analyzed using Light Cycler 480 software 1.5. Viral DNA was detected using LANA specific primers and normalized to cellular DNA detected by the ACTB

specific primer pair. The number of viral copies per cell was extrapolated using a modified ΔCp method, taking into account that the cellular genome harbors 2 copies of the ACTB gene:

$$Viral\ copy\ number/cell = 2 * 2^{Cp_{LANA} - Cp_{ACTB}}$$

2.2.6 Spheroid sprouting assay

Spheroids from rKSHV-HuARLT cells were embedded in fibrin gels according to a protocol described in[86]. 6-8 spheroids were mixed with in fibrin solution (3 mg/ml) supplemented with 2 U/ml thrombin and 0.25% methyl cellulose in Hanks' Balanced Salt Solution. The mixtures were cast onto a 96-well plate and allowed to solidify for 30 minutes at 37° C. The respective compounds were added in EGM media using the concentrations listed in Table 1 and incubated for 5 days. Quantification of spheroid sprouting was performed from fluorescence microscopy images using ImageJ software[171]. To this end, the area covered by sprouts at the representative focus plane was measured and normalized against the spheroid's core area (sprouting index).

$$Sprouting\ index = \frac{Total\ area - core\ area}{Core\ area}$$

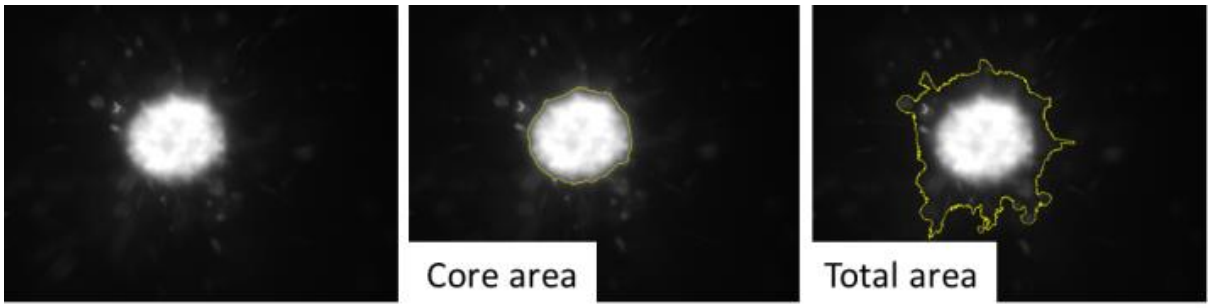

Figure 2. 1 Quantification of *in vitro* sprouting (representative pictures).
The total area and the core area was measured using ImageJ software and the sprouting index was calculated as indicated for one representative section per spheroid.

2.2.7 Relative gene expression (RT-qPCR)

Total RNA was isolated from 5×10^5 rKSHV-HuARLT cells using RNAeasy mini kit according to the manufacturer's instructions and measured with the ND-1000 spectrophotometer. cDNA was synthetized from 500 ng of RNA using Reverse-Aid First Strand cDNA Synthesis Kit according to the manufacturer's instructions. Quantitative PCR was performed as described above using the primers specified above. Relative expression of genes in relation to cellular ACTB or C1ORF43 was calculated using the standard ΔCp method.

2.2.8 Flow cytometry

In order to analyze GFP expression, rKSHV-HuARLT or HuARLT cells were washed and detached with trypsin/EDTA and resuspended in PBS supplemented with 2% FCS. Flow cytometric analysis was performed on a FACSCalibur™ analyzer. Non-infected cells were used as a negative control. The data were processed with FlowJo v10 software.

For analysis of surface markers of endothelial cells, the cells were harvested ad described above followed by fixation in 4% formaldehyde for 20 minutes. For intracellular staining (Vimentin) the cells were permeabilized by 0,2% of triton X-100. The cells were incubated with primary antibodies for 30 minutes at 4° C followed by washing with PBS and incubation with secondary antibodies for 30 minutes at 4° C at the dilutions indicated above. The samples were analyzed with BD™ LSRII analyzer. The cells treated with secondary antibodies only were used as a control.

2.2.9 Uptake of acetylated low-density lipoproteins

For the uptake of acetylated low-density lipoproteins (AcLDL) the cells were cultivated for 4 hours with 10 mg/ml AlexaFluor™ 488 labeled AcLDL at 37° C. Following the incubation the cells were trypsinized, resuspended in FACS buffer and analyzed by flow cytometry.

2.2.10 Detection of senescence-associated beta-galactosidase activity

Fluorescence based assay to detect senescence-associated beta-galactosidase activity were performed according to previously published protocol[199]. In brief, the cells were pretreated with 100 nM bafilomycin A1 for 1 hour followed by addition of C_{12}FDG to the final concentration of 33 µM. After 2 hours of incubation the cells were trypsinized and suspended in ice-cold FACS buffer followed by FACS analysis.

2.2.11 Matrigel tube formation assay

Matrigel tube formation assay was performed according to previously published protocols[200,201]. Briefly, 24-well plates were coated with Matrigel for 30 min at 37° C. $1.2x10^5$ cells were seeded per well and cultivated for 16 h in EGM medium in presence or absence of doxycycline. The formation of tube-like structure was evaluated by microscopic analysis using Angiogenesis Analyser plug-in for ImageJ[202].

2.2.12 Gene expression profiling by gene arrays

In this study, the 'Whole Human Genome OligoMicroarray' (AMADID 014850, Agilent Technologies) was used containing 45015 oligonucleotide probes covering the entire human transcriptome. Total RNA utilized for microarray experiments was prepared with the RNeasy Mini Kit. The microarray experimentswere realized as biological duplicates. Quality and integrity of the total RNA was controlled on an AgilentTechnologies 2100 Bioanalyzer. 50 ng of total RNA were applied for Cy3-labeling reaction using the one color Quick Amp Labeling protocol (Agilent Technologies). Labeled cRNA was hybridized to Agilent's human 4 9 44k V1 microarrays for 16 h at 68° C and scanned using the Agilent DNA Microarray Scanner G2505C US84903606. Expression valueswere calculated by the software package Feature Extraction 10.5.1.1 (Agilent Technologies). Statistical analysis of the expression datawas performed using theGene SpringGX Software V.12 (Agilent Technologies). Entities that showed technical impairments were excluded from final analysis.

The raw data were imported into R, log2-transformed according to the recommended default procedure and interarray quantile normalized. The genes were considered to be differentially regulated if expression change is higher than 2 fold and adjusted p-value is less than 0.01 as determined by ANOVA test. Canonical pathways enriched in Gene Ontology analysis by differentially expressed genes was visualized by ClusterProfiler[203] tool. Network visualization of selected enriched biological processes was achieved by EnrichMap[204] tool, using Kamada-Kawai layout.

2.2.13 Gene expression profiling by RNA-Seq

Quality and integrity of total RNA was controlled on Agilent Technologies 2100 Bioanalyzer. The RNA sequencing library was generated from 500ng total RNA using Dynabeads® mRNA DIRECT™ Micro Purification Kit for mRNA purification followed by ScriptSeq v2 RNA-Seq Library Preparation Kit according to manufacture´s protocols. The libraries were sequenced on Illumina HiSeq2500 using TruSeq SBS Kit v3-HS (50 cycles, single ended run) with an average of 3 x107 reads per RNA sample. Each FASTQ file gets a quality report generated by FASTQC tool[205]. Before alignment to reference genome each sequence in the raw FASTQ files were trimmed on base call quality and sequencing adapter contamination using Trim Galore![206] wrapper tool. Reads shorter than 20 bp were removed from FASTQ file. Trimmed reads were aligned to the reference genome using open source short read aligner STAR[207] with settings according to log file. Feature counts[208] were determined using R package Rsubread. Only genes showing counts greater 5 at least two times across all samples were considered for further analysis (data cleansing). Gene annotation was done by R package bioMaRt[209]. Before starting the statistical analysis steps, expression data was log2 transform

and normalized according to 50th percentile (quartile normalization using edgeR[210]). Differential gene expression was calculated by R package edgeR. Functional analysis was performed by R package clusterProfiler[203].

2.2.14 B cell based high throughput screening of natural compound library against KSHV lytic replication

The screening of the natural compounds library was done by T. Schultz and G.Beauclair. In brief, Brk.219, a BJAB cell line stably infected with rKSHV.219[211,212] was used to screen a library of 260 natural compounds. Brk.219 cells were seeded into round bottom 96 well plates at a density of 10^5 cells per well in 100 µl RPMI medium. Compounds were added at a final concentration of 10 µM and the viral lytic cycle induced by the addition of an antibody to human IgM on the BJAB cell surface as described[211.] Forty-eight hours later the supernatant of individual wells was collected and used to infect HEK293 cells. After a further 48 hours the number of GFP positive HEK293 cells was quantified by a Biotek fluorescence reader. The viability of the treated Brk.219 cells was determined by MTT assay.

2.2.15 Immunofluorescence microscopy

rKSHV-HuARLT cells were plated on 0.5% gelatin-coated cover glass slips and fixed for 20 min with 4% formaldehyde in PBS followed by permeabilization with 0.5% Triton X-100 in PBS for 10 min. Blocking of the samples was done in PBS supplemented with 2% BSA for 1h. The coverslips were stained with primary antibodies in PBS with 0.1% saponin Quillaja sp. at 4°C overnight, diluted as inducated above. Staining with secondary antibodies was performed in in PBS with 0.1% saponin at RT for 1h. Coverslips were mounted on glass slides with Fluoroshield™ containing DAPI and incubated at room temperature overnight. Images were acquired using a Zeiss LSM META confocal laser scanning microscope. Brightness and contrast were adjusted using ImageJ software.

2.2.16 Mouse experiments

rKSHV-HuARLT cells were transplanted to mice as described before[194]. In brief, 1.2×10^6 cells were seeded into each well of AggreWell™400, centrifuged for 3 minutes at 100 g and cultivated for 3 days at 37° C. 400 spheroids were used for each matrigel implant containing 0.2% methyl cellulose, 3 mg/ml fibrinogen in EGM media supplemented with 10 µg/ml FGF, 0.5 µg/ml VEGF, 1 U/l thrombin and 300 µl of Matrigel HC, growth factor reduced. The mixture was injected subcutaneously to $Rag2^{-/-}\gamma c^{-/-}$ mice.

For singe cell analysis, the plugs were isolated 4 weeks after transplantation, cut into smaller pieces, and digested with Collagenase H (1 mg/ml) in PBS at 37° C for 1 hour. Digested cell suspension was filtrated via cell strainer to eliminate cell clumps. The flow-through was centrifuged down, the cells were resuspended in FACS buffer and analyzes by FACS as described above.

Starting from day 1 after implantation, the mice were treated with the drugs according to the route, dose and regime adapted from previous studies. Animal experiments were performed in accordance to the local animal law.

Table 2. 9 Dosage, administration route and regime of in vivo application of selected compounds

Compound	Route	Dose, [mg/kg]	Frequency	Solvent	Volume, [µL]	Reference
Chondramide B	i.v.	0,5	Once a week	PBS+5% DMSO	100	[213]
Pretubulysin D	i.v.	1	Once a week	PBS+5% DMSO	100	[214,215]
Epothilon B	i.v.	2,5	Once a week	PBS+5% DMSO	100	[216,217]
Soraphen A	oral	50	3x/week	Water	100	[218]
FK506	i.p.	2	3x/week	PBS+5% EtOH	100	[219]
Rapamycin	i.p.	1	3x/week	PBS+5% EtOH	100	[219]
Phosphonoformic acid	i.p.	200	3x/week	PBS	100	[220]

2.2.17 Immunohistological stainings

After 4 weeks of treatment, Matrigel implants were extracted and fixed with 4% formalin, embedded in paraffine, sectioned and stained with hematoxylin-eosin or with immunohistochemistry staining. The antibodies and their dilutions are listed above. Diameters of the lesions were measured on histological sections, stained for human vimentin. Human endothelial cells were marked applying *in situ* hybridization technique (ALU). The ALU probe was purchased from Ventana/Roche Diagnostics GmbH applying Ventana ISH detection kit.

3. Results

3.1. Evaluation of conditionally immortalized HuARLT cells as a system to investigate KSHV infection

The investigation of KSHV pathogenesis and the identification of potential antiviral compounds are compromised by the lack of scalable and robust *in vitro* cell culture models that reflect the virus-induced changes observed in patients. Recently, conditionally immortalized human endothelial cells (HuARLT) were developed, which preserve the properties of primary endothelial cells[193]. It has been shown that the cells express key markers of blood endoderm and maintain many endothelial functions, such as tube formation, barrier functions, eNOS activity and uptake of AcLDL[193,194]. Moreover, the cell line gives rise to functional blood vessels when transplanted into immunocompromised mice[194]. To evaluate this cell line as a model for KSHV infection, the capacity of the cell line to reflect the changes, observed upon KSHV infection of primary cells was investigated.

3.1.1. HuARLT cells are tightly growth controlled

HuARLT cells carry immortalizing genes and rtTa driven by bidirectional tet-promoter[193] (Fig. 3.1A). This construct allows the expression of immortalizing genes, and, as a result, cell proliferation only on presence of doxycycline. In order to confirm that the cells are tightly growth-controlled even after prolonged passaging, $1x10^4$ cells were seeded in 12-well plates and cell numbers were measured upon cultivation with or without doxycycline for 13 days. Cell samples were counted every 2-3 days. The result shows that the cell number increases in presence of doxycycline, whereas it remains constant when doxycycline is withdrawn, thus confirming doxycycline-dependent growth control (Fig. 3.1B). Cell proliferation slowed down after day 8 of the culture, likely due to contact inhibition of the cell growth, since the cells were maintained within the same cell culture dish for the whole experiment. Of note, non-proliferating cells show less than two fold increase in senescence-associated β-galactosidase staining, indicating marginal signs of senescence within the first 9 days. (Fig. 3.1E).

In order to evaluate the frequency of proliferating cells in the culture, expression of Ki-67, the cellular proliferation marker, was evaluated by immunofluorescence staining of the cells cultured in presence or absence of doxycycline for 3 days (Fig 3.1C and D). The percentage of Ki-67 positive cells was quantified as the number of Ki-67 positive cells related to the number of nuclei visualized by DAPI staining per field of view. As a result, 89,40±1,16% of Ki-67 positive cells were observed in doxycycline-treated samples, whereas only 0,96±0,06% of the cells were Ki-67 positive upon withdrawal of doxycycline. Taken together, the data confirm that the cells are tightly growth-controlled.

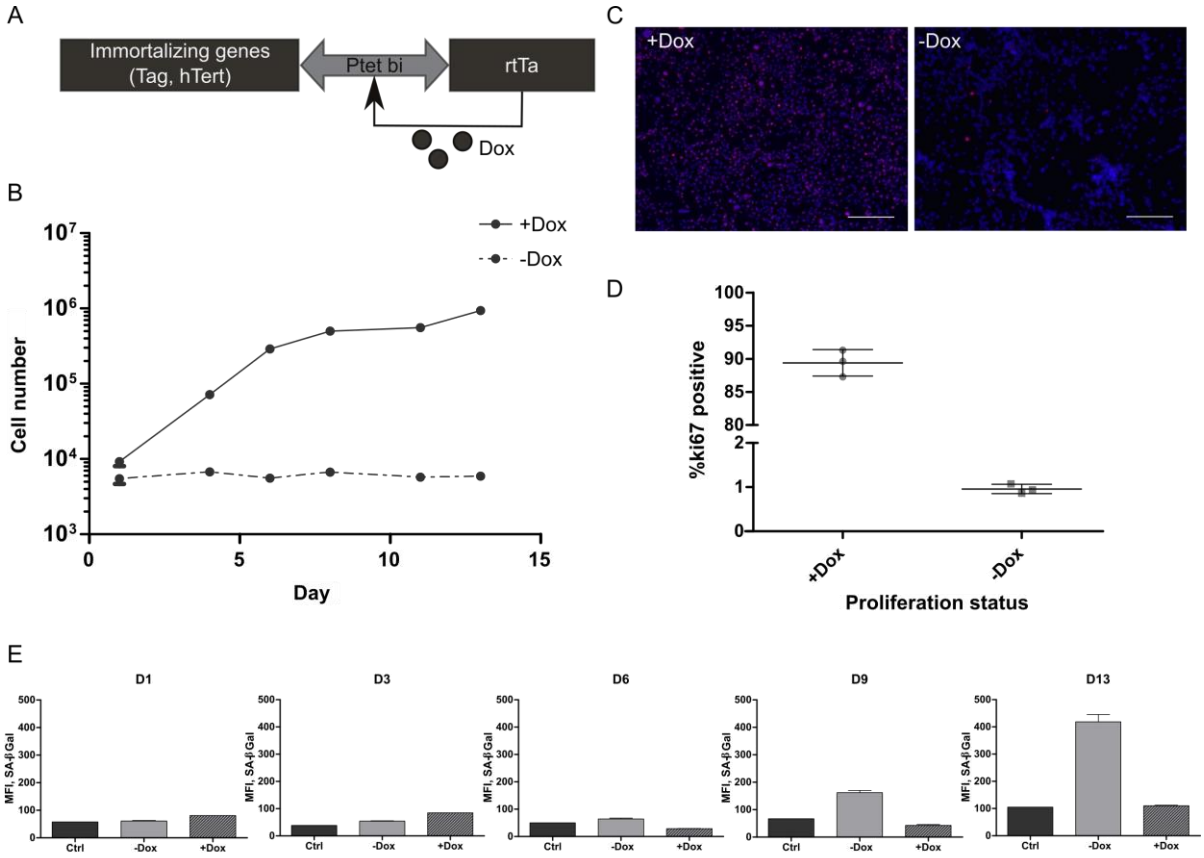

Figure 3. 1 HuARLT cells are tightly growth controlled.
A) a scheme of the immortalization cassette (adapted from[193]). Transactivator protein (rtTA) binds to the operator sequences within the tet promoter and initiates transcription of the immortalizing genes only in presence of doxycycline (Dox). Bidirectional tet promoter allows co-expression of rtTa and immortalizing genes. B) Cell numbers of HuARLT cells upon cultivation with and without doxycycline. 10^4 cells were cultured on gelatin-coated plates with or without doxycycline, respectively. Cell numbers were counted every 2-3 days, the mean of 4 replicates is shown per time point. C) Representative images of immunofluorescence staining for Ki-67. HuARLT cells were cultured in presence or absence of doxycycline for 3 days followed by fixation and the staining with an anti-Ki-67 antibody. The primary antibody was detected by Cy3 conjugated anti-IgG, scale bar 100 µm. D) Quantification of relative Ki-67/DAPI ratio shown in C, 3 biological replicates were analyzed with 3 fields if view per replicate. E) HuARLT cells were stained for senescence-associated β-galactosidase using a 5-dodecanoylaminofluorescein di-beta-D-galactopyranoside (C_{12}FDG), a fluorogenic substrate for β-galactosidase activity. .The expression level was quantified by flow cytometry at indicated days. Shown is the mean fluorescence intensity (MFI) of HuARLT cells cultured either in absence or in presence of doxycycline for 13 days. The data based on 3 replicates per condition at each time point.

3.1.2 Conditionally immortalized endothelial cells preserve properties of primary cells

It has been shown before that conditionally immortalized human endothelial cells preserve endothelial functions, as measured by AcLDL uptake, and express of endothelial specific markers CD31, CD105, CD102 to similar levels as primary endothelial cells[193]. In order to confirm that the cells kept these properties upon prolonged cultivation, total RNA was isolated from primary HUVEC cells and HuARLT cells on passage 60 and the expression levels of several endothelial-specific markers were measured by RT-qPCR. The result showed that the expression levels of *VEGFR1*, *Tie-1*, *CD31* and *VE-Cadherin* were moderately reduced in HuARLT cells compared to the levels in primary cells. Expression of *VEGFR2* and *Tie-2* could be detected in conditionally immortalized cells, but it was markedly reduced in comparison with HUVECs. Interestingly, the expression levels on *VEGFR2*,

CD31 and *VE-Cadherin* was significantly lower in proliferating HuARLT cells, compared to non-proliferating cells (Fig. 3.2.A) indicating that non-proliferating HuARLT cells closer resemble primary endothelial cells.

Transcriptome analysis confirmed that non-proliferating HuARLT cells express more endothelial-specific genes than proliferating cells, indicating that proliferation status influences endothelial phenotype[194]. In order to verify that this observation reflects intrinsic properties of endothelial cells rather than a cell culture artifact, HUVEC cells were treated with 5-Fluoro-2'-deoxyuridine (FuDR), a small molecule inhibiting DNA synthesis and thereby reducing cell proliferation. After 7 days of cultivation, the total RNA was isolated and the expression levels of selected proliferation-sensitive genes (as identified by transcriptome analysis) was measured by RT-qPCR. HuARLT cells cultured either in absence or in presence of doxycycline for 7 days were used as a control. The analysis shows that reduction of cell proliferation increases expression of MMP2, MMP10 and VE-Cadherin expression in both primary HUVECs and conditionally immortalized HuARLT cells (Fig. 3.2 B and C).

The ability to uptake of acetylated low density lipoproteins is regarded as a specific feature of endothelial cell and macrophages. To see weather proliferation can affect this function, the uptake of fluorescently labeled AcLDL was measured by FACS-analysis of HUVECs treated with FuDR for 7 days and HuARLT cells cultured either in presence or in absence of doxycycline. The results show that both the primary and the immortalized cells reduce the uptake of AcLDL upon proliferation (Fig 3.2 D and E).

Taken together, the data confirmed that HuARLT cells maintained the endothelial properties upon prolonged cultivation and showed that the proliferation specific changes in the endothelial phenotype reflect the changes in primary cells.

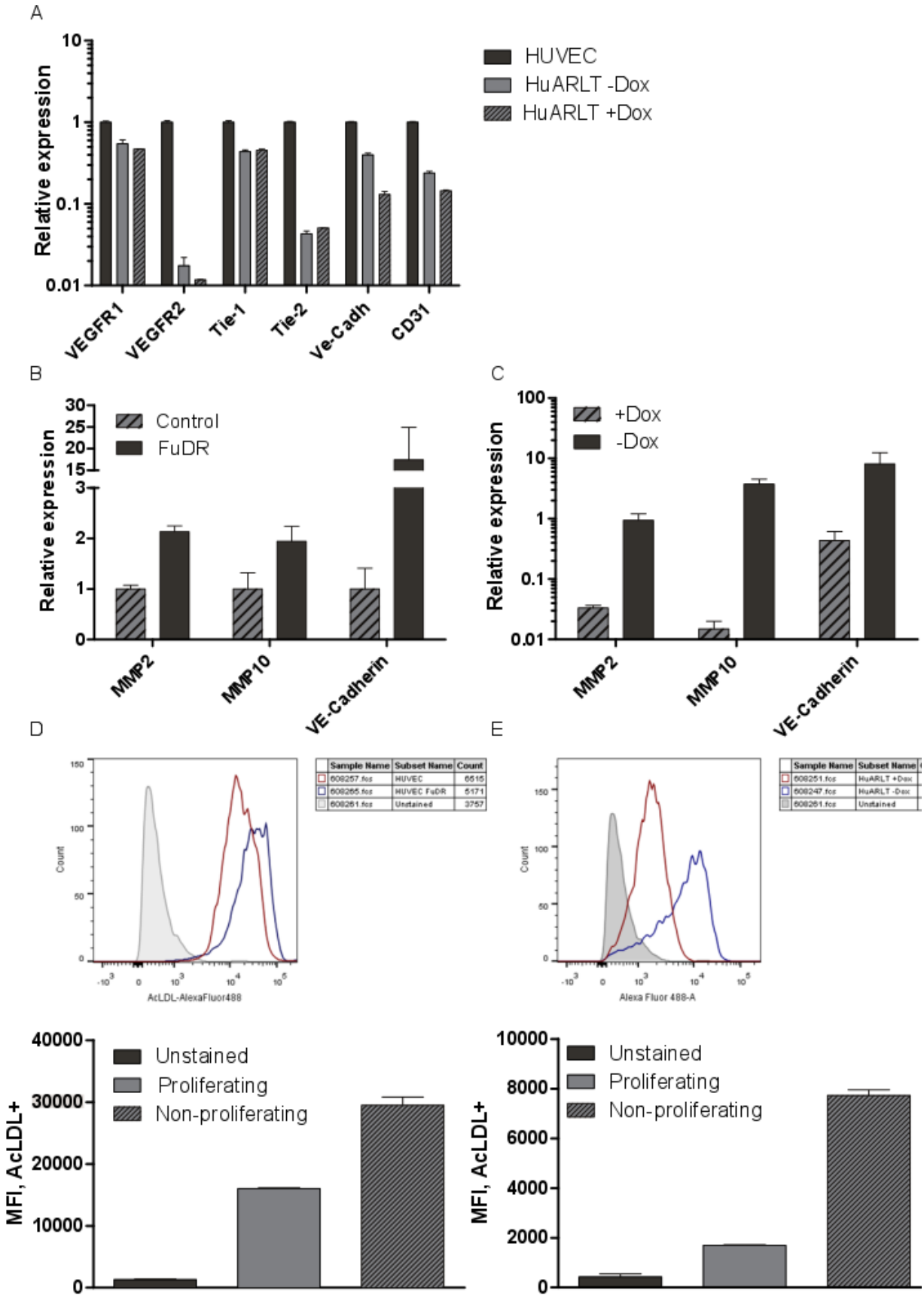
A
Relative expression
HUVEC
HuARLT -Dox
HuARLT +Dox
VEGFR1
VEGFR2
Tie-1
Tie-2
Ve-Cadh
CD31
B
Relative expression
Control
FuDR
MMP2
MMP10
VE-Cadherin
C
Relative expression
+Dox
-Dox
MMP2
MMP10
VE-Cadherin
D
Count
AcLDL-AlexaFluor488
Sample Name
Subset Name
Count
608257.fcs
HUVEC
6515
608265.fcs
HUVEC FuDR
5171
608261.fcs
Unstained
3757
E
Count
Alexa Fluor 488-A
Sample Name
Subset Name
608251.fcs
HuARLT +Dox
608247.fcs
HuARLT -Dox
608261.fcs
Unstained
MFI, AcLDL+
Unstained
Proliferating
Non-proliferating
MFI, AcLDL+
Unstained
Proliferating
Non-proliferating

Figure 3. 2 HuARLT cells maintain properties of primary endothelial cells.
A) Relative expression of endothelial specific genes analyzed by RT-qPCR of total mRNA isolated from primary HUVECs or HuARLT cells cultured in absence or presence of doxycycline for 3 days. B) Relative expression of proliferation-sensitive genes was measured by RT-qPCR on total mRNA of HUVEC cells cultured for 7 days either with or without 3µM FuDR. C) Relative expression of proliferation-sensitive genes was measured by RT-qPCR on total mRNA of HuARLT cells cultured in presence or absence of doxycycline. Expression levels in primary HUVECS are set to 1. D) and E) AcLDL uptake was measured in HUVECs or HuARLT cells by FACS analysis 7 days after treatment with FuDR or removal of doxycyline, respectively.

3.1.3 HuARLT cells are susceptible for KSHV infection

To validate HuARLT cells as a cell culture model for KSHV infection, the cells were infected with rKSHV.219[196] at MOI 10. The virus constitutively expresses the GFP and puromycin acetyl transferase genes, which allows for selection and monitoring of the infected cells. Infected cells show punctuated localization of the latency associated nuclear antigen LANA in the nuclei indicating the association of viral episomes with the cellular chromosomes (Fig. 3.3A). If cultivated under selection pressure, the rKSHV.219-infected HuARLT cells (rKSHV-HuARLT) are 100% GFP-positive (Fig 3.3B) and display the characteristic spindle-like morphology (Fig 3.3C), indicating that HuARLT cells are permissive for KSHV-infection.

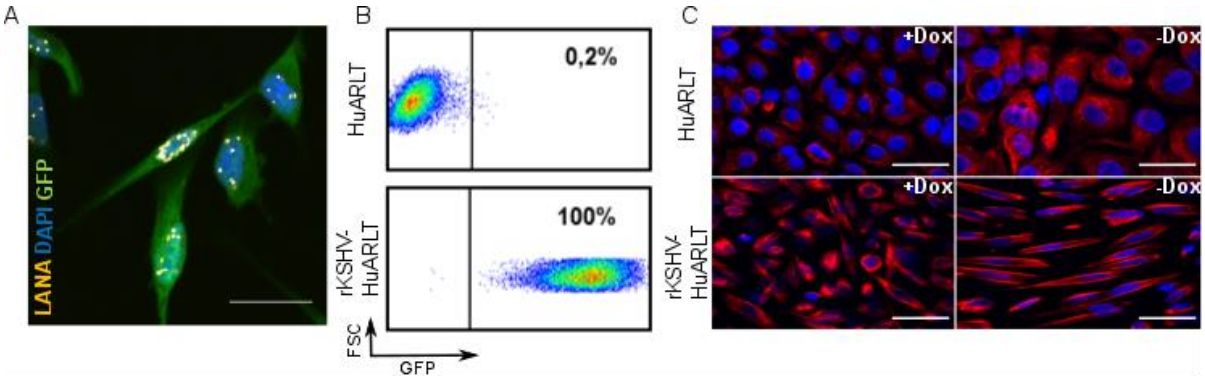

Figure 3. 3 HuARLT cells are susceptible to KSHV infection.
A) A representative confocal image of immunofluorescence staining for viral LANA. rKSHV-HuARLT cells were cultured in presence of doxycycline and puromycin followed by cell fixation and LANA staining. Nuclei were visualized by DAPI staining, GFP is encoded by the virus. Scale bar 25 µm. B) Expression of virus-derived GFP was measured by FACS analysis of HUARLT cultured in presence of doxycycline and rKSHV-HuARLT cultured in presence of doxycycline and puromycin. C) Representative confocal images of spindle cell formation upon KSHV infection. HuARLT or rKSHV-HuARLT were cultured in presence or absence of doxycycline, respectively, and stained with an anti-vimentin antibody and DAPI for better visualization. Scale bar 50 µm (Image by Ch. Lipps)

3.1.4 KSHV establishes latency in HuARLT cells

In order to characterize the stage of KSHV infection in rKSHV-HuARLT cells, the expression of RFP driven by the lytic *PAN* viral promoter was evaluated via fluorescence microscopy and FACS analysis. A significant fraction of RFP expressing cells could not be detected by any method, suggesting that the lytic phase is not detectable in standard cultivation conditions and the virus has established latency in the infected cells. It was tested, if lytic reactivation can be induced by 12-O-Tetradecanoylphorbol 13-acetate (TPA), sodium acetate, or decitabine. However, even in presence of

the agents, reactivation of rKSHV-HuaARLT cells could not be efficiently achieved (Fig 3.4A and B), which is in agreement with the studien in other adherent cell lines[159,160].

In order to confirm the predominant latent stage of the virus, the expression levels of typical latent and lytic viral genes relative to cellular ACTB was measured using RT-qPCR. The result showed elevated levels of latent mRNAs, such as *LANA, vCyclin, vFLIP* and *kaposin*, whereas mRNAs of

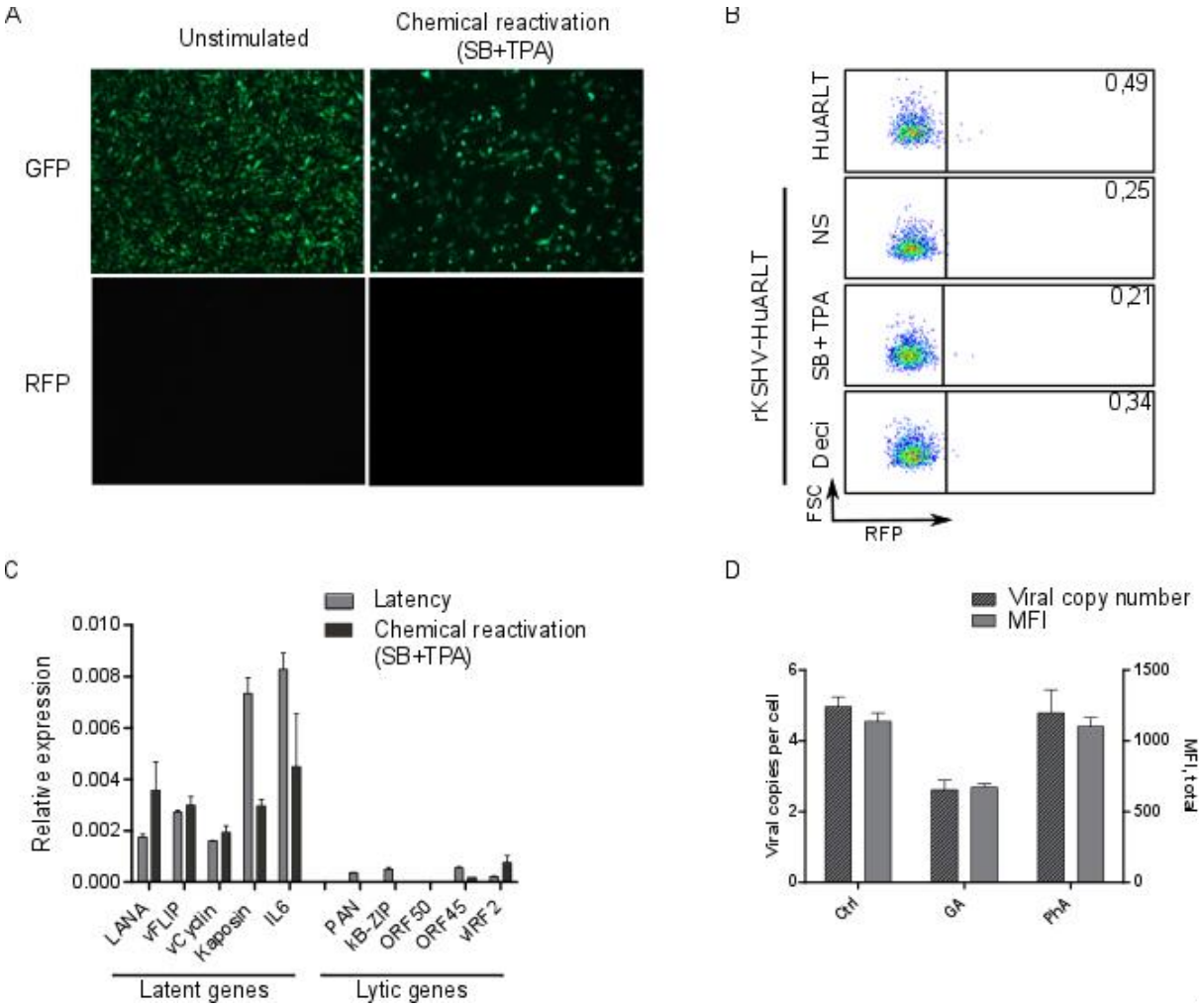

Figure 3. 4 KSHV establishes latency in HuARLT cells.
A) Representative pictures of fluorescence imaging of rKSHV-HuARLT cells cultured either in presence or absence of 20 ng/ml TPA and 1 mM sodium butyrate (SB), respectively, for 72h. Scale bar 50 µm B) FACS plots showing RFP expression of HuARLT and rKSHV-HuARLT cells cultured in presence or absence of 20 ng/ml TPA and 1 mM sodium butyrate (SB) or 100 nM decitabine (Deci), respectively, for 72h. C) Relative expression of latent and lytic viral transcripts was measured by RT-qPCR in latent or upon addition of 20 ng/ml TPA and 1 mM sodium butyrate, respectively, for 72h. D) Viral copy number and GFP expression level (MFI) of rKSHV-HuARLT cells treated for 14 days with either 25 µM GA or 100 µM PhA.

viral lytic genes, such as *PAN, kB-ZIP, ORF50, ORF45* were expressed at lower levels or could not be detected at all, confirming that the vast majority of infected cells had established latency (Fig. 3.4C). Similar to the absence of RFP expressing cells even in conditions of reactivation, expression of lytic viral transcripts could not be increased by addition of sodium butyrate and TPA, thus confirming lack of reactivation of the virus from infected cells in 2D cell culture.

To confirm that the viral genome is maintained episomally in the immortalized cells the cells were treated with glycyrrhizinic acid (GA). GA downregulates LANA, the protein responsible for tethering viral episomes to the cellular genome[221]. rKSHV-HuARLT cells were treated with GA for two weeks. Then, GFP expression was determined and the viral copy number per cell was assessed by qPCR. As depicted in Figure 3.3D, the GA treatment induced substantial viral loss as determined by both qPCR for viral copy number, as well as MFI of the treated cells. This confirms that the viral genome is in an episomal state rather than aberrantly integrated into the cellular genome in this cell line.

In contrast, treatment of the infected cells with phosphonoformic acid (PhA), an inhibitor of the lytically expressed viral DNA polymerase[136], did not have an effect on the viral copy number. These data support the conclusion that the cells are predominantly latently infected and lytic reactivation does not play a role in viral maintenance in 2D culture.

Taken together, the data shows that rKSHV.219 established a latent episomal state in HuARLT cells with no detectable levels of lytic reactivation.

3.1.5 KSHV infection changes the endothelial phenotype of HuARLT cells

Based on transcriptional profiling, it was previously shown that in virus infected cells 1839 genes were up-regulated by two-fold while 1693 genes were found to be down-regulated[194]. In order to evaluate to which extent these changes reflect Gene ontology pathway analysis showed that the differentially regulated genes are enriched in pathways connected with angiogenesis, cell migration and organ development (Fig. 3.5A and B).

It has been reported that the expression profile of the cells from Kaposi's sarcoma lesions closer resemble the profile of lymphatic endothelial cells (LECs) rather than blood endothelial cells (BECs)[69]. In particular, the cells from Kaposi's sarcoma lesions express VEGFR3[59], the marker of lymphatic and precursor endothelium as well as PROX1, a master regulator of lymphatic endothelium cell differentiation. Infection of BEC with KSHV leads their lymphatic reprogramming and induction of the main lymphatic endothelial genes expression[69,70]. Similarly, rKSHV-HuARLT cells upregulate VEGFR3 and PROX1 relative to cellular ACTB as measured by RT-qPCR. In contrast, expression of blood endothelial specific markers, such as VEGFR1, Tie1, Tie2 and VE-Cadherin is markedly reduced or not detectable at all in rKSHV-HuARLT infected cells (Fig. 3.5C). Immunofluorescence detection of CD31, ZO-1 and CD144, other blood endothelial-specific markers, showed

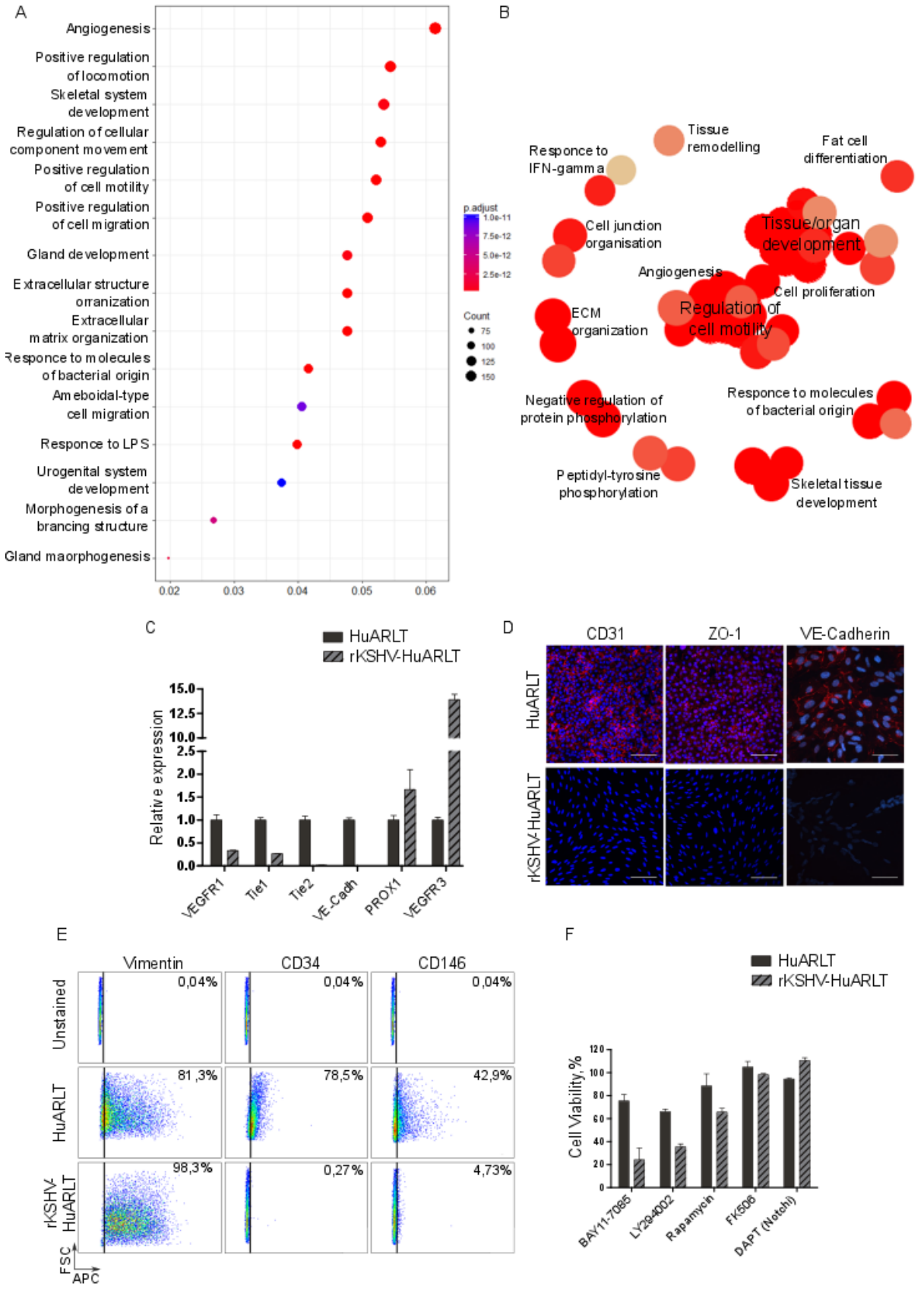

Figure 3. 5 KSHV infection changed phenotypic characteristics of HuARLT cells.
A) Top 20 canonical pathways enriched in Gene Ontology analysis by differentially expressed genes in the rKSHV-HuARLT and HuARLT cells. The set of differentially expressed genes was obtained by transcriptome analysis of the cells via Gene arrays and visualized by ClusterProfiler[203] tool. The genes were considered to be differentially regulated if

expression change is higher than 2 fold and adjusted p-value is less then 0.01 as determined by ANOVA test. B) Network visualization of selected enriched biological processes upon KSHV infection of HuARLT cells. The networks were assembled and visualized by EnrichMap[204] tool, using Kamada-Kawai layout. The node size represents the number of genes assigned to a biological process and overlap is proportional to the number of overlapping genes between two nodes. The higher color intensity reflects lover adjusted p-value. C) Relative expression of blood or lymphatic endothelial cell markers was measured by RT-qPCR. The expression level of HuARLT cells was set to 1. D) Representative images of immunofluorescence staining of HuARLT cells and rKSHV-HuARLT cells for hCD31, ZO-1 (scale bar 100 µm, image by Ch. Lipps) and hCD144 (VE-Cadherin, scale bar 50 µm). Primary antibodies were detected by cy3-labeled secondary anti-IgG antibodies. E) Expression of Vimentin, hCD34 and hCD146 was measured by FACS analysis of antibody stained samples. Primary antibodies were detected via APC-labeled secondary anti-IgG antibodies. F) The percentage of viable HuARLT and rKSHV-HuARLT cells was measured by WST assay after 3 days of treatment with 1.25 mg/ml rapamycin, 1.25 mg/ml FK506, 10 µM BAY11-7085, 12.5 µM LY294002 or 100 µM DAPT respectively.

homogeneous expression of the markers in HuARLT cells, whereas rKSHV-HuARLT cells did not exhibit detectable levels of hCD31, ZO-1 or CD144 (Fig. 3.5D). Similarly, FACS analysis revealed that CD34 and CD146 expression was abolished in KSHV-infected cells. Interestingly, Vimentin, a mesenchymal marker, which is found in histological sections of oral Kaposi's sarcoma[63], was expressed in both KSHV-infected and non-infected HuARLTs (Fig. 3.5E). Taken together, the data confirm that similar to primary BEC and the cells isolated from KS lesions, HuARLT cells undergo lymphatic transcriptional reprogramming.

3.1.6 Survival of KSHV-infected cells is dependent on the PI3K-mTOR pathway

The crucial role of various cellular signaling pathways for the survival of virus-infected cells was previously highlighted[141]. To confirm the relevance of these pathways in infected HuARLT cells, the viability of infected cells were tested upon inhibition of the respective pathways. Differential cell viability was observed upon treatment of the infected and non-infected cells with rapamycin, BAY11-7085 and LY294002, which block mTOR, PI3K and NFkB pathways, respectively. FK506, which is structurally related to rapamycin and shares a number of molecular targets with it, except for mTOR, was used as a negative control in this assay. DAPT, a small molecule inhibitor of γ-secretase and Notch, exhibited no difference on viability of infected and non-infected cells (Fig. 3.5D). In agreement with previous studies in primary cells[141] these data indicate that mTOR, PI3K and NFkB, rather than Notch pathway are important for survival of KSHV-infected HuARLT cells.

3.1.7 KSHV infection enhances tube formation of HuARLT cells in vitro

rKSHV.219 infection of HuARLT cells leads to numerous transcriptional and phenotypic changes that correspond to those observed in primary endothelial cells and cells in KS lesions. To investigate whether the phenotypic changes described above have an impact on endothelial function of KSHV-infected cells, we conducted Matrigel tube formation assay. The assay measures an ability of endothelial cells to form capillary-like structures, or tubes, and is employed to demonstrate the angiogenic activity of vascular endothelial cells *in vitro*[222–224].

To investigate the ability of KSHV-infected cells to form tubes, the cells were seeded on growth-factor reduced Matrigel™-coated plates to achieve subconfluence and incubated overnight either in

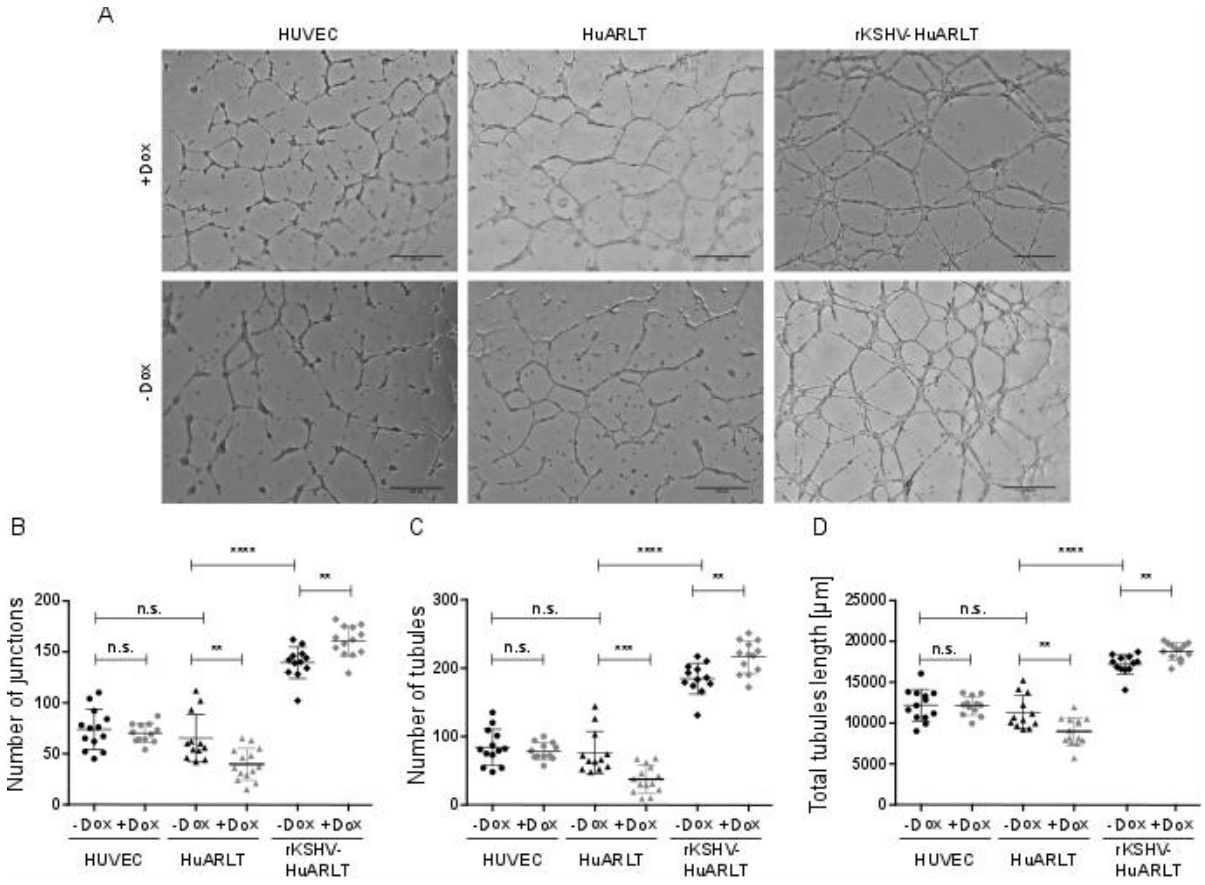

Figure 3. 6 Infection with rKSHV promotes tubules formation in Matrigel assay.
$1.2*10^5$ HUVEC, HuARLT or rKSHV-HuARLT cells were seeded onto Matrigel coated 24-well plates either in presence or absence of doxycycline. Tube formation was evaluated 16 hours later by bright field microscopy. A) Representative images, scale 500 µm. B, C, D) Quantification of the number of junctions, number of tubules and length of tubes from independent fields of view of a representative experiment, each dot represents an independent field of view. Statistical significance is shown by asterisks: *$p \leq 0.05$, **$p \leq 0.01$, ***$p \leq 0.001$, **** $p \leq 0.0001$.

presence or absence of doxycycline. As control, HUVEC cells were used under the same conditions. Tube formation was evaluated with phase contrast microscopy. Total tubules length as well as number of tubules and junctions was calculated with the use of angiogenesis analyzer plugin for ImageJ software[225]. The results showed that HuARLT cells cultured in absence of doxycycline are as efficient

in forming tubules as primary HUVECs. Interestingly, culture in presence of doxycycline significantly reduced the angiogenic potential of HuARLT cells in this assay.

Of note, KSHV infection induced a significant increase in tube length, number of tubes and junctions as compared to both uninfected HuARLT and primary HUVECs. This is in line with the studies showing that KSHV infection increases the ability of primary HUVEC cells to form tubes in matrigel assay even in serum-deprived conditions [141]. Thus, these results confirm that HuARLT cell undergo similar change in endothelial cell function as primary HUVEC cells do.

3.1.8. KSHV infection increases the invasiveness of the cells in 3D cell culture

To investigate the invasive properties of KSHV infected cells, rKSHV-HuARLT cells as well as non-infected HuARLT cells were embedded into fibrin gels, as was previously described[86] and the ability to form sprouts was observed by phase contrast microscopy for 7 days (Fig. 3.7A).

Both rKSHV-HuARLT and HuARLT cells form visible sprouts 3 days after embedding, however, the sprouting has different nature in these cells. Upon day 5-7 of cultivation, the sprouts formed by HuARLT cells transform into vessel-like structures growing out from the spheroid body. Of note, only proliferating HuARLT are capable of building these structures, whereas non-proliferating cells fail to do so. In contrast, spheroids formed from rKSHV-HuARLT cells continue invasive growth and sprouting without developing vessel-like structures in both presence and absence of doxycycline.

Together, the results indicate that transcriptional reprogramming of KSHV-infected HuARLT cells described in chapter 3.1.5 is accompanied with loss of vessel formation capacity and gain of an invasive phenotype.

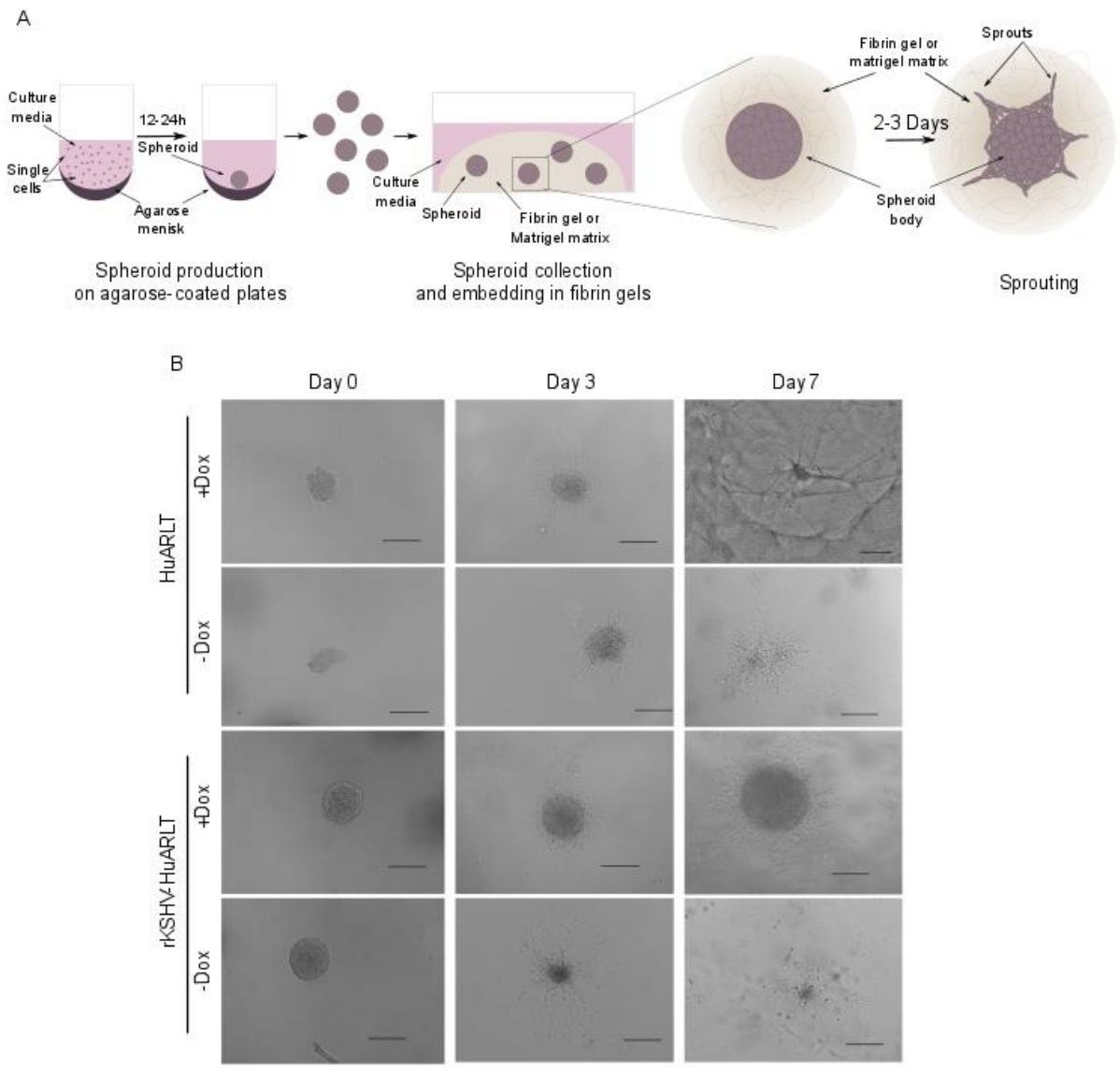

Figure 3. 7 KSHV induces the migration and invasiveness of the infected cells.
A) Schematic depiction of experimental procedure. B) Phase contrast microscopy of HuARLT and rKSHV-HuARLT spheroids embedded into fibrin gels was performed on day 0, day 3 and day 7. Scale bar 200 µm.

3.1.9 rKSHV-HuARLT induce lesions upon transplantation into mice

To investigate the tumorigenic potential of rKSHV-HuARLT cells, rKSHV-HuARLT as well as the control HuARLT cells were aggregated to spheroids and transplanted into immunocompromised Rag2$^{-/-}\gamma c^{-/-}$ mice according to a previously described protocol[194] (Fig. 3.8A). After 4 weeks, the plugs were isolated. Sections were stained for human vimentin and the morphology of transplanted cells was examined via microscopy (Fig.3.8B). As described before, HuARLT cells form functional blood vessels upon transplantation in presence of doxycycline, whereas rKSHV-HuARLT cells form KS-like lesions[194]. The lesions were positive for virus encoded GFP and LANA well as for human ALU sequences and hCD141, but not for mouse CD31, confirming that they are originated from transplanted KSHV-infected cells. (Fig. 3.8C).

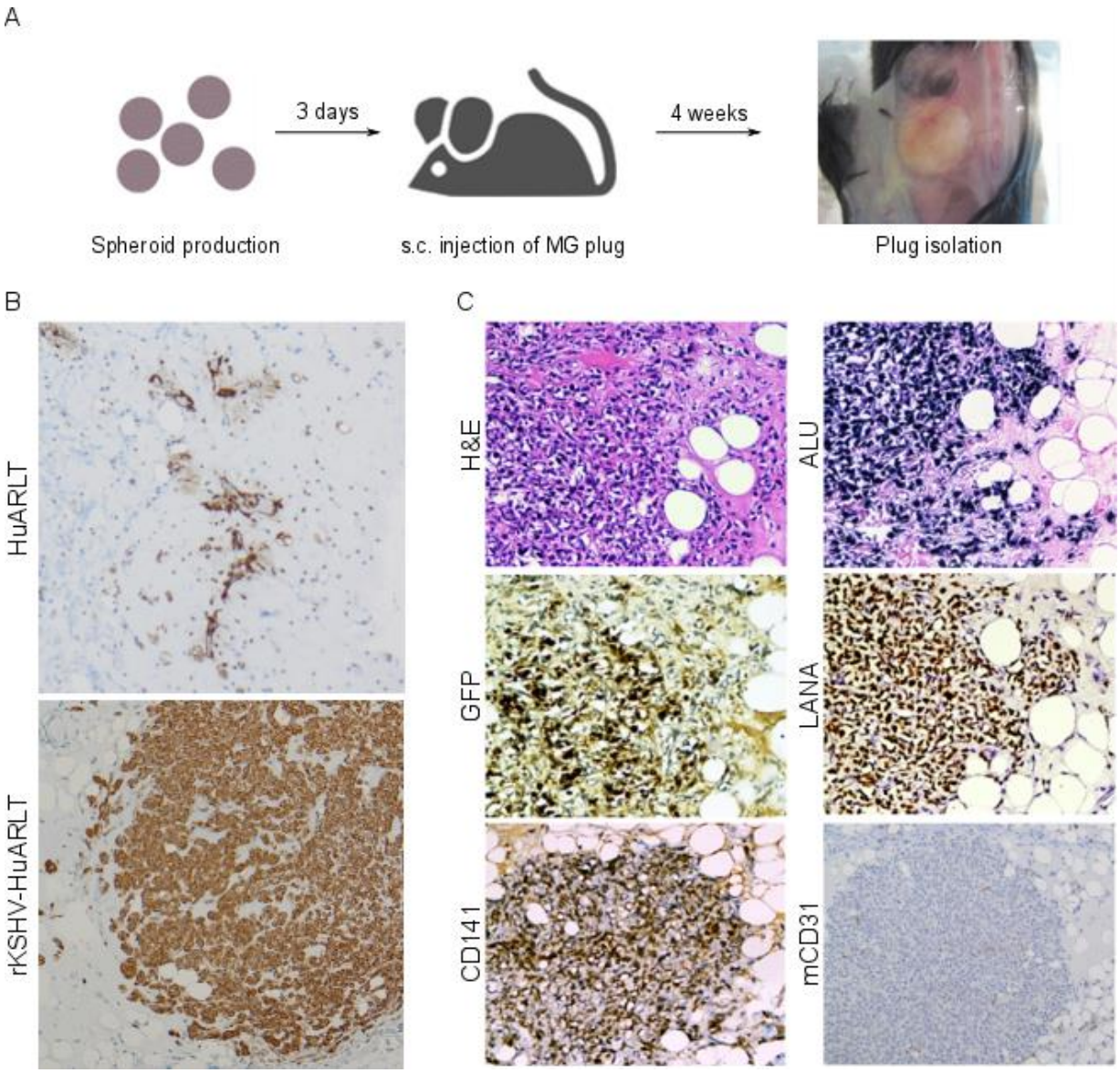

Figure 3. 8 Characterisation of rKSHV-HuARLT cells upon transplantation to Rag2$^{-/-}\gamma c^{-/-}$.
A) Experimental setup. B) Representative pictures of engrafted cells isolated 4 weeks after transplantation upon staining for human vimentin. Magnification 100x. C) Lesions obtained from transplanted rKSHV-HuARLT cells were stained for H&A as well as ALU-positive nuclei, GFP, LANA, CD141 (staining was performed by G. Büsche, magnification 250x) and mouse CD31 (magnification 50x). Representative immunohistochemistry sections are shown.

3.2. Molecular mechanism of maintenance of KSHV in latently infected endothelial cells

Unlike KSHV-infected B-cells, spindle cells isolated from KS lesions[153–155] as well as newly KSHV-infected HUVECs[156] fail to maintain viral episomes during cell culture using standard 2D conditions. It led to the hypothesis that viral loss in endothelial cell culture is a consequence of in vitro cell proliferation. If latent viral episomes are not replicated as efficiently as the host cell genome, rapidly proliferating endothelial cells will lose the viral genome. This indicates that not spindle cells, but rather slowly proliferating memory B-cells are the primary reservoir of KSHV in the patients[156]. However, this observation is in conflict with the clinical data showing that depending on the stage of the disease, up to 90% of spindle cells are infected with the virus[59]. This chapter will describe differential KSHV maintenance in latently infected HuARLT cells upon various culture conditions and the elucidation of underlying molecular mechanisms involved in viral maintenance.

3.2.1. Maintenance of KSHV upon cultivation without selection pressure

rKSHV.219 encodes the puromycin resistance gene, which allows selection of infected cells in culture, thereby achieving 100% KSHV-positive population, as accessed by FACS analysis of virus-encoded GFP. Upon culture rKSHV-HuARLT cells in presence of doxycycline and without puromycin for 2 weeks, a fraction of GFP-negative, LANA-negative cells appear in the culture, as was observed by LANA immunofluorescence staining and FACS analysis (Fig. 3.9A and B). Similarly, the number of viral genomes measured by qPCR is reduced from 9.19±1,88 to 4,61±0,61 viral copies per cell upon cultivation without selection pressure for 14 days (Fig. 3.9B). The viral copy number as well as the amount of GFP-positive cells decreased further upon prolonged cultivation without puromycin (Fig. 3.9B and C).

Taken together, the findings indicate that similar to primary cells and KS-isolated spindle cells, proliferating rKSHV-HuARLT fail to retain the virus upon prolonged cultivation without selection pressure.

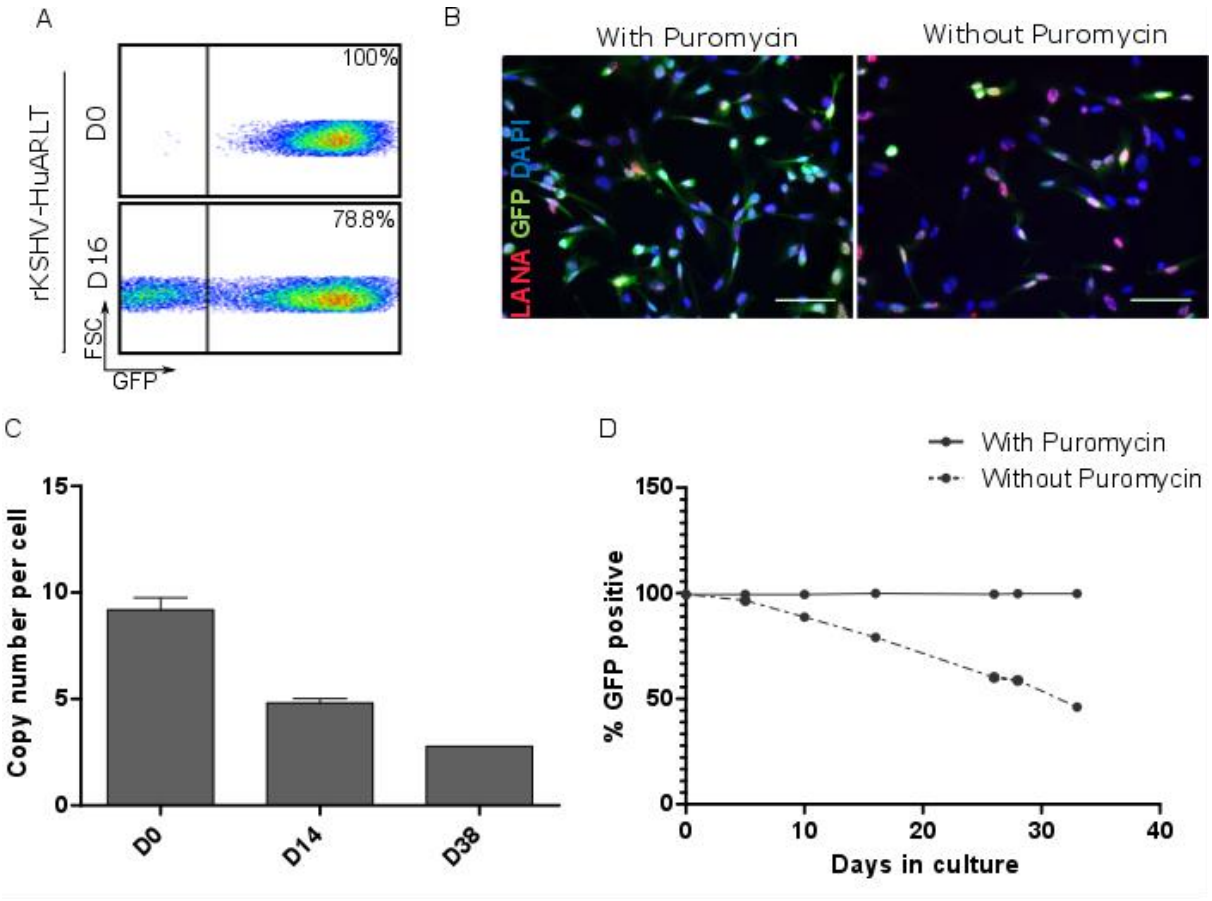

Figure 3. 9 Viral loss in proliferating rKSHV- HuARLT cells.
FACS analysis (A) and fluorescence imaging (B) of the rKSHV-HuARLT cells cultured in presence of doxycycline and in absence of puromycin for 14 days indicate appearance of GFP-negative cells upon cultivation without selection pressure. Scale bar 50 µm. C) Relative viral copy number of proliferating rKSHV-HuARLT cells was measured by qPCR on day 0, 14 and 38 upon cultivation without puromycin. D) Percentage of GFP positive cells was measured by FACS analysis of proliferating rKSHV-HuARLT cells cultured with and without puromycin for 33 days.

3.2.2. Viral loss in cell culture is not only the result of cell proliferation

Based on the observation that newly infected SLK and primary HUVECs fail to retain viral copies in vitro, it has been hypothesized that the loss of KSHV in endothelial cells is connected with cellular proliferation[156]. In particular, if viral episomes replicate less efficient than the cellular genome, every cell division will result in reduction of viral copies per cell. To test this hypothesis we investigated viral loss in rKSHV-HuARLT cells either in absence or in presence of doxycycline. First, the proliferation capacity of KSHV-infected cells was tested. To this end, the cells were cultured for 13 days either in presence or absence of doxycycline. Similarly to non-infected HuARLT, rKSHV-HuARLT cells exhibit robust cell growth in presence of doxycycline, whereas cell numbers in a culture without doxycycline remains constant (Fig. 3.10A), showing that infection with rKSHV does not interfere with doxycycline-dependent growth control.

After it was established that proliferation status of rKSHV-HuARLT cells depends on presence of doxycycline, the effect of proliferation on the viral copy number was investigated. The cells were cultured without selection pressure with or without doxycycline for 14 days followed by evaluation of viral copy number either by qPCR of viral DNA or by counting LANA dots per cells, as the latter has been shown to reflect viral copy numbers[181]. As a result, the population cultured in presence of selection pressure had 10.53±0.56 virus per cell as determined by qPCR and 10.55±4.47 as measured by immunofluorescence, indicating that both readouts give rise to consistent results. Strikingly, both proliferating and non-proliferating cells show a viral copy number reduction to 5.77±1.86 in presence of doxycycline and 5,43±1,07 in absence of doxycycline as measured by qPCR (Fig. 3.10B). The data shows that the proliferation status of the cells does not have an impact on KSHV maintenance, rejecting the hypothesis that viral maintenance in cell culture is simply a result of an imbalance between cellular and viral replication.

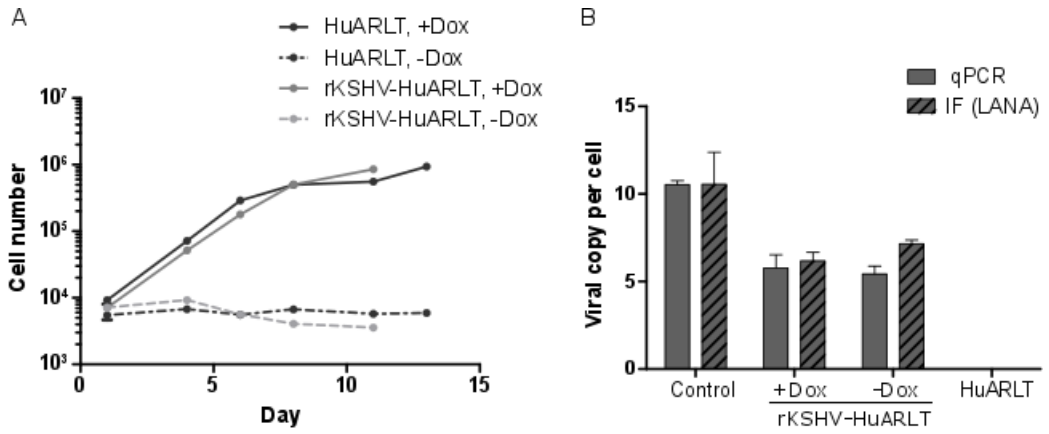

Figure 3. 10 KSHV loss in cell culture is not the result of cellular proliferation.
A) KSHV does not interfere with doxycycline-dependent growth control. 104 cells were seeded on gelatin-coated plates and cultured for 13 days with or without doxycycline, respectively. Cell numbers were counted every 2-3 days, 4 replicates were evaluated per each time point. B) rKSHV-HuARLT cells were cultured without selection pressure in presence or absence of doxycycline for 14 days followed by either immunofluorescence LANA staining or DNA isolation and measuring of viral load by qPCR. 3 replicates were analyzed per condition and independent fields of view per replicate were alalyzed to measure LANA dot count.

3.2.3 3D culture conditions rescue for viral maintenance

To investigate, whether viral maintenance depends on cell culture conditions, viral load per cell was measured in the cells cultured in standard 2D or advanced 3D cell culture for 14 days. For this assay the spheroids were embedded in Matrigel, rather than fibrin, as described before[86,194], because fibrin cultures are not stable enough to support long-term cultivation and were completely degraded on day 9-10 of cultivation. Matrigel-embedded spheroids were cultured in presence of doxycycline and in absence of puromycin selection pressure. As a result, the cells cultured in 2D cell culture had 9,61±0,92 copies per cell in presence of puromycin and 4,82±0,49 copies per cells in absence of puromycin, whereas cell cultured in 3D had 9.75±2.66 viral copy per cell with no significant difference from puromycin-treated cells (Fig. 3.11A).

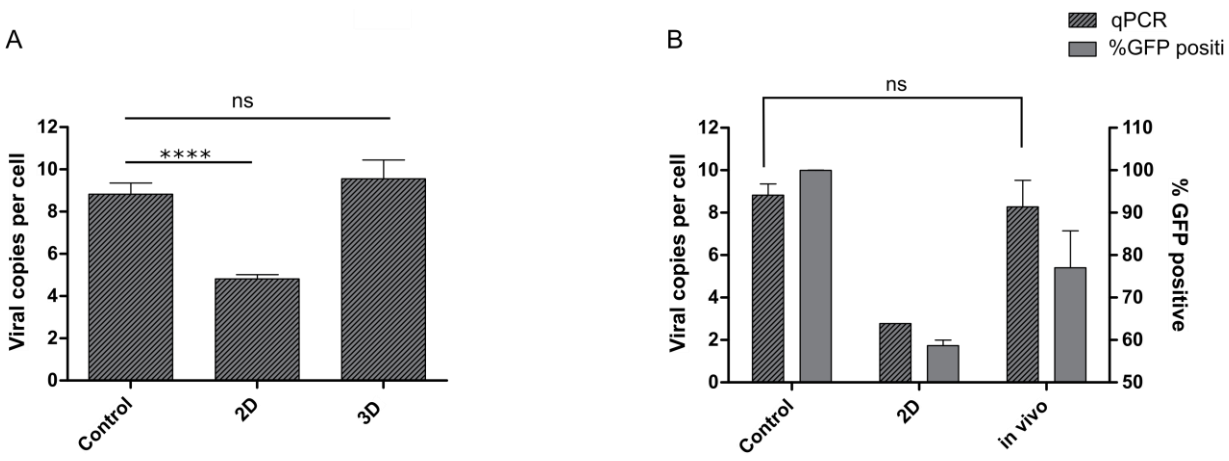

Figure 3. 11 Viral maintenance is supported by 3D cell culture conditions and is also observed upon transplantation in vivo. A) rKSHV-HuARLT cells were cultured either in standard 2D culture or 3D matrigel culture for 14 days in presence of doxycycline followed by FACS analysis and viral copy number measurement by qPCR. Control refers to the cells cultured in 2D conditions in presense of selection pressure. B) Viral copy number and presence of GFP positive cells were quantified in rKSHV-HuARLT cells isolated from mice 1 month after transplantation or cultured in standard 2D culture in presence of doxycycline. For in vivo tests doxycycline was added to the drinking water throughout the experiment.

In order to confirm that 3D cell conditions are supportive for viral maintenance in vivo, viral copy number change was investigated in humanized mouse model. To this end, rKSHV-HuARLT cells were transplanted as described before[194] and the plugs were isolated 1 month after transplantation. In order to discriminate human and mouse cells, the cells isolated from mice, the plugs were stained for human vimentin and isolated by FACS. Based on this cell fraction, the viral copy number per cell was measured. The analysis showed 12,23±3,97 copies for the engrafted human cells with no significant difference to the cells cultured in vitro in presence of puromycin. Similarly, also the amount of GFP-positive cells in the resulting population was significantly higher than in 2D culture, confirming the results observed by qPCR (Fig. 3.11B).

These observations are in agreement with previous studies indicating a higher LANA dots-per-cell count in 3D cultured endothelial cells[86] as well as improved KSHV maintenance in 3D cultured B cells[172]. Taken together, the data indicate that advanced 3D culture or *in vivo* conditions are required for viral maintenance.

3.2.4 Lytic reactivation in 3D cell culture conditions

To investigate whether mechanisms of viral maintenance differ between 2D and 3D cell culture, the cells were treated with of GA and PhA, targeting LANA and viral DNA polymerase respectively, in 3D cell culture conditions. To this end, the cells were cultured for 14 days in different cell culture conditions either in presence or in absence of inhibitors. Similarly to latently infected cells in 2D, 3D cultured cells were susceptible to GA, confirming that KSHV established episomal maintenance in 3D. However, viral copy number in 3D was reduced by PhA from 10.97±1.12 to 6.84±0.17 viral copies per cells, in contrast to standard 2D cell culture conditions (Fig. 3.4D). The data indicate

indicating that the mechanism of viral maintenance in 3D depends on viral DNA polymerase (Fig.

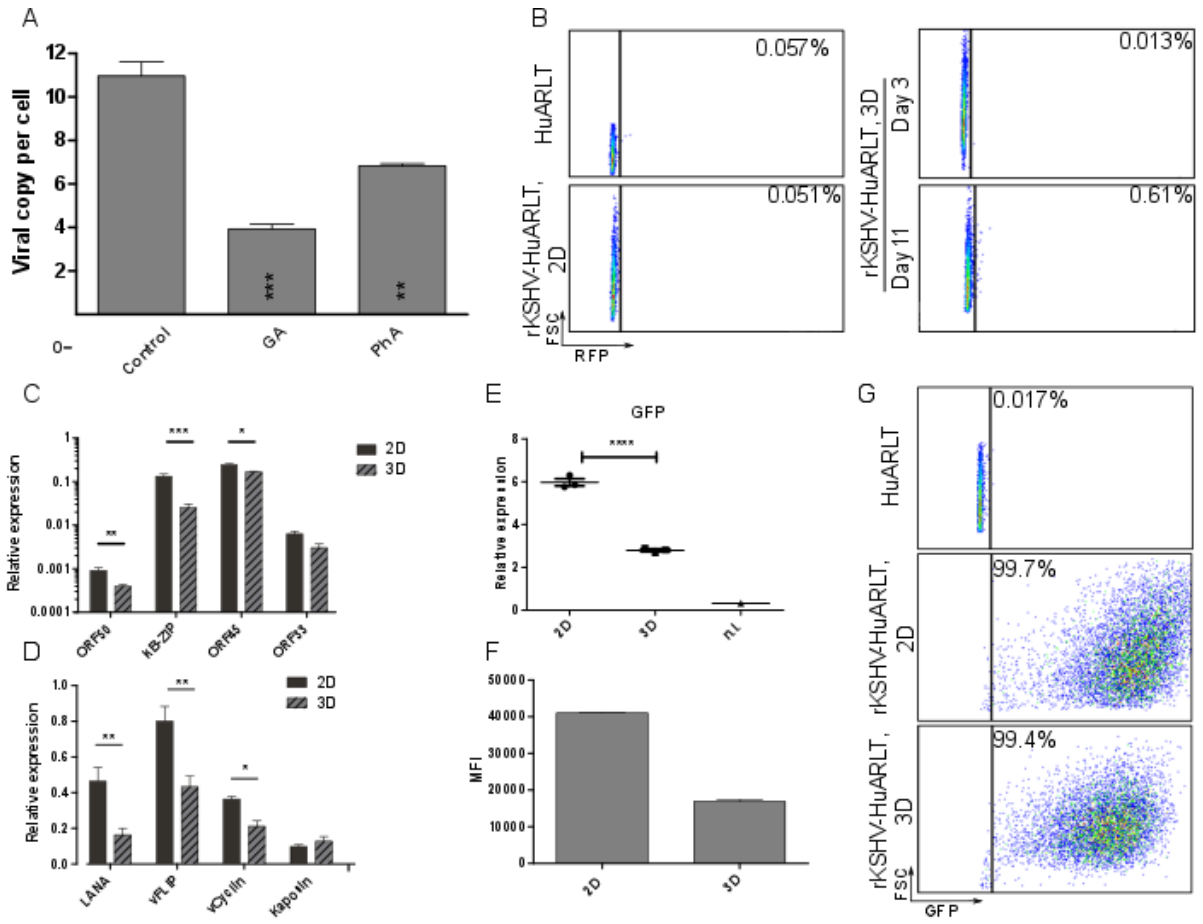

Figure 3. 12 KSHV reactivation in 3D cell culture conditions.
A) Viral copy number of rKSHV-HuARLT cells embedded in Matrigel 3D cell culture for 14 days and treated with 25 µM GA or 100 µM PhA; untreated rKSHV-HuARLT cells were used as a control. B) FACS analysis on RFP expression of rKSHV-HuARLT cells either cultured in 2D or in 3D cell culture conditions for the indicated days. C) Lytic, latent (D) and GFP (E) gene expression in rKSHV-HuARLT cells cultured in indicated cell culture conditions for 3 days was measured by RT-qPCR relative to the cellular housekeeping gene NICE3 (c1orf43); n.i.: non-infected HuARLT cells. G) Percentage of GFP-positive cells and MFI (F) in rKSHV-HuARLT cells cultured in different cell culture conditions for 3 days as analyzed by FACS.

3.12A) and differs from the one observed in 2D culture conditions.

rKSHV.219 encodes RFP, driven by viral immediate early PAN promoter, which allows monitoring of lytically reactivated cells in culture. To address the role of lytic reactivation, the amount of RFP cell was measured by FACS analysis after 3 and 14 days of 3D cultivation. Of note, no significant increase in RFP expression in any of these conditions (Fig. 3.12B). Thus, expression of viral lytic transcripts was measured in cell cultured in 3D for 3 days. No elevation in expression of tested lytic genes could be observed in either of the conditions. Rather, ORF50, k-bZIP, ORF45, ORF33 transcripts were even downregulated in 3D cell culture (Fig. 3.12C).

To investigate, whether downregulation of viral genes is restricted to lytic transcripts only, expression of viral latent (LANA, vFLIP, vCyclin) was measured by RT-qPCR. Unexpectedly, also the latent genes were expressed to a lower level (Fig. 3.12D). Similarly, expression of GFP, which is controlled

by cellular EF1a promoter, but encoded by the viral episome, was reduced, as observed by RT-qPCR (Fig. 3.12E). Although the amount of GFP-negative cells did not decrease upon 3 days of 3D culture (Fig 3.12F), a significant decrease of MFI could be observed by FACS-analysis (Fig. 3.12G), confirming lower levels of GFP expression in 3D cell culture.

3.2.5 Role of hypoxia in KSHV maintenance

According to their structure, 3D spheroid cultures develop gradients of various factors (e.g. nutrients, catabolites) and, particularly, oxygen (reviewed in[165]). The spheroids cultured in standard cell culture conditions without additional oxygen supply form a hypoxic core, expressing various hypoxic markers[226,227]. KSHV genome carries hypoxia-responsive regions[228] and hypoxic conditions induce viral reactivation[36,229,230]. To test whether hypoxic conditions alone could be responsible for better maintenance of the virus in 3D culture and are sufficient to increase viral copy number in 2D the cells were subjected to hypoxic conditions. To this end, the cells were cultured either in normoxic (20% O_2) or hypoxic conditions (5% O_2). Treatment of the cells in the normoxic chamber with $CoCl_2$, a chemical inducer of HIF-1a, was utilized as another way to mimic hypoxic conditions in cell culture. The cells were treated for 14 days followed by measurement of the viral copy number. As a result, neither the cells cultured in the hypoxic chamber, nor the chemically induced hypoxic conditions were able to increase viral copy number compared to the standard normoxic 2D culture (Fig. 3.13A).

It has been shown that increase in media volume can significantly impact the pericellular oxygen concentration[231]. To enhance the effect of hypoxic chamber the cells were cultured in 6 well plates either with 2,5 ml of media (medium height 2 778 µm, corresponding to ≈2.83% of oxygen) or 5 ml

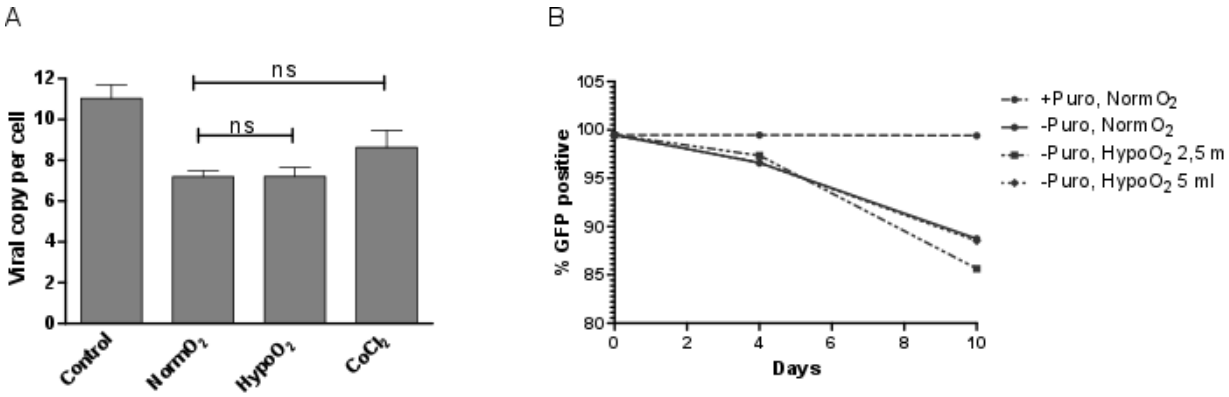

Figure 3. 13 KSHV maintenance is not affected by hypoxic cell culture conditions.
A) The viral copy number of rKSHV-HuARLT cells cultured for 14 days either in normoxic (20% O2), hypoxic (5% O2) conditions or in presence of 100 µM of $CoCl_2$ was measured by qPCR. rKSHV-HuARLT cells cultured in normoxic conditions in presence of selection pressure were used as a control. B) Percent of GFP positive cells in rKSHV-HuARLT cells cultured either in normoxic conditions (20% O_2) or in hypoxic conditions enhanced by increased media volume without selection pressure as quantified by FACS analysis on day 4 and day 10. As control rKSHV-HuARLT cells cultured in presence of puromycin in normoxic conditions were used.

of media (medium height 5 556 µm) for 10 days. The amount of GFP-positive cells was measured by FACS analysis on day 4 and day 10. In both time points the amount of GFP-positive cells did not differ between the conditions (Fig.3.13B). Taken together, the data indicates that hypoxic conditions alone are not sufficient to increase viral copy number in 2D culture and cannot explain better viral maintenance in 3D.

3.2.6 The PI3K-mTOR pathway is deregulated in 3D cell culture conditions

In order to determine which pathways contribute to viral maintenance in 3D cell culture, the expression profile of cells was analyzed by RNA-Seq. To this end, in rKSHV-HuARLT cells were cultured in either standard cell culture conditions or in 3D spheroids. Total RNA was extracted from these cells after 3 days of cultivation and subjected to next generation sequencing. The raw data obtained during sequencing were mapped to the reference human and KSHV genomes. As a result, 736 cellular genes were upregulated and 542 cellular genes were downregulated upon 3D cultivation (Fig 3.14A). Differentially regulated genes strongly enriched in several cellular pathways, among which are: pathways in cancer, PI3K-Akt and MAPK pathways (Fig. 3.14B). Of note, downstream targets of Pi3K-Akt pathway were not homogeneously regulated (Fig. 3.14C and S3).

In order to confirm these data, relative expression of selected candidate genes was evaluated by RT-qPCR in an independent experiment. RT-qPCR analysis confirmed that *TLR2, Jak2, PI3K, Notch1, Hes1* and *S6K1* were significantly upregulated in 3D culture conditions with a fold change of 1,4 or higher. Interestingly, TLR2 gene showed a 2.6fold upregulation in 3D cell culture by RT-qPCR in contrast to downregulation by RNA-Seq. In contrast, expression of *TLR4, cRaf, Jag1, Hey1, MEK and Akt* genes was not significantly changed, as measured by both RT-qPCR and RNA-Seq. Although *mTOR* gene expression appeared to be moderately upregulated in the RNA-Seq experiment, the data could not be confirmed by RT-qPCR (Fig. 3.14D). Taken together, the RT-qPCR data largely confirmed the RNA-Seq analysis and indicated upregulation of several genes associated with the PI3K-Akt pathway. However, it has to be taken into account that the pathway is mainly regulated on post-transcriptional level; thus, evaluation of the contributing genes on the level of RNA can only be taken as a hint. This might also explain the heterogeneous deregulation of individual factors as well as the minimal fold change.

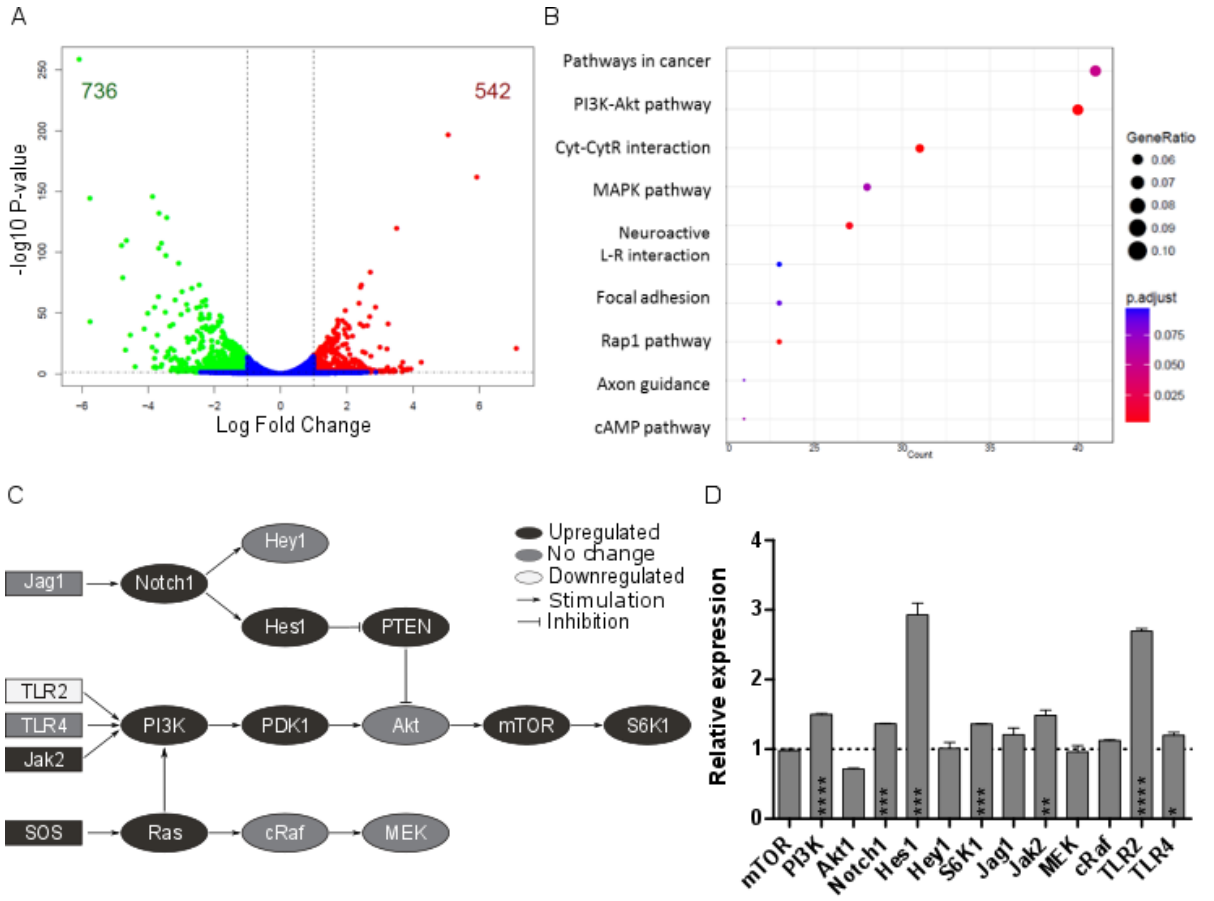

Figure 3. 14 Upregulation of PI3K pathway in 3D cell culture.
A) Volcano plot of total deregulated genes upon 3 days of cultivation in 3D cell culture conditions as determined by RNA-Seq. Green indicates the genes downregulated in 3D culture and red indicates the genes upregulated in 3D cell culture. Fold change of 2 and adjusted p-value of 0.05 were selected as a threshold (data analysis by R. Geffers). B) Top 9 canonical pathways enriched in KEGG pathways by differentially expressed genes from the RNA-Seq analysis of rKSHV-HuARLT cell cultured either in 2D or 3D cell culture for 3 days (data analysis by R. Geffers). C) PI3K pathway regulation as determined by RNA-Seq analysis. The genes, upregulated more then 1.5 fold are indicated in dark grey, downregulated gene is shown in white and the genes with no detected change of expression are shown in light grey. C) Relative expression of the selected genes from PI3K pathway as measured by RT-qPCR. The expression level in 2D culture was set to 1.

3.2.7 Inhibition of the PI3K-mTOR pathway induces viral loss in 3D cell culture

Previous studies indicate that the PI3K, as well as the Ras-cRaf-MAPK and the NF-kB pathways are stimulating KSHV reactivation[38,39]. Another study shows that 3D cell culture of KSHV-infected cells leads to higher viral gene expression and upregulation of Notch signaling[86]. Taking into account the multiple interactions between these pathways, it is not possible to distinguish them based on the KEGG database. Rather, they are recognized as a single PI3K-Akt pathway. In order to determine which part of the pathway is responsible for better viral maintenance in 3D cell culture, the cells were embedded into matrigel matrix and cultured for 14 days in presence of small molecules that specifically target the activity of various proteins within these pathways (Fig. 3.15A).

As a result, treatment with LY294002, a chemical inhibitor of PI3K, as well as treatment with Rapamycin, an inhibitor of mTOR, led to the reduction in viral copy number in 3D culture up to 20%, whereas FK506, which shares a number of molecular targets with rapamycin, except for mTOR showed no effect. Interestingly, the inhibitors showed no significant effect in 2D conditions. (Fig. 3.15B). In contrast, inhibition of the factors in the associated Notch, NF-kB, or Ras-cRaf pathways showed no influence of viral copies number both in 2D and 3D culture. Interestingly, GW5074, an inhibitor of cRaf even increased the viral copy number both in 2D and 3D up to 30%.

Taken together, the data indicate that the PI3K-Akt-mTOR axis is crucial for viral maintenance in 3D cell culture, but not the other branches of the pathway.

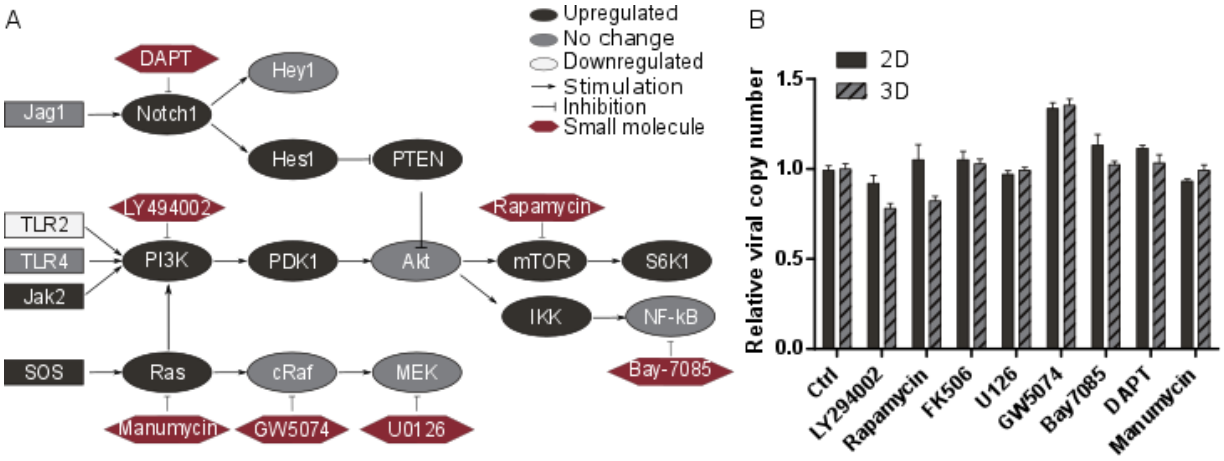

Figure 3. 15 Inhibition of the PI3K-Akt-mTOR pathway leads to viral loss in 3D culture.
A) Schematic representation of the pathway and the inhibitors used. B) Relative viral copy number was measured in rKSHV-HuARLT cells after 14 days of treatment with the selected compounds: 2.5 µM LY294002, 2.5 µg/ml rapamycin, 2.5 µg/ml FK506, 10 µM U0126, 10 µM GW5074, 2,5 µM Bay7085, 50 µM DAPT, 5 µM manumycin. Viral load in the respective control samples was set to 1.

3.2.8 Differential role of the DNA damage response in viral maintenance in 2D and 3D cell culture

KSHV infection induces DNA damage response early upon infection. The activation of the pathway and specifically ATM-induced H2AX phosphorylation is beneficial for establishment of latency and viral maintenance[108]. Another study indicates that both DNA-PK dependent protein kinase (DNA-PK) and the MRE11/Rad50/MBS1 (MRN) complex play a differential role in KSHV reactivation. The data suggest that the MRN complex supports KSHV reactivation, whereas DNA-PK/Ku70/Ku80 complex restricts it[232]. In order to determine if DNA damage response and in particular the MRN complex plays a role in KSHV maintenance, the pathway was perturbed by small molecules (Fig.16 A and B).

To this end, rKSHV-HuARLT cells were either cultured in standard 2D cell culture conditions, or in the previously described matrigel-embedded 3D culture conditions in presence of the inhibitors. The cells were treated for 14 days followed by evaluation of the relative viral copy number. In accordance

with the literature data, inhibition of ATM led to substantial viral loss in both 2D and 3D cell culture, supporting the conclusion that it is required for maintenance of KSHV latency. Interestingly, treatment with NU7441, a chemical inhibitor of DNA-PK, resulted in viral loss, which was more pronounced in 2D rather than 3D culture conditions. On the contrary, treatment, with mirin, an inhibitor of the MRN complex led to a moderate increase in viral copy number up to 15% in 2D cell culture. However, it had no effect in 3D culture.

Taken together, the data suggest that differential regulation of the DNA damage response pathway in 2D and 3D cell culture might contribute to the differential viral maintenance.

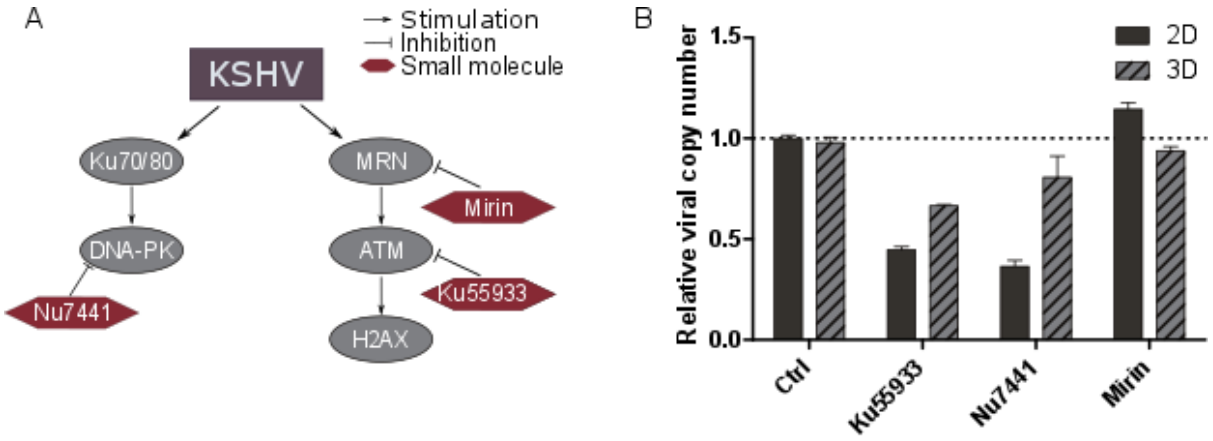

Figure 3. 16 Role of the DNA damage response pathway in KSHV maintenance.
A) Schematic representation of the pathway and the inhibitors used. B) Relative viral copy number was measured in rKSHV-HuARLT cells after 14 days of treatment with the selected compounds: 10 µM Ku55933, 1 µM Nu7441 or 10 µM mirin. Viral load in the respective control samples was set to 1.

3.2.9 Role of Eya phosphatases in KSHV maintenance

Recent studied demonstrated that H2AX phosphorylation on the Tyr142 site regulated by eye absent (Eya) phosphatases plays a crucial role in apoptosis or DNA repair decisions[93]. Mammalian cells express four Eya phosphatases, known as Eya 1-4. Of note, careful evaluation of the RNA array data revealed that expression of one of the phophatases, Eya1, was 2-fold lower in 3D cell culture, as determined by RNA-Seq.

To confirm this finding, total mRNA was isolated from independent experiment and the expression of all four Eya genes, as well as their target H2AX was evaluated via RT-qPCR. The result showed significant downregulation of Eya1, Eya2 and Eya4 in 3D cell culture, confirming the RNA-Seq analysis. The expression of H2AX did not change upon different cell culture conditions which in line with the posttranslational rather than a transcriptional regulation of this protein.

These results open the possibility that Eya expression in 2D conditions might compromise viral maintenance. To investigate whether downregulation of Eya expression in 3D culture conditions could be the reason for better viral maintenance, it was tested if blocking of Eya would result in better

maintenance of the virus. To this end, rKSHV-HuARLT cells were cultured in 2D conditions and treated with MLS000544460, a small molecule inhibitor of Eya2[233,234] for 14 days followed by viral copy number analysis. 3D cell culture was used as control. However, the treatment of the cells with the inhibitor did not result in an increase of viral copy number in 2D as well as in 3D cell culture condition. Rather, a moderate decrease in viral copy number compared to the control was observed. These results thus suggest that Eya2 is not a negative factor but rather supports viral maintenance.

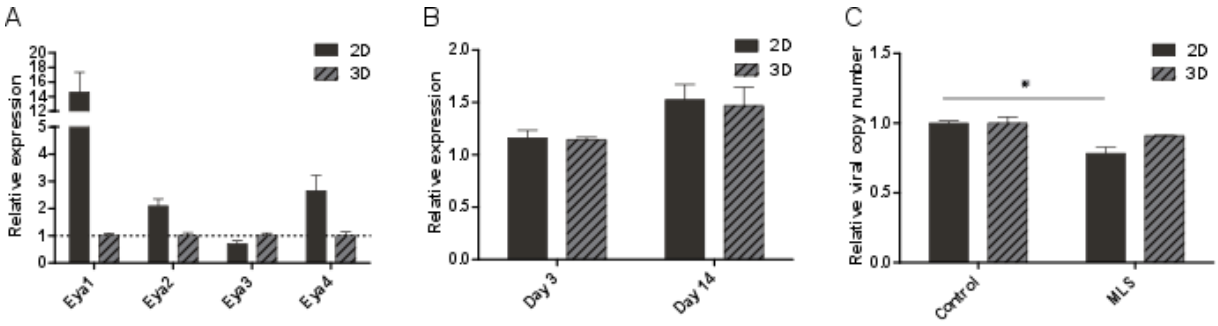

Figure 3. 17 Role of Eya phosphatases in KSHV maintenance.
A) The relative expression of Eya phosphatases in 2D or 3D rKSHV-HuARLT cell culture was measured by RT-qPCR after 3 days of cultivation. Expression levels in 3D culture were set to 1. B) The relative expression of H2AX in rKSHV-HuARLT cells cultured in 2D or 3D conditions was measured by RT-qPCR on days 3 and day 14 of cultivation. Expression levels on day 1 of culture were set to 1. C) Relative viral copy number in rKSHV-HuARLT cells cultured for 14 days in 2D or 3D cell conditions in presence of 5 µm MLS000544460. The viral copy numbers in absence of the drug in the respective culture conditions are set to 1. * indicated p-value less than 0,05

3.3 rKSHV-HuARLT for screening and validation of novel antiviral compounds

HuARLT cells closely mimic the changes observed in primary cells upon KSHV infection. They undergo transcriptional reprogramming, which corresponds to lymphatic transdifferentiation, as we as endothelial-to-mesenchymal transition. Moreover, rKSHV-HuARLT cells depend on PI3K and NF-kB pathways for survival, as described for primary HUVEC cells. Together with transcriptional changes, the cells also undergo phenotypic and functional transformation, as shown by loss of the ability to form vessels and acquisition of the invasiveness in 3D culture as well as in vivo. Taken together, these properties make rKSHV-HuARLT cells an attractive model for KSHV-induced tumorigenesis. In this chapter the relevance and the predictive power of the system will be evaluated upon treatment with compounds with known pharmacological targets, followed by evaluation of novel compounds for their ability to reduce viral load and decrease invasiveness in 3D cell culture.

3.3.1 Purging cells from virus abolishes the tumorigenic phenotype

From existing literature data it remained unclear if the loss of the viral genome could revert the phenotype of infected cells and abrogate tumor formation in vivo. To this end, rKSHV-HuARLT cells were cultured for 38 days without selection pressure and isolated the GFP negative cells by FACS (designated as KF-HuARLT cells, Fig. 3.18A). Analysis of the viral copy number in KF-HuARLT cells confirmed a significant reduction of viral genomes down to 0.07±0.04 copies per cell indicating the absence of the KSHV genome in the vast majority of these cells (Fig.3.18 B).

To see if loss of KSHV reverted the transcriptional profile of the cells, total RNA was isolated and used for gene array analysis. Pathway analysis showed that differentially expressed genes upon loss of KSHV enriched pathways in angiogenesis, cell migration and organ/tissue development (Fig. 3.18C and D). These changes are opposite to those observed between rKSHV-HuARLT and HuARLT cells, suggesting that the cells reverted their phenotype upon loss of the virus.

To investigate if the transcriptome changes of KF-HuARLT cells would result in a reduced tumor potential, KF-HuARLT as well as the control rKSHV-HuARLT and HuARLT cells were aggregated to spheroids and transplanted into immunocompromised Rag2$^{-/-}\gamma c^{-/-}$ mice. After 4 weeks, the plugs were isolated. Sections were stained for human vimentin and the morphology of transplanted cells was examined via microscopy. The virus-infected rKSHV-HuARLT cells formed KS-like lesions as described above (see section 3.1.9). Also transplantation of KF-HuARLT cells resulted in engraftment of individual cells. However, no KS-like lesion could be found indicting lack of tumorigenic potential of these cells (Fig.3.18E). Thus, elimination of viral genomes from KSHV-infected HuARLT cells completely reverted the tumorigenic phenotype and impaired the formation of lesions indicating that continuous expression of KSHV genes is crucial for tumor formation.

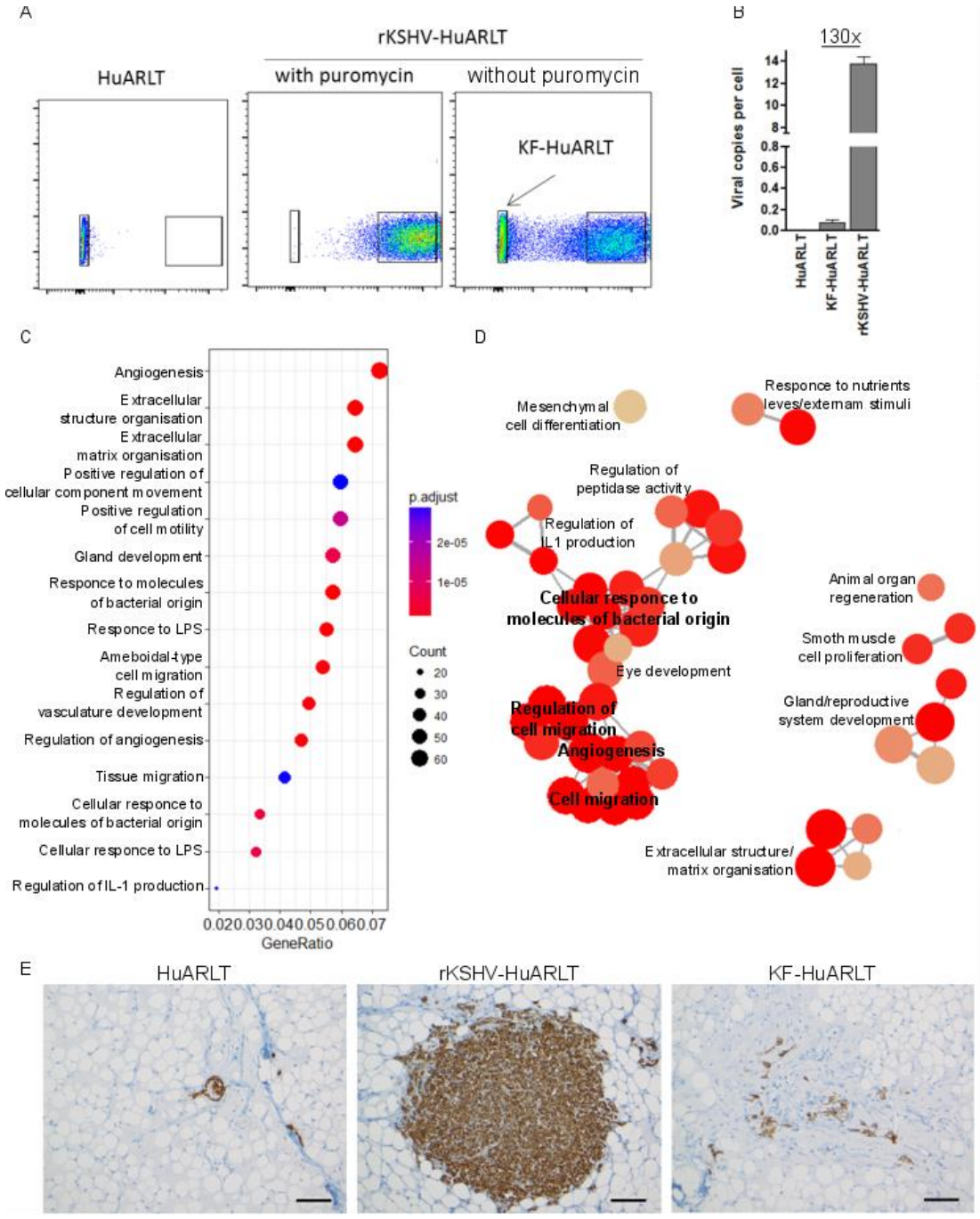

Figure 3. 18 Purging rKSHV-HuARLT cells from the virus.
A) Flow cytometry of non-infected HuARLT cells as well as rKSHV-HuARLT cells upon culture in presence or absence of puromycin for 38 days. The gate used to sort the GFP-negative KF-HuARLT cells from the puromycin-free culture conditions is indicated. B) Viral load of the indicated cell populations as assessed by qPCR. C) Top 20 canonical pathways enriched in Gene Ontology analysis based on the differentially expressed genes in the infected rKSHV-HuARLT and purged KF-HuARLT cells. The set of differentially expressed genes was obtained by transcriptome analysis of the cells via gene arrays and is visualized with the help of the ClusterProfiler[203] tool. The genes were considered to be differentially regulated if the change of expression was higher than 2fold and if the adjusted p-value was less then 0.01 as determined by ANOVA test. The size of the nodes reflects the number of contributing genes ('count') and the colour code indicates the significance level. D) Network visualization of selected enriched biological processes upon purging rKSHV-HUARLT cells from the virus. The networks were assembled and visualized by the EnrichMap[204] tool, using the Kamada-Kawai layout. The node size represents the number of genes assigned to a biological process and overlap is proportional to the number of overlapping genes between two nodes. The higher color intensity reflects a lower adjusted p-value. E) Representative pictures of engrafted cells isolated 4 weeks after transplantation upon staining for human vimentin. Scale bar 100µm.

3.3.2 Establishment of *in vitro* assays for compound validation

Loss of tumorigenic properties upon elimination of the virus indicates that the reduction of viral copy number is a useful parameter to identify antitumor compounds. Several therapeutic strategies targeting lytic reactivation of the virus were proposed recently, however, targeting the predominant latent stage of the virus is still a challenge[124]. Chapter 3.2 showed that KSHV maintenance crucially depends on the cell culture conditions. Although it is a common understanding that viral maintenance is largely governed by latent proteins chapter 3.2 indicates that viral maintenance relies on a tightly regulated balance between latency and lytic reactivation.

To consider this complexity, different assay systems were established (summarized in Figure 3.19A). 3D cell culture conditions were employed since they represent a physiologically relevant system, where most of the cells are latently infected with only minor proportion of cells undergoing lytic reactivation, resembling situation within the tumors. Treatment of 3D spheroid cultures with GA (which impairs LANA association) and with PhA (inhibitor of viral DNA polymerase) resulted in a significant reduction of the viral load (Fig. 3.12A), indicating that the system is sensitive to inhibitors of both latent and lytic replication.

A 2D cell culture system was also tested for validation of antiviral compounds, since it allows selection of the compounds selectively targeting latent virus. As depicted in Figure 3.4D, treatment of cells with GA induced substantial viral loss as determined by qPCR and FACS analysis. In contrast, treatment of the infected cells with PhA did not have an effect on the viral copy number and GFP expression. These data indicate that the 2D cell culture system is highly selective for inhibitors of viral latent proteins.

Although purging cells completely from the virus reverted their tumorigenic phenotype, it is unclear how compounds which only partially reduce viral load would impact invasiveness of the infected cells. For evaluation of the invasiveness of KSHV-infected cells upon compound treatment a 3D culture system was adapted that was previously described for KSHV-infected primary endothelial cells[86]. rKSHV-HuARLT cells were first aggregated to spheroids and then embedded in a fibrin matrix. Three days after embedding, the KSHV-infected cells exhibited pronounced sprouting and invaded into the surrounding matrix (Fig. 3.19B). To validate the specificity of the assay with respect to KSHV, the effect of KSHV-specific inhibitors on sprouting in 3D culture conditions was investigated. To this end the cell were treated with GA, PhA, and rapamycin, which is shown to reduce tumor progression in post-transplant KS patients as well as inhibit KSHV-induced angiogenesis[139]. The embedded spheroids were treated with the compounds for five days. The effect of the compounds was evaluated by microscopy and quantified by measuring the area covered by sprouts and relating it to the spheroid body area in the same section (Fig. 2.1). Quantification revealed

a significant reduction of sprouting for GA and rapamycin. In contrast, treatment with the control drugs FK506 and PhA did not reduce the sprouting activity (Fig. 3.19C).

Together, the three assay systems allow selection of the compounds, which reduce viral copy number both in strictly latent conditions and with a limited level of viral reactivation, as well as directly access virus-induced invasiveness. Moreover, these test systems are sensitive to inhibitors with known mechanisms of action, which highlights that the systems are appropriate to test antiviral and antitumor activities of novel compounds. (3.19A).

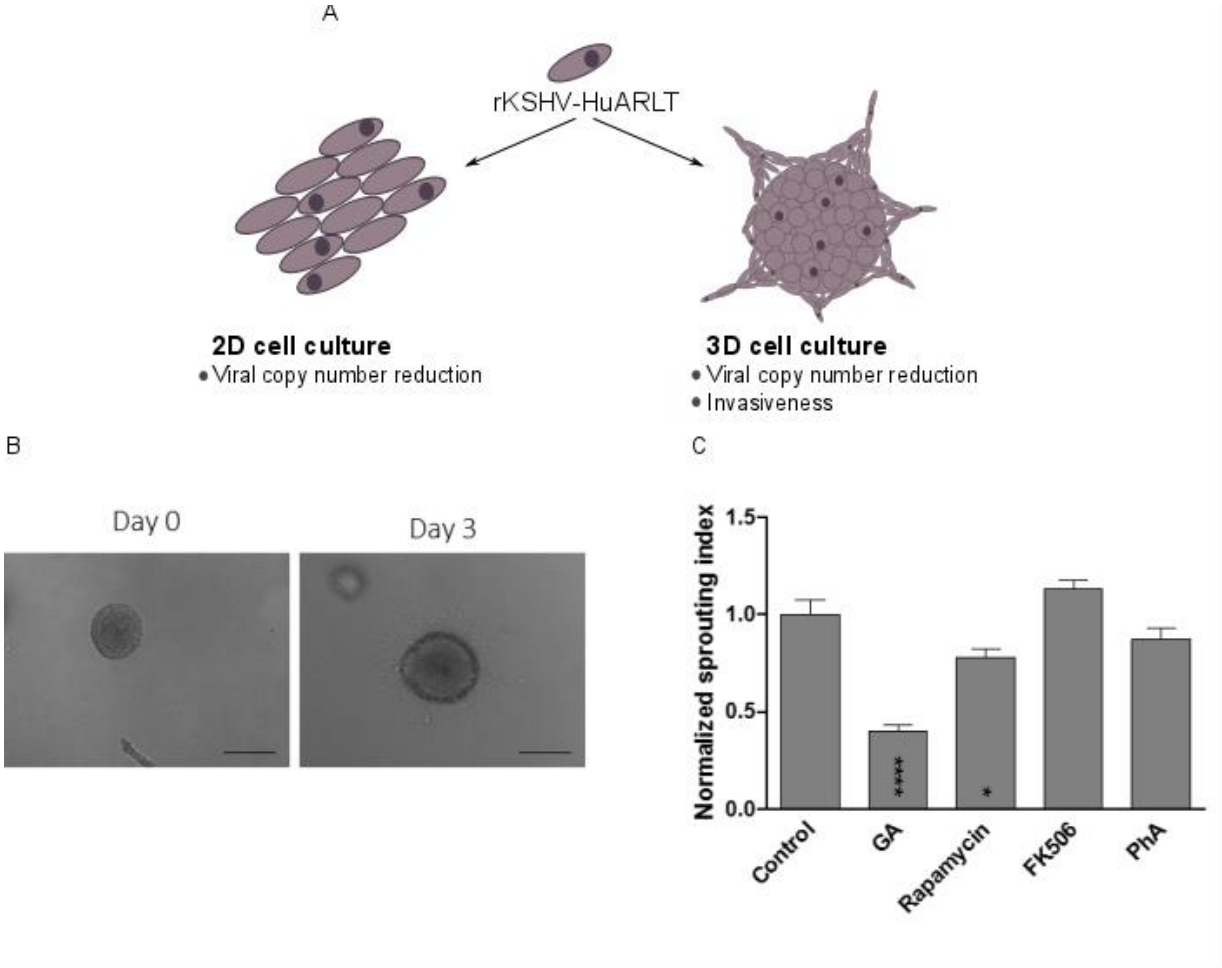

Figure 3. 19 *In vitro* systems for validation of novel anti-KS compounds.
A) Schematic representation of the tests used for validation of the hits in vitro. B) Phase contrast microscopy of representative 3D spheroids before and 3 days after embedding in fibrin gels. Scale bar 50 µm. C) Relative sprouting index upon treatment of rKSHV-HuARLT cells with GA, PhA, Rapamycin or FK506 for 5 days. Statistical significance is indicated by asterisks: * $p \leq 0.05$, ** $p \leq 0.01$, *** $p \leq 0.001$, **** $p \leq 0.0001$.

3.3.3 Evaluation of novel compounds for viral loss and invasiveness in 2D and 3D culture models

To search for novel anti-KSHV agents in a pilot screen, a library of 260 natural compounds was studied in a previously described reactivation assay in KSHV-infected BJAB cells (Brk.219 cells)[211,212]. The library mainly consisted of secondary metabolites from Myxobacteria, which were

selected by previous natural product screening programs[235]. The supernatant from compound-treated reactivated Brk.219 cells was used to infect HEK 239T cells. Infection rate of HEK 293 was measured via fluorescence microscopy. Fig. 3.20A indicates the compounds that showed reduction of GFP expression in HEK293 cells and at the same time exhibited low to moderate toxicity in Brk.219 cells.

To evaluate the capability to reduce viral load in latently KSHV-infected endothelial HuARLT cells 26 compounds were selected including pretubulysin D, a chemically accessible precursor of tubulysins[197]. First, their impact on viral copy number was tested in KSHV-infected HuARLT cells using drug concentrations that had little influence on cell viability (Table 2.8). The KSHV latently infected HuARLT cells were cultured in standard 2D conditions and treated with the compounds for two weeks followed by evaluation of viral copy number by qPCR. Out of the 26 compounds tested, seven showed a reduction of the cellular viral load to 75%: epothilon E, myxochelin A, eliamid, saframycin Mx1, stigmatellin F, chondramides B and C (Fig. 3.20B). This set of compounds was tested under the more physiologically relevant 3D conditions. To this end, matrigel embedded spheroids formed from KSHV-infected cells were treated for 14 days with the compounds and then evaluated for the viral copy number per cell. A total of nine compounds were identified that showed a reduction to 60%. In addition to five compounds that already showed positive effects in the 2D assay (epothilon E, myxochelin A, eliamid, chondramides B and C) four compounds showed copy number reductions in 3D culture only: trichangion, pellasoren, tubulysin A, tubulysin X (Fig. 3.20C).

To investigate whether the selected compounds have an impact on the cell invasiveness in 3D culture conditions, their effect on the cell's sprouting activity was evaluated in 3D cell culture. To this end fibrin gel embedded spheroids produced from rKSHV-HuARLT cells were treated with the compounds for 5 days followed by evaluation of the sprouting index. Overall, 13 compounds significantly reduced sprouting to 60% or less in the 3D sprouting assay, indicating pronounced reduction in the invasive potential of the cells (Fig. 3.20D). In Fig. 3.20E, the results of the three in vitro assays are summarized.

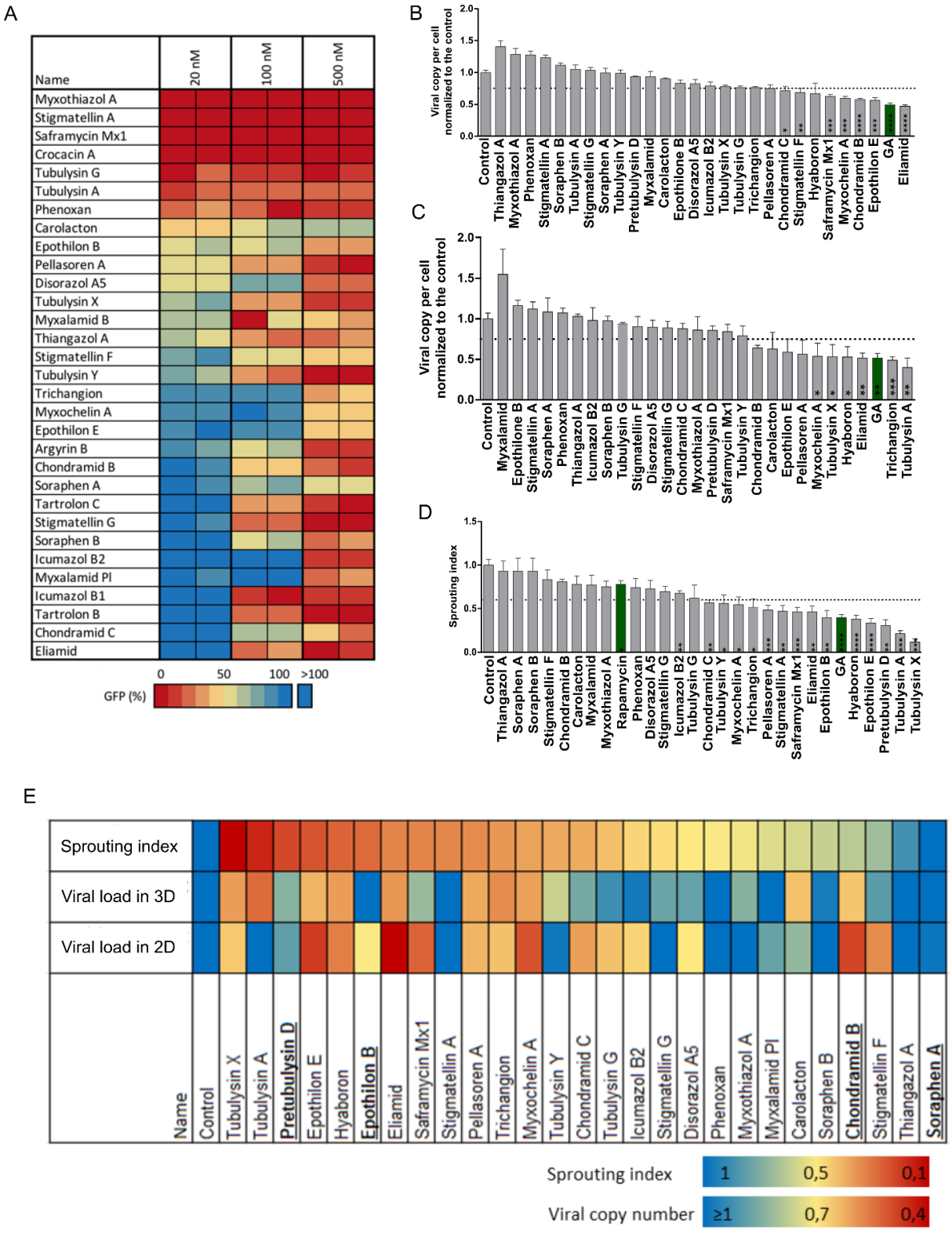
A
Name
20 nM
100 nM
500 nM
Myxothiazol A
Stigmatellin A
Saframycin Mx1
Crocacin A
Tubulysin G
Tubulysin A
Phenoxan
Carolacton
Epothilon B
Pellasoren A
Disorazol A5
Tubulysin X
Myxalamid B
Thiangazol A
Stigmatellin F
Tubulysin Y
Trichangion
Myxochelin A
Epothilon E
Argyrin B
Chondramid B
Soraphen A
Tartrolon C
Stigmatellin G
Soraphen B
Icumazol B2
Myxalamid PI
Icumazol B1
Tartrolon B
Chondramid C
Eliamid
0
50
100
>100
GFP (%)
B
Viral copy per cell normalized to the control
Control
Thiangazol A
Myxothiazol A
Phenoxan
Stigmatellin A
Soraphen B
Tubulysin A
Stigmatellin G
Soraphen A
Tubulysin Y
Pretubulysin D
Myxalamid
Carolacton
Epothilone B
Disorazol A5
Icumazol B2
Tubulysin X
Tubulysin G
Trichangion
Pellasoren A
Chondramid C
Stigmatellin F
Hyaboron
Saframycin Mx1
Myxochelin A
Chondramid B
Epothilon E
GA
Eliamid
C
Viral copy per cell normalized to the control
Control
Myxalamid
Epothilone B
Stigmatellin A
Soraphen A
Phenoxan
Thiangazol A
Icumazol B2
Soraphen B
Tubulysin G
Stigmatellin F
Disorazol A5
Stigmatellin G
Chondramid C
Myxothiazol A
Pretubulysin D
Saframycin Mx1
Tubulysin Y
Chondramid B
Carolacton
Epothilon E
Pellasoren A
Myxochelin A
Tubulysin X
Hyaboron
Eliamid
GA
Trichangion
Tubulysin A
D
Sprouting index
Control
Thiangazol A
Soraphen A
Soraphen B
Stigmatellin F
Chondramid B
Carolacton
Myxalamid
Myxothiazol A
Rapamycin
Phenoxan
Disorazol A5
Stigmatellin G
Icumazol B2
Tubulysin G
Chondramid C
Tubulysin Y
Myxochelin A
Trichangion
Pellasoren A
Stigmatellin A
Saframycin Mx1
Eliamid
Epothilon B
GA
Hyaboron
Epothilon E
Pretubulysin D
Tubulysin A
Tubulysin X
E
Sprouting index
Viral load in 3D
Viral load in 2D
Name
Control
Tubulysin X
Tubulysin A
Pretubulysin D
Epothilon E
Hyaboron
Epothilon B
Eliamid
Saframycin Mx1
Stigmatellin A
Pellasoren A
Trichangion
Myxochelin A
Tubulysin Y
Chondramid C
Tubulysin G
Icumazol B2
Stigmatellin G
Disorazol A5
Phenoxan
Myxothiazol A
Myxalamid PI
Carolacton
Soraphen B
Chondramid B
Stigmatellin F
Thiangazol A
Soraphen A
Sprouting index
1
0,5
0,1
Viral copy number
≥1
0,7
0,4

Figure 3. 20 Evaluation of novel compounds for viral loss and cellular invasiveness.
A) Natural compounds inhibiting KSHV lytic reactivation in BJAB cells. A library of natural compounds was screened for the ability to reduce the production of infectious virus by lytically induced KSHV-infected BJAB (Brk.219) cells. The amount of infectious virus released from Brk.219 cells was measured by plating supernatants on HEK293 cells and measuring the GFP signal in a BioTek plate reader. Replicates are depicted (Data from T. Schultz and G.Beauclair). (B-E) Selected compounds were tested on rKSHV-HuARLT cells. The relative viral load was assessed in rKSHV-HuARLT cells upon culture in presence of the indicated drugs in standard 2D conditions (B) or in 3D matrigel (C). Non-treated cells were included as reference (control). 40% viral copy reduction in viral copy number was chosen as a cut-off value to select active compounds (dashed line). D) rKSHV-HuARLT cells were treated with the compounds in 3D cell culture conditions. The relative sprouting index was determined after 2 weeks treatment. 40% reduction on sprouting index viral copy reduction was chosen as a cut-off value for active compounds (dashed line). For drug concentrations used in this experiment see Table 2.8. Control compounds are indicated in green. Statistical significance is shown by asterisks: *p ≤ 0.05, **p ≤ 0.01, ***p ≤ 0.001, **** p ≤ 0.0001. E) Heat map summarizing the activity of the compounds in indicated assays (some of the compounds were tested by A. Lieske).

3.3.4 Validation of hits *in vivo*

Four compounds with various degrees of inhibition in the three in vitro test systems were selected investigated for the ability to reduce the formation of KS-like lesions in the xenograft model. Chondramid B was chosen as a compound that significantly reduced the viral load in 2D and 3D culture, but with a moderate effect on the sprouting index. In contrast, pretubulysin D and epothilon B were selected for their strong effect on sprouting but no significant effect on the viral copy number. As a drug with minor activities we selected soraphen A. In addition, we used the mTOR inhibitor rapamycin (and its control FK506) as well as PhA with known antiviral activities. Starting directly after transplantation of the virus-infected cells, the mice were treated with the respective drugs for 4 weeks. Then, the mice were sacrificed and the plugs were isolated. The lesion size was assessed by microscopy analysis of vimentin stained sections.

While the control compound FK506 showed no significant effect on tumor size, a certain reduction of lesion size down to about 70-80% of the size of untreated controls was found in mice treated with rapamycin and PhA. Interestingly, a comparable effect was observed for chondramid B and soraphen A. However, the strongest impairment was observed for epothilon B and pretubulysin D, both of which resulted in a complete regression of the tumor growth (Fig. 3.20A and B).

Moreover, the drug-mediated reduction of invasiveness of rKSHV-HuARLT cells in the 3D cell culture conditions strongly correlates with tumor size reduction (R^2=0,9266, Fig. 3.20C). In contrast, viral copy number reduction, measured both in 2D and 3D cell culture show poor correlation with the in vivo outcome (R^2=0.0863 and 0.0517 respectively). Taken together these observations highlight the predictive power of the 3D invasiveness assay with respect to tumor size reduction in vivo.

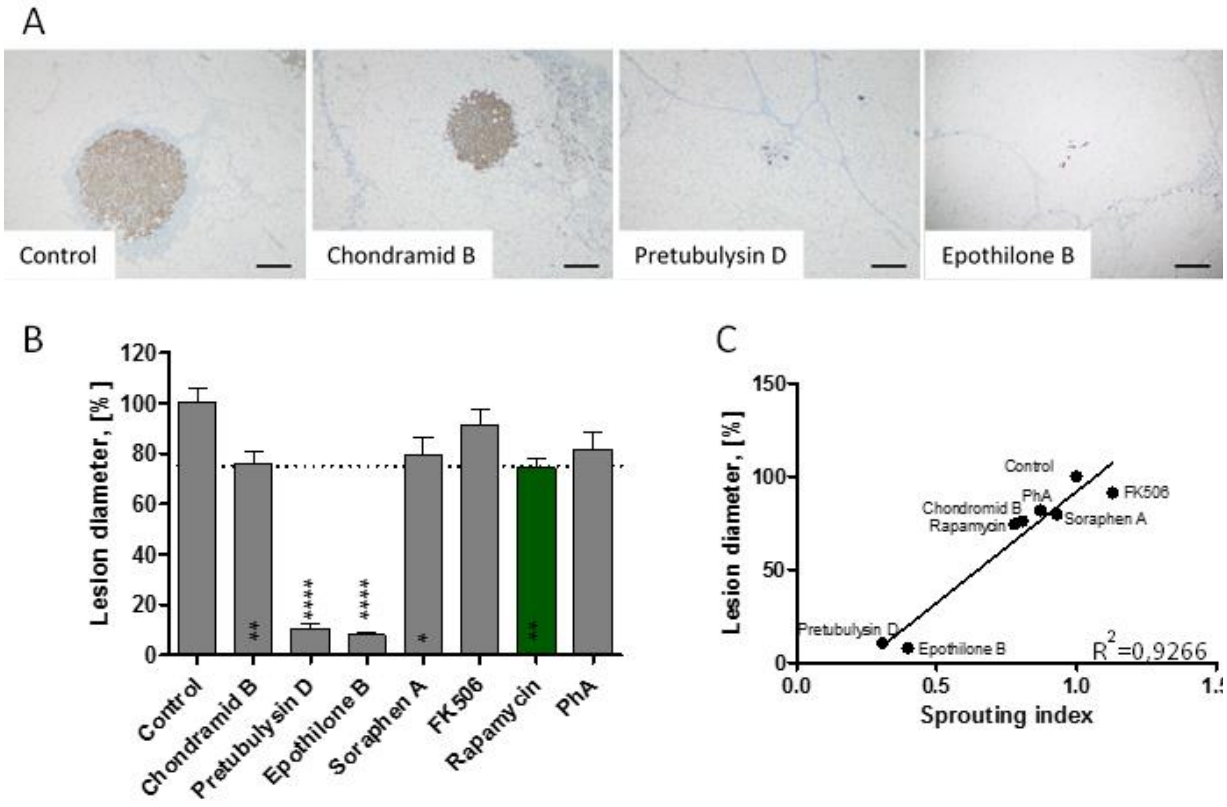

Figure 3. 21 Compound validation *in vivo*.
A) Representative immunohistochemistry sections from lesions observed without treatment or upon 4 weeks treatment with indicated compounds. Cells were stained for human vimentin, scale bar 200 µm. Scale bar 200 µm. B) The lesion size was measured and is indicated as % of non-treated control (n=6 per compound). 25% tumor size reduction was chosen as a cut-off value for active compounds. Statistical significance is shown by asterisks: * $p \leq 0.05$, ** $p \leq 0.01$, *** $p \leq 0.001$, **** $p \leq 0.0001$, (10 to 80 lesions out of 6 plugs). C) Correlation analysis of 3D sprouting index vs. lesion size diameter *in vivo.*

4. Discussion

Immunocompromised patients, as patients with HIV or organ recipients, have higher risks of developing Kaposi's sarcoma than the general population. Currently there are about 36,7 million people living with HIV with an estimated 1,8 million of newly infected patients per year worldwide[236]. With the recent development of organ transplantation, the amount of transplantations increases worldwide[237]. This statistics indicates that high-risk groups for developing KS continue to grow and highlights the need for efficient anti-KS therapeutics. The current therapies of Kaposi's sarcoma are mainly based on standard antitumor treatments, and have several limitations, such as high overall toxicity, low efficiency, and strong side effects. Currently there is no targeted therapy and no vaccines available. While some drugs that block the virus in its lytic stage have been discussed recently[124], the latent stage of the virus that is predominant in KS lesions can so far not be specifically targeted.

Since KSHV infection is restricted to humans, investigation of KS pathogenesis as well as the development of novel therapeutics relies on model systems that aim to recapitulate viral-induced cell transformation *in vitro* and therefore can be predictive for *in vivo* outcome. In this study, the properties of the previously developed conditionally immortalized human endothelial cell line HuARLT[194] were investigated upon KSHV infection.

4.1. HuARLT cells as a model for KSHV infection

HuARLT cells were generated based on primary human umbilical vein endothelial cells (HUVECs)[193] commonly used in endothelial cell research. HUVECs represent blood endothelial cells (BECs) in classic 2D cell culture conditions, but they exhibit certain plasticity and transdifferentiation towards lymphatic linage in 3D cell culture conditions[238]. HuARLT cells represent a tightly growth-controlled cell line that preserves the phenotype of the primary cells. This is reflected both by the expression profile as well as the functional properties, such as the uptake of macromolecules and tube formation in Matrigel assay[193]. Importantly, the cells are able to form functional perfused blood vessels upon transplantation in Rag2$^{-/-}\gamma c^{-/-}$ mice. No aberrant cell proliferation and no tumor formation is detected upon transplantation of HuARLT even upon prolonged obsevation[194]. Similar to primary cells, HuARLT increased the expression of endothelial-specific markers upon growth arrest (Fig. 3.2A and B). Uptake of macromolecules, as well as tube formation, was more efficient in non-proliferating cells, suggesting that growth-arrested cells more closely reflect endothelial phenotype (Fig. 3.2D and E, 3.6). The use of primary cells in drug screening is limited due to high donor-to-donor variability and limited cell numbers. HuARLT cell line overcomes these limitations and represents an expandable, reproducible cell culture system.

HuARLT cells are susceptible for KSHV infection and like the cells within Kaposi's sarcoma[239–241] the majority of rKSHV-HuARLT cells established latency upon infection with KSHV. Similar to

other adherent cell lines upon infection[159,160], rKSHV-HuARLT cells could not be efficiently reactivated with the use of TPA or epigenetic modifiers, such as sodium butyrate or decitabine.

KSHV induced a number of functional and transcriptional changes in the infected cells. These changes mainly affected genes associated with cell migration, innate immune response and cell differentiation, as assessed by transcriptome analysis (Fig. 3.5 A and B). Although HuARLT cells expressed a number of BEC-specific markers, such as VEGFR1, Tie1, Tie2 and VE-Cadherin, the expression was abrogated upon KSHV infection and the expression of LEC-specific markers, such as POX1 and VEGFR3, increased (Fig. 3.5 C-E). These changes reflect endothelial transdifferentiation observed upon infection of primary cells and typical for spindle cells within KS tumors, which express both BEC and LEC markers. Further, this study showed that they critically depend on PI3K/Akt/mTOR and NF-κB pathways which have been shown to provide a survival advantage to infected cells[141].

Unlike HuARLT cells, rKSHV-HuARLT cells form KS-like lesions upon transplantation to $Rag2^{-/-}\gamma c^{-/-}$ mice, opening the opportunity to investigate the fate of infected cells in vivo[194]. In situ hybridization with Alu polymerase showed that the lesions were originated from human cells. Majority of the cells carried the virus, as was demonstrated by immunohistochemistry staining for LANA and virus-encoded GFP, as well as FACS analysis (Fig. 3.8 C and Fig. 3.11 B). Similar to KS biopsies[242] and KSHV-infected SKL cells[243], the lesions were positive for the human thrombomodulin (CD141), which is recognized as a marker of lymphatic endothelium and expressed in many endothelium-derived tumors[244] (Fig. 3.8 C). Tumorigenic phenotype was recapitulated in 3D fibrin cell culture, where rKSHV-HuARLT cells showed increased invasiveness and loss of vessel formation, as compared to non-infected cells.

Notably, the overall expression of pan-endothelial genes[245] is decreased upon infection[194], whereas the transcriptome analysis indicated changes in genes connected with cell motility (Fig. 3.5 A and B). Together with the loss of the ability of infected cells to form vessels, the increased migration, and acquired invasiveness of infected cells in 3D culture and *in vivo,* these transcriptional changes indicate that the cells lost their endothelial properties and underwent endothelial-to-mesenchymal transition, typical for KS lesions and KSHV-infected primary cells[84,86].

Increased and aberrant angiogenesis with extravasated erythrocytes is a key feature of Kaposi's sarcoma lesions. KSHV is able to induce angiogenesis by a complex interplay of viral and cellular pro-angiogenetic and pro-inflammatory signaling affecting both KSHV-infected cells as well as neighboring cells in paracrine manner[49,246]. Interestingly, although rKSHV-HuARLT lost the ability to form vessels in 3D fibrin gels and upon transplantation to mice, the cells showed increased tube formation in the matrigel tube formation assay in agreement with previous studies in primary KSHV-infected cells[122,247].

Matrigel tube formation assay is typically employed to demonstrate the angiogenic activity of vascular endothelial cells *in vitro.* However, recently it has been shown that the tumor cells, such as

melanoma B16F1 cells, glioblastoma U87 cells, and breast cancer MDA-MB-435, are able to form tube-like structures in Matrigel assay[248]. Thus, matrigel tube formation assay is not specific for endothelial sprouting and can also be used also to study vasculogenic ability of tumor cells, referred to as vasculogenic mimicry. Likely, the ability of rKSHV-HuARLT cells to form tubular network in the matrigel assay might represent the ability of the infected cells to employ alternative angiogenetic mechanisms and cannot be considered as an increased endothelial function.

Taken together, the results of this study give further evidence that HuARLT cells reflect the properties of primary cells upon KSHV infection. The cells undergo transcriptional reprogramming as well as acquire an invasive and tumorigenic phenotype recapitulating the changes observed in patients, thus highlighting the relevance of the cell line for investigation of KSHV pathogenesis and the validation of novel antiviral compounds.

4.2 Tumorigenicity of the cells depends on virus gene expression

While it has been shown that the plasma level of KSHV is a poor prognostic or diagnostic biomarker for KS[249,250], it was highlighted that rather the viral load within tumor cells correlates with the tumor burden in the patients and reflects the severity of the disease[250]. This suggests that the reduction of viral load within KSHV-infected cells may result in loss of tumorigenic potential.

To test this hypothesis, in this study a virus-free cell population was established by passaging rKSHV-HuARLT cells in absence of selection pressure. The virus free cell population was characterized by an altered transcription profile and the main changes include deregulation of the genes associated with cell migration, angiogenesis and innate immune response (Fig.3.18 C and D). The transcriptome changes corresponded to a change of the in vivo phenotype, as the virus-free cell population lost its tumorigenic potential upon transplantation in vivo (Fig. 3.18 E).

While some systems have been used before to establish KS-like lesions in nude mice upon transplantation of the cells carrying KSHV genome[161,185–187], this study shows for the first time that the cellular phenotype can be reverted upon purging the cells from the virus. Thus, the expression of viral genes, rather than the permanent virus-induced cell transformation is essential for KSHV-induced tumorigenesis. Since the virus-induced changes are reversible when the cells are cured targeting the pathways effecting viral maintenance in latently infected cells can be considered to be a viable strategy for treatment of KS.

Studies indicate that viral proteins induce genomic instability both directly[251–253] or via manipulation of DNA damage response (reviewed in[105]). This process may lead to irreversible cell transformation and undoubtedly contributes to KSHV-induced tumorigenesis on later stages. Still, this study indicates that at least on early stages of KS development expression of viral genes is necessary and sufficient to induce tumorigenesis.

4.3 Molecular mechanisms of viral maintenance

Clinical data suggest that the amount of KSHV infected cells[59] as well as the KSHV burden within the tumor increases with the progression of the disease[250]. Surprisingly, in vitro studies showed that although spindle cells in KS carry the KSHV genome directly after isolation, they fail to retain it in 2D culture[153–155]. Similarly, primary endothelial cells[156] as well as the majority of telomerase-immortalized endothelial cells[161] rapidly lose the KSHV genome upon cultivation.

It has been hypothesized that viral loss in endothelial cells is a result of cell proliferation and inefficient viral replication. This would also imply that not endothelial, but rather non-proliferating memory B cells are the main reservoir of KSHV[156]. HuARLT cells are tightly growth controlled with less than 1% proliferating cells in absence of doxycycline, as measured by Ki67 staining (Fig. 3.1 C and D). In order to test, if cell proliferation affects viral maintenance, viral copy number was evaluated in proliferating and growth-arrested conditions. No difference in viral copy number was observed (Fig. 3.10), demonstrating that viral loss upon cultivation in 2D cell culture conditions is not the result of cellular proliferation. Moreover, efficient maintenance of the virus in 3D conditions and upon transplantation in vivo indicates that 3D cell culture conditions (Fig. 3.11) are beneficial for virus persistence. Together with the observation that 3D cell culture conditions better reflect EndMT, as addressed by changes in transcriptional profile[86] as well as invasive phenotype, the results of this study indicate higher relevance of 3D cell culture systems for investigation of viral pathogenesis.

4.3.1 Viral reactivation in 3D cell culture conditions

Previous studies showed higher levels of lytic reactivation in 3D cultivated B cells[172] and endothelial cells[86]. KSHV viral copy number in 3D cell culture was markedly reduced upon treatment with phosphonoformic acid (Fig. 3.12 A), an inhibitor viral DNA polymerase[136], suggesting that lytic reactivation contributed to the efficiency of viral maintenance. Surprisingly, neither the expression of lytic genes addressed by RT-qPCR, nor PAN-driven RFP expression, was increased in 3D cell culture conditions (Fig 3.12 B and C). The discrepancy between the results can be explained by different sensitivity of the methods. Histological data indicate that only a minor fraction of the cells with KS lesions undergo spontaneous reactivation[68]. Based on these observations only few percent of KSHV infected cells are expected to reactivate at the time, which would not be possible to detect via RT-qPCR due to the dilution of the signal in the latent population. Moreover, some reports indicate that virus-encoded fluorescence proteins do not always reflect the infection status correctly, likely due to variable episomal silencing and different expression dynamic compared to ‘native’ viral genes.[254,255]. Besides, lytically reactivated cells undergo apoptosis, and therefore are likely to be washed or gated out during sample preparation and FACS analysis, which could explain the inability to detect the RFP

positive cells in 3D cultures. Therefore, the lack of any prove for a lytic state based on these two methods can not exclude a small proportion of reactivating cells in the 3D culture.
In contrast, continuous treatment with PhA, the inhibitor of lytically expressed DNA polymerase, would affect all reactivating cells thought-out the prolonged treatment. Therefore it had more prominent cumulative effect on the inhibition of viral replication and was more likely to be detected. Thus, reduction of viral copy number in 3D cell culture by PhA indicated that viral lytic replication at least partially contributes to viral maintenance in 3D cell culture.
Interestingly, the cells cultured in 3D conditions showed consistent downregulation of the genes encoded on the viral episome. Considering that both latent and lytic genes, as well as virus encoded GFP driven by a cellular promoter, are downregulated in a similar fashion (Fig. 3.12 C-G), it is tempting to speculate that the viral episome is kept in an altered epigenetic state in 3D cell culture conditions. Additional studies would be required to confirm this hypothesis and to determine if the epigenetically altered viral episome has an effect on viral maintenance.

4.3.2 Role of the PI3K pathway in KSHV maintenance

In order to determine which cellular pathways are differentially expressed in 2D and 3D cell culture conditions, and therefore might be responsible for increased viral maintenance, transcriptome analysis of the cells was carried out. As a result, a prominent alteration of the PI3K/Akt/mTOR pathway was detected (Fig. 3.14 B). The specific pharmacological inhibition of PI3K and mTOR could confirm that the pathway is crucial for viral maintenance in 3D, but not in 2D cell culture (Fig. 3.14 D).
Several studies indicate that the PI3K pathway is involved in KSHV reactivation upon coinfection with HIV or Herpes Simplex virus type 1. Inhibition of the pathway leads to lack of viral reactivation in these conditions[38,39]. Higher levels of PI3K in 3D cell culture conditions might thus enable lytic reactivation and therefore result in more efficient viral maintenance.
The other studies show that PI3K pathway is activated as early as 5 minutes p.i. PI3K activation leads to the Rho-GTPase dependent assembly of microtubules, their association with the viral genome, and its transfer to the nucleus. Pharmacological inhibition of the PI3K pathway results in lower efficiency of infection[20]. 3D cell culture provides more favorable conditions for virus spread due to cell compaction and increased cell-cell contacts. Of note, inhibition of the lytically expressed viral DNA polymerase in 3D cell culture results in loss of viral copies, indicating that the better viral maintenance in 3D cell culture is likely due to higher virus production and dissemination. In that case, activated PI3K pathway would not only support viral reactivation, but also assure better cell-to-cell transmission.
Besides direct interaction with KSHV PI3K/mTOR pathway regulates various cellular processes that might impact viral replication, such as cellular metabolism, autophagy, and protein synthesis. Autophagy is shown to restrict viral infection and initiate antiviral immune response by cooperating

with pattern recognition receptors[256]. It is a key part of viral pathogenesis for several human pathogens, including Zika virus[257]. To test if differential regulation of autophagy by PI3K contributes to differential viral maintenance in 2D and 3D cell culture, the expression of autophagy-associated genes was analyzed by RNA-Seq. The analysis showed no difference in expression of genes in neither Autophagy database[258] comprising 1383 genes nor HADb[259] comprising 232 genes (data not shown). This data indicate that it is unlikely that autophagy contributes to differential KSHV maintenance in 2D and 3D cell culture.

A recent study by McCormick showed that although mTOR is crucial for early stages of viral reactivation, its role in viral protein synthesis is dispensable[260]. The study demonstrated that translation efficiency of viral proteins is independent from eIF4F and, therefore from mTOR. This suggests that the differences observed in 2D and 3D might probably also not be attributed to regulation of protein synthesis by mTOR.

4.3.3 DNA Damage response and its role in viral maintenance

Differential viral maintenance in 2D and 3D cell culture could be a result of two independent processes, namely, an increase of viral replication in 3D cell culture or viral degradation in 2D conditions. Detection and specific degradation of episomal viral genomes by the cell thus represents an antiviral strategy. An increasing body of evidence suggests that DNA damage response can serve as a part of an intrinsic intracellular defense against viruses. KSHV triggers the DDR on various stages on viral infection and complex interactions between DDR and KSHV is illustrated in Fig.4.1. The detection of viral DNA by DDR sensors leads to the induction of several innate immune pathways, such as type-1 interferon and NF-kB.

Of note, a differential expression of genes associated to the DNA damage response pathway was not detected via RNA-Seq analysis (data not shown). However, this does not argue against an involvement of this pathway since the regulation of the pathway is mainly realized on the posttranscriptional level, such as protein phosphorylation, and therefore cannot be evaluated on the transcriptional level. Accumulating evidence shows that the activation of PI3K/Akt/mTOR regulates the DNA damage response. In the following, several hypotheses are discussed that might explain the contribution of DDR to differential viral maintenance in the various culture conditions, thereby including results from the current study as well as reports from literature.

A. The role of ATM and γH2AX

Histological studies indicate that markers of DNA damage response, such as γH2AX, pT-Chk2 and 53BP1, are also activated in early KSHV lesions[261]. H2AX phosphorylation (γH2AX), a marker of DNA damage response activation, can be detected as early as 30 minutes post-infection in primary endothelial cells and colocalizes with viral DNA[108]. The binding of γH2AX to TRs enables the tethering of viral episome to cellular chromatin via direct interaction between γH2AX and C-terminal

domain of LANA. The interaction is crucial for the establishment and maintenance of KSHV latency and its disruption, either by inhibition of H2AX phosphorylation or by mutation of the interaction cites, leads to the reduction of the viral copy number[108,262].

In line with this literature data, viral copy number can be significantly reduced by treatment with Ku55933, a small molecule inhibitor of the ATM (Fig. 3.16 B). This data confirms that ATM activity supports maintenance of latency both in 2D and 3D cell culture conditions.

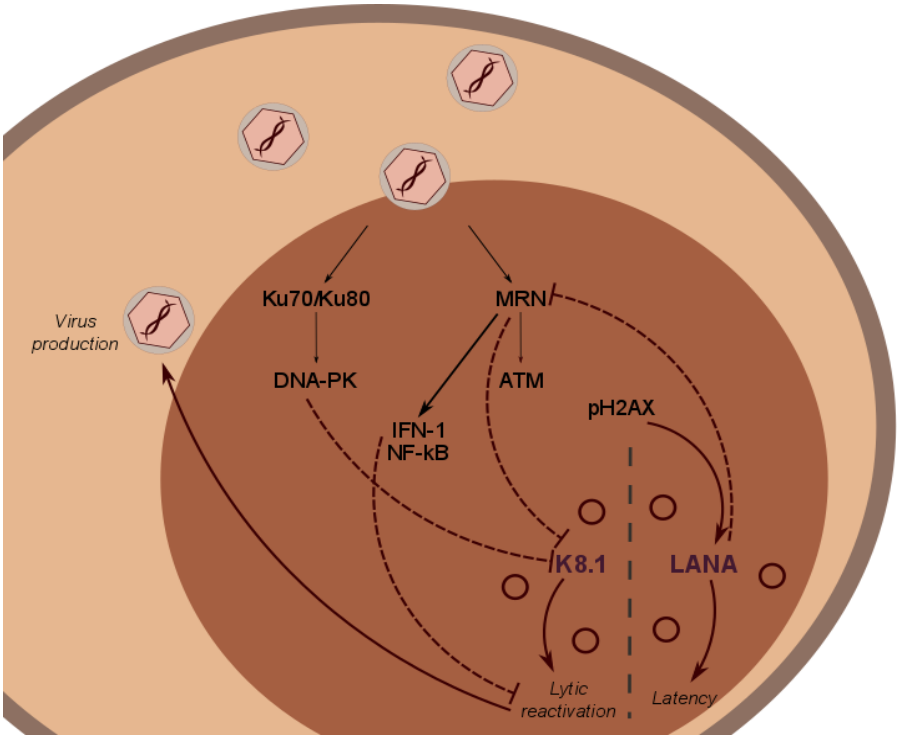

Figure 4. 1 Summary of the interplay between KSHV and DNA damage response during viral latency and reactivation (based on literature data).

B. The role of Eya phosphatases

Of note, while the expression of H2AX did not change from 2D to 3D cell culture conditions, the expression levels of Eya1, 2, and 4 are markedly reduced in 3D cell culture of rKSHV-HuARLT cells, as addressed by RNA-Seq and RT-qPCR (fig. 3.17 A and B). Recent studies suggest that phosphorylation at the Tyr142 site of H2AX determines cell death or DNA repair decisions by regulating the binding of apoptotic proteins and proteins responsible for DNA repair[93]. This observation led to the hypothesis that an increased expression of Eya in 2D cell culture conditions might restrict KSHV maintenance by an unknown mechanism. To test this hypothesis, the cells were treated with MLS000544460, a small molecule inhibitor of Eya2, but not the other Eya phosphatases[233]. This inhibitor was chosen as the only commercially available inhibitor of Eya phosphatases. If Eya2 activity were restrictive for viral maintenance in 2D, the treatment would increase the viral copy number. In contrast, the treatment with the inhibitor lead to the minor decrease in viral copy number, suggesting that Eya2 might be supportive for viral maintenance in 2D cell culture (Fig. 3.17 C). Of note, the expression levels of Eya2 was the lowest among the four

phosphatases (data not shown) and Eya1 showed the highest fold change in 3D cell culture conditions. Therefore, to finally exclude or confirm the role of the Eya phosphatases additional studies with more selective inhibitors or knockout/knockdown should be done.

C. Impact of the DNA dependent protein kinase DNA-PK

The DNA-PK complex, a heterotrimeric complex consisting of the Ku70/Ku80 heterodimer and the catalytic subunit of the DNA dependent serine protein kinase DNA-PK, was identified as a cytoplasmic sensor for DNA that is important for the innate immune response to intracellular DNA[101]. Lytic reactivation of KSHV induces ATM-CHK2 and DNA-PK response, but not ATR-CHK1, and inhibition of DDR kinases results in alterations of virus production in B cells[263]. Recent studies showed that knockdown or inhibition of Ku70/Ku80 or DNA-PK enhances the amplification of KSHV DNA, indicating that DNA-PK restricts viral replication upon lytic reactivation in the endothelial cell line EA.hy926[232]. In contrast, when the DNA-PK activity was blocked in latently infected rKSHV-HuARLT cells a reduction in viral copy number was observed, indicating that the complex supports latent viral maintenance. Moreover, no difference was observed for 2D and 3D culture conditions, suggesting that DNA-PK is not responsible for the differential maintenance of viral genomes.

D. The role of the MRN complex

Another factor contributing to DDR is the MRN complex. RPA32 and Mre11 localize to the sites of viral DNA synthesis during viral reactivation[263]. So far, its role in KSHV is controversial. One study showed that inhibition of the MRN complex by a small molecule leads to a decrease in virus production in lytically reactivated endothelial cells[232] suggesting a beneficial role of MRN for lytic replication. On the contrary, another study showed that the silencing of the MRN complex leads to increase of KSHV lytic replication in an NF-κB dependent manner in KSHV-infected B cells[109]. In addition, the study showed that LANA recruits the MRN complex to the cytosol and antagonizes MRN-induced innate immune response against KSHV, thus supporting lytic reactivation in HeLa and B cells[109]. This suggests that the MRN complex impairs lytic reactivation. Interestingly, when the role of the MRN complex was studied in rKSHV-HuARLT cells the pharmacological inhibition of MRN by mirin (Fig. 3.16) showed no effect in 3D cell culture. At the same time, the treatment showed a moderate increase in viral copy number in 2D cell culture. This observation thus supports the idea that the MRN complex has a restrictive role on KSHV maintenance in 2D cell culture (Fig 4.2 A). However, since pharmacological inhibitor studies are limited due to dose restriction, toxicity, and off-target effects, more detailed studies with a specific knockout of the components of MRN complex are needed to confirm this conclusion. This might be achieved by introducing frame-shift mutations via CRISPR-Cas9 to Mre11, Rad50 or NSB1 genes.

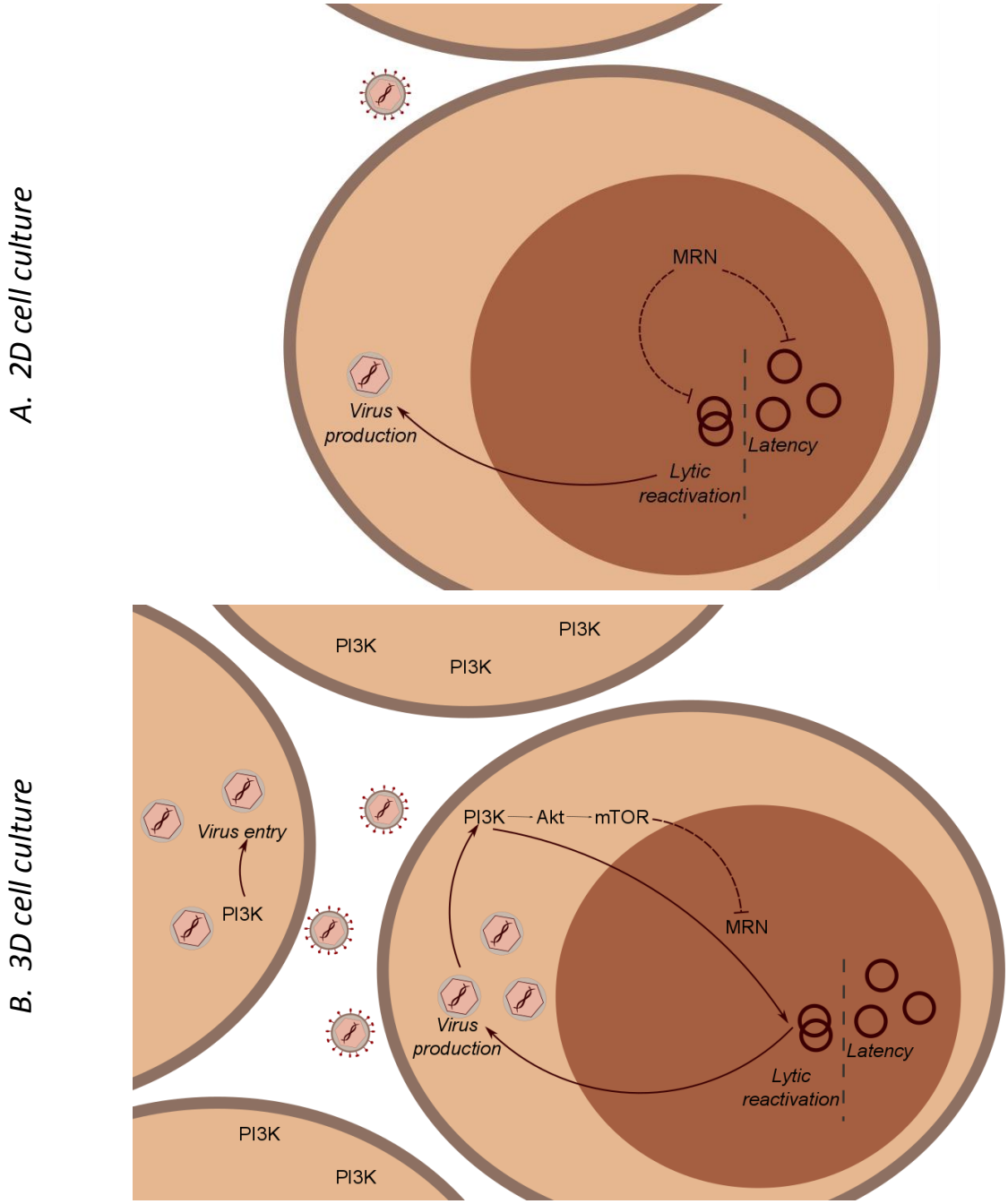

Figure 4. 2 A scheme illustrating a hypothesis of PI3K-governed maintenance.
PI3K supports KSHV reactivation and virus entry to neighboring cells. MRN-dependent viral degradation might explain loss of viral copies in 2D cell culture. Overactivation of PI3K pathway in 3D cell culture inhibits the effect of MRN complex supporting better viral maintenance.

The activation of PI3K/Akt/mTOR regulates the DNA damage response by degradation of MRN complex[264] as well as imparing activity of RNF168, a E3 ligase, which is shown to be involved in H2AX ubiquitination and amplification of the DDR signal[265]. These data suggest that upregulation of the PI3K pathway in 3D cell culture may lead to downregulation of MRN dependent response and result in increased viral maintenance (Fig. 4.2 B). Together with increased viral reactivation and dissemination, regulation of MRN might be an additional mechanism by which PI3K/Akt contributes to KSHV maintenance in 3D cell culture.

4.4. rKSHV-HuARLT cells for testing of novel antiviral compounds

Based on the rKSHV-HuARLT three in vitro tests for preselection of novel antiviral compound were developed, namely the viral copy number reduction in 2D and 3D cell culture and a 3D invasiveness assay. While 2D cell culture allowed selection of drugs targeting exclusively latent virus, 3D cell culture provided conditions in which both inhibitors of viral latent and lytic replication could be tested. The two assays were complemented with a 3D sprouting assay, which allowed direct assessment of the invasiveness of the cells in presence of the tested compounds. All three assay systems were validated by using compounds with known pharmacological targets, such as GA, PhA and rapamycin, targeting viral latent maintenance, viral DNA replication or KSHV induced invasiveness and angiogenesis, respectively. The fact that the compounds performed as predicted highlights the relevance of the system for validation of novel compounds.

A selected set of natural compounds derived from a myxobacterial library was validated for antiviral and antitumor effects using standard and advanced cell culture assays. The combination of the results of 2D and 3D in vitro assays allowed the identification of potential therapeutic candidates. These compounds were finally challenged in a humanized mouse model that allows monitoring the tumor formation of KSHV-infected human endothelial cells.

Interestingly, only the 3D invasiveness assay, but not the assays addressing viral copy number, showed high correlation with in vivo outcome, indicating high predictive power of the assay.

Although 2D cell culture is a valuable tool for high throughput drug screening and target validation, it does not fully reflect virus-induced transformation of endothelial cells and it is insufficient for viral maintenance. 3D cell culture supports conditions under which the cells obtain a more invasive phenotype, as evident by transcriptome analysis, and are able to achieve a certain level of viral reactivation, sufficient for viral maintenance. KSHV-infected endothelial cells show increased invasiveness and angiogenesis and these effects are dependent on several viral proteins expressed either during the latent (e.g. LANA[266–269], vFLIP[270], vCyc[271]) or lytic (e.g. vIL-6[272,273], vGPCR[274,275], K1[276], K15[121,277]) phase of the viral life cycle. Lytically expressed viral cytokines induce angiogenesis and invasiveness both in autocrine and paracrine manner. The drugs inducing viral loss are likely to target either viral latent genes, or viral DNA replication machinery, but not necessary have an effect on viral cytokines, which are not necessary for viral latent or lytic replication. This might explain why a simple viral copy number reduction in 2D cell culture has very poor correlation with the antitumor effect of the drugs in vivo. However, poor correlation with in vivo outcome may also be a result of non-representative drug selection. Due to restrictions in animal law, only compounds with known pharmacokinetics and pharmacodynamics could be tested. As a result, the drugs selected for the in vivo study did not include the novel compounds with the strongest effect on the viral copy number reduction.

Still, even these drugs showed a strong correlation between sprouting in 3D cell culture and tumor size reduction in vivo. However, both assays do not allow distinguishing between antitumor and antiviral effect of the compounds and are sensitive not only to the KSHV-specific drugs, but also to the drugs targeting cell motility, proliferation or survival. This highlights the need for combination of virus-specific test systems with highly predictive 3D assays for faithful pre-selection of active compounds in vitro.

Four compounds (tubulysin Y, pretubulysin D, epothilon B and stigmatellin A) that did not reduce the viral copy number but were efficient in reducing sprouting were identified with the use of the system. Tubulysin Y, pretubulysin D and epothilon B are known to interact with the cytoskeleton by acting on tubulins, thereby inducing apoptosis of proliferating cells[214,215,217,278,279], a property that qualifies these drugs as antitumor agents. Both epothilon B and pretubulysin D abolished tumor formation in the xenograft mice, which qualifies them as novel therapeutic options against KS. Although the compounds showed no KSHV-specific effect, they efficiently reduce tumor formation in vivo, outperforming rapamycin, a drug that is in clinical use for KSHV-infected organ transplant recipient with KS.

The tests also identified chondramid B that induced a moderate, but significant tumor size reduction comparable with the effect of rapamycin. This effect is in line with previously published data, characterizing chondramid B as an actin-polymerizing myxobacterial compound diminishing angiogenesis in vitro and in vivo[213]. Interestingly, in the assays chondramid B also significantly reduced the viral copy number in 2D and 3D cell culture, which suggests that in addition to antiangiogenic properties it has a specific antiviral effect. While it remains to be elucidated if the effect of chondramid B depends on its function on actin or is a result of the interaction with other molecular targets, these findings highlight chondramid B as a potential novel anti-KSHV therapeutic.

Animal tests play a crucial role in drug development, because they allow not only the confirmation of selective drug activity, but also access its pharmacokinetics, pharmacodynamics and safety in vivo. Humanized mouse models expand the toolbox and allow us to study human-specific diseases, like Kaposi's sarcoma, as well. In this study a novel humanized mouse model was developed which allows testing of novel compounds that inhibit KSHV induced tumor growth. However, animal experiments remain constrained by ethical considerations, are laborious and cost-intensive. In this regard, predictive in vitro tests are required to limit the requirement of animal experiments to a minimum. This will allow reducing the numbers of experimental animals and ensure compliance with 3R principles.

5. Outlook

This study showed that HuARLT cells reflect the properties of primary endothelial cells upon infection with KSHV, thus confirming that the cell line represent a reliable and scalable system for investigation of KSHV infection and screening of potential antiviral drugs.

In depth characterization indicated that viral maintenance is dependent on cell culture conditions and on the activity of the PI3K/mTOR pathway. Regulation of MRN stability by mTOR might represent one of the molecular mechanisms governing viral stability in 3D cell culture, however the results have to be confirmed with the other methods. Also, the detailed molecular mechanisms that govern MRN-dependent virus degradation need to be further investigated.

The system was used to validate anti-KS activity a selection of natural metabolites. To this end, the ability of the compounds to reduce viral load and invasiveness of the infected cells was evaluated in vitro. Based on the in vitro performance, three compounds were selected for test in humanized mouse model. In vivo tests revealed that the selected compounds reduce tumor size with similar or greater effect than rapamycin, which is clinically used to treat post-transplantation KS. This result shows the power of the system to validate novel potent KS therapeutics. Two out of the compound, which showed high potency in vivo, have no effect on KSHV maintenance, indication that they might not antiviral, but rather antitumor drugs. Screening of a bigger compound library will allow identification of specific antiviral compounds and establishment of targeted KS therapy.

This study showed that HuARLT cell line closely mimicked the properties of primary endothelial cells and allowed investigation of endothelial-specific infection in vitro and in vivo. This indicates the potential of the system to be extended to other endothelial-specific pathogens. In particular, the cell line is permissive for human cytomegalovirus infection and the cells support full replication cycle of the virus. With the use of the cells line the change of the cellular phenotype upon hCMV infection can be further investigated. Similar to KSHV, hCMV is a human-specific virus and therefore has no small animal model available. The potential of HuARLT cells to mimic hCMV infection in vivo and be used for validation of novel hCMV drugs has to be evaluated in the further studies.

References

1. Sternbach, G. & Varon, J. Moritz Kaposi: Idiopathic pigmented sarcoma of the skin. *J. Emerg. Med.* **13,** 671–674 (1995).
2. Friedman-Kien, A. E. Disseminated Kaposi's sarcoma syndrome in young homosexual men. *J. Am. Acad. Dermatol.* **5,** 468–471 (1981).
3. Chang, Y. *et al.* Identification of herpesvirus-like DNA sequences in AIDS-associated Kaposi's sarcoma. *Science* **266,** 1865–9 (1994).
4. IARC Monographs on the Evaluation of Carcinogenic Risks to Humans. in *A review on human cancerogens. Part B: biological agents.* **100B,** 169–214 (International Agency for research on Cancer, World Health Organization, 2012).
5. International Committee on Taxonomy of Viruses (ICTV). Available at: https://talk.ictvonline.org/taxonomy/. (Accessed: 31st May 2018)
6. Chakraborty, S., Veettil, M. V. & Chandran, B. Kaposi's Sarcoma Associated Herpesvirus Entry into Target Cells. *Front. Microbiol.* **3,** 6 (2012).
7. Wu, L. *et al.* Three-Dimensional Structure of the Human Herpesvirus 8 Capsid. *J Virol* **74,** 9646–9654 (2000).
8. Deng, B., O'Connor, C. M., Kedes, D. H. & Zhou, Z. H. Cryo-electron tomography of Kaposi's sarcoma-associated herpesvirus capsids reveals dynamic scaffolding structures essential to capsid assembly and maturation. *J. Struct. Biol.* **161,** 419–427 (2008).
9. Russo, J. J. *et al.* Nucleotide sequence of the Kaposi sarcoma-associated herpesvirus (HHV8). *Proc. Natl. Acad. Sci. U. S. A.* **93,** 14862–7 (1996).
10. Barbera, A. J. *et al.* The Nucleosomal Surface as a Docking Station for Kaposi's Sarcoma Herpesvirus LANA. *Science (80-.).* **311,** 856–861 (2006).
11. Ballestas, M. E., Chatis, P. A. & Kaye, K. M. Efficient persistence of extrachromosomal KSHV DNA mediated by latency-associated nuclear antigen. *Science* **284,** 641–4 (1999).
12. Mesri, E. a, Cesarman, E. & Boshoff, C. Kaposi's sarcoma and its associated herpesvirus. *Nat. Rev. Cancer* **10,** 707–19 (2010).
13. Chang, H. *et al.* Non-human primate model of Kaposi's sarcoma-associated herpesvirus infection. *PLoS Pathog.* **5,** e1000606 (2009).
14. Kumar, B. & Chandran, B. KSHV entry and trafficking in target cells - Hijacking of cell signal pathways,actin and membrane dynamics. *Viruses* **8,** 305 (2016).
15. Veettil, M., Bandyopadhyay, C., Dutta, D. & Chandran, B. Interaction of KSHV with Host Cell Surface Receptors and Cell Entry. *Viruses* **6,** 4024–4046 (2014).
16. Raghu, H., Sharma-Walia, N., Veettil, M. V., Sadagopan, S. & Chandran, B. Kaposi's sarcoma-associated herpesvirus utilizes an actin polymerization-dependent macropinocytic pathway to enter human dermal microvascular endothelial and human umbilical vein endothelial cells. *J. Virol.* **83,** 4895–911 (2009).
17. Inoue, N., Winter, J., Lal, R. B., Offermann, M. K. & Koyano, S. Characterization of entry

mechanisms of human herpesvirus 8 by using an Rta-dependent reporter cell line. *J. Virol.* **77,** 8147–52 (2003).

18. Veettil, M. V. *et al.* RhoA-GTPase facilitates entry of Kaposi's sarcoma-associated herpesvirus into adherent target cells in a Src-dependent manner. *J. Virol.* **80,** 11432–46 (2006).
19. Naranatt, P. P., Krishnan, H. H., Smith, M. S. & Chandran, B. Kaposi's sarcoma-associated herpesvirus modulates microtubule dynamics via RhoA-GTP-diaphanous 2 signaling and utilizes the dynein motors to deliver its DNA to the nucleus. *J. Virol.* **79,** 1191–206 (2005).
20. Naranatt, P. P., Akula, S. M., Zien, C. A., Krishnan, H. H. & Chandran, B. Kaposi's sarcoma-associated herpesvirus induces the phosphatidylinositol 3-kinase-PKC-zeta-MEK-ERK signaling pathway in target cells early during infection: implications for infectivity. *J. Virol.* **77,** 1524–39 (2003).
21. Purushothaman, P., Thakker, S. & Verma, S. C. Transcriptome analysis of Kaposi's sarcoma-associated herpesvirus during de novo primary infection of human B and endothelial cells. *J. Virol.* **89,** 3093–111 (2015).
22. Li, Q., Zhou, F., Ye, F. & Gao, S.-J. J. Genetic disruption of KSHV major latent nuclear antigen LANA enhances viral lytic transcriptional program. *Virology* **379,** 234–244 (2008).
23. Lan, K., Kuppers, D. A. & Robertson, E. S. Kaposi's sarcoma-associated herpesvirus reactivation is regulated by interaction of latency-associated nuclear antigen with recombination signal sequence-binding protein Jkappa, the major downstream effector of the Notch signaling pathway. *J. Virol.* **79,** 3468–78 (2005).
24. Lu, F., Day, L., Gao, S.-J. & Lieberman, P. M. Acetylation of the latency-associated nuclear antigen regulates repression of Kaposi's sarcoma-associated herpesvirus lytic transcription. *J. Virol.* **80,** 5273–82 (2006).
25. Cai, Q. *et al.* Kaposi's sarcoma herpesvirus upregulates Aurora A expression to promote p53 phosphorylation and ubiquitylation. *PLoS Pathog.* **8,** (2012).
26. Chen, W., Hilton, I. B., Staudt, M. R., Burd, C. E. & Dittmer, D. P. Distinct p53, p53:LANA, and LANA complexes in Kaposi's Sarcoma--associated Herpesvirus Lymphomas. *J. Virol.* **84,** 3898–3908 (2010).
27. Radkov, S. A., Kellam, P. & Boshoff, C. The latent nuclear antigen of Kaposi sarcoma-associated herpesvirus targets the retinoblastoma-E2F pathway and with the oncogene Hras transforms primary rat cells. *Nat. Med.* **6,** 1121–7 (2000).
28. Di Bartolo, D. L. *et al.* KSHV LANA inhibits TGF-beta signaling through epigenetic silencing of the TGF-beta type II receptor. *Blood* **111,** 4731–40 (2008).
29. Cai, Q. *et al.* Kaposi's sarcoma-associated herpesvirus latent protein LANA interacts with HIF-1 alpha to upregulate RTA expression during hypoxia: Latency control under low oxygen conditions. *J. Virol.* **80,** 7965–75 (2006).
30. Alkharsah, K. R. *et al.* Deletion of Kaposi's sarcoma-associated herpesvirus FLICE inhibitory protein, vFLIP, from the viral genome compromises the activation of STAT1-responsive cellular

genes and spindle cell formation in endothelial cells. *J. Virol.* **85,** 10375–88 (2011).

31. Liu, L. *et al.* The human herpes virus 8-encoded viral FLICE inhibitory protein physically associates with and persistently activates the Ikappa B kinase complex. *J. Biol. Chem.* **277,** 13745–51 (2002).
32. Guasparri, I., Keller, S. A. & Cesarman, E. KSHV vFLIP is essential for the survival of infected lymphoma cells. *J. Exp. Med.* **199,** 993–1003 (2004).
33. Chen, X. *et al.* Human immunodeficiency virus type 1 Tat accelerates Kaposi sarcoma-associated herpesvirus Kaposin A-mediated tumorigenesis of transformed fibroblasts in vitro as well as in nude and immunocompetent mice. *Neoplasia* **11,** 1272–84 (2009).
34. Li, X., Feng, J. & Sun, R. Oxidative Stress Induces Reactivation of Kaposi's Sarcoma-Associated Herpesvirus and Death of Primary Effusion Lymphoma Cells. *J. Virol.* **85,** 715–724 (2011).
35. Ye, F. *et al.* Reactive Oxygen Species Hydrogen Peroxide Mediates Kaposi's Sarcoma-Associated Herpesvirus Reactivation from Latency. *PLoS Pathog.* **7,** e1002054 (2011).
36. Zhang, L. *et al.* Inhibition of KAP1 enhances hypoxia-induced Kaposi's sarcoma-associated herpesvirus reactivation through RBP-Jkappa. *J. Virol.* **88,** 6873–6884 (2014).
37. Purushothaman, P., Uppal, T. & Verma, S. C. Molecular biology of KSHV lytic reactivation. *Viruses* **7,** 116–53 (2015).
38. Qin, D. *et al.* Activation of PI3K/AKT and ERK MAPK signal pathways is required for the induction of lytic cycle replication of Kaposi's sarcoma-associated herpesvirus by herpes simplex virus type 1. *BMC Microbiol.* **11,** 240 (2011).
39. Zhu, X. *et al.* Human immunodeficiency virus type 1 induces lytic cycle replication of Kaposi's-sarcoma-associated herpesvirus: role of Ras/c-Raf/MEK1/2, PI3K/AKT, and NF-kappaB signaling pathways. *J. Mol. Biol.* **410,** 1035–1051 (2011).
40. Shin, H. J., DeCotiis, J., Giron, M., Palmeri, D. & Lukac, D. M. Histone Deacetylase Classes I and II Regulate Kaposi's Sarcoma-Associated Herpesvirus Reactivation. *J. Virol.* **88,** 1281–1292 (2014).
41. Li, Q., He, M., Zhou, F., Ye, F. & Gao, S.-J. Activation of Kaposi's Sarcoma-Associated Herpesvirus (KSHV) by Inhibitors of Class III Histone Deacetylases: Identification of Sirtuin 1 as a Regulator of the KSHV Life Cycle. *J. Virol.* **88,** 6355–6367 (2014).
42. Lin, C. L. *et al.* Kaposi's sarcoma-associated herpesvirus lytic origin (ori-Lyt)-dependent DNA replication: identification of the ori-Lyt and association of K8 bZip protein with the origin. *J. Virol.* **77,** 5578–88 (2003).
43. Song, M. J., Deng, H. & Sun, R. Comparative study of regulation of RTA-responsive genes in Kaposi's sarcoma-associated herpesvirus/human herpesvirus 8. *J. Virol.* **77,** 9451–62 (2003).
44. Lukac, D. M., Renne, R., Kirshner, J. R. & Ganem, D. Reactivation of Kaposi's sarcoma-associated herpesvirus infection from latency by expression of the ORF 50 transactivator, a homolog of the EBV R protein. *Virology* **252,** 304–12 (1998).
45. Sun, R. *et al.* A viral gene that activates lytic cycle expression of Kaposi's sarcoma-associated

herpesvirus. *Proc. Natl. Acad. Sci. U. S. A.* **95,** 10866–71 (1998).

46. Gradoville, L. *et al.* Kaposi's sarcoma-associated herpesvirus open reading frame 50/Rta protein activates the entire viral lytic cycle in the HH-B2 primary effusion lymphoma cell line. *J. Virol.* **74,** 6207–12 (2000).
47. Izumiya, Y. *et al.* Kaposi's sarcoma-associated herpesvirus K-bZIP is a coregulator of K-Rta: physical association and promoter-dependent transcriptional repression. *J. Virol.* **77,** 1441–51 (2003).
48. Ganem, H. H. C. and D. A unique herpesviral transcriptional program in KSHV-infected lymphatic endothelial cells leads to mTORC1 activation and rapamycin sensitivity. *Cell Host Microbe* **144,** 724–732 (2013).
49. Ojala, P. M. & Schulz, T. F. *Manipulation of endothelial cells by KSHV: Implications for angiogenesis and aberrant vascular differentiation*. *Seminars in Cancer Biology* **26,** 69–77 (2014).
50. Mariggiò, G., Koch, S. & Schulz, T. F. Kaposi sarcoma herpesvirus pathogenesis. *Philos. Trans. R. Soc. B Biol. Sci.* **372,** 20160275 (2017).
51. Gramolelli, S. & Ojala, P. M. Kaposi's sarcoma herpesvirus-induced endothelial cell reprogramming supports viral persistence and contributes to Kaposi's sarcoma tumorigenesis. *Curr. Opin. Virol.* **26,** 156–162 (2017).
52. Gallo, R. C. The enigmas of Kaposi's sarcoma. *Science* **282,** 1837–9 (1998).
53. Beral, V., Peterman, T. A., Berkelman, R. L. & Jaffe, H. W. Kaposi's sarcoma among persons with AIDS: a sexually transmitted infection? *Lancet* **335,** 123–128 (1990).
54. Antman, K. & Chang, Y. Kaposi's Sarcoma. *N. Engl. J. Med.* **342,** 1027–1038 (2000).
55. Wabinga, H. R. *et al.* Trends in the incidence of cancer in Kampala, Uganda 1991-2010. *Int. J. Cancer* **135,** 432–439 (2014).
56. Dupin, N. *et al.* Herpesvirus-like DNA sequences in patients with Mediterranean Kaposi's sarcoma. *Lancet* **345,** 761–762 (1995).
57. Boshoff, C. *et al.* Kaposi's sarcoma-associated herpesvirus infects endothelial and spindle cells. *Nat. Med.* **1,** 1274–1278 (1995).
58. Staskus, K. A. *et al.* Kaposi's sarcoma-associated herpesvirus gene expression in endothelial (spindle) tumor cells. *J. Virol.* **71,** 715–719 (1997).
59. Dupin, N. *et al.* Distribution of human herpesvirus-8 latently infected cells in Kaposi's sarcoma, multicentric Castleman's disease, and primary effusion lymphoma. *Proc. Natl. Acad. Sci. U. S. A.* **96,** 4546–4551 (1999).
60. Regezi, J. A. *et al.* Oral Kaposi's sarcoma: a 10-year retrospective histopathologic study. *J. oral Pathol. Med. Off. Publ. Int. Assoc. Oral Pathol. Am. Acad. Oral Pathol.* **22,** 292–297 (1993).
61. Pyakurel, P. *et al.* Lymphatic and vascular origin of Kaposi's sarcoma spindle cells during tumor development. *Int. J. cancer* **119,** 1262–1267 (2006).
62. Jussila, L. *et al.* Lymphatic Endothelium and Kaposi's Sarcoma Spindle Cells Detected by Antibodies against the Vascular Endothelial Growth Factor Receptor-3. *Cancer Res.* **58,** 1599 LP-

1604 (1998).

63. Ramirez-Amador, V., Martinez-Mata, G., Gonzalez-Ramirez, I., Anaya-Saavedra, G. & de Almeida, O. P. Clinical, histological and immunohistochemical findings in oral Kaposi's sarcoma in a series of Mexican AIDS patients. Comparative study. *J. oral Pathol. Med. Off. Publ. Int. Assoc. Oral Pathol. Am. Acad. Oral Pathol.* **38,** 328–333 (2009).
64. Dubina, M. & Goldenberg, G. Positive staining of tumor-stage Kaposi sarcoma with lymphatic marker D2-40. *J. Am. Acad. Dermatol.* **61,** 276–280 (2009).
65. Kahn, H. J., Bailey, D. & Marks, A. Monoclonal antibody D2-40, a new marker of lymphatic endothelium, reacts with Kaposi's sarcoma and a subset of angiosarcomas. *Mod. Pathol. an Off. J. United States Can. Acad. Pathol. Inc* **15,** 434–440 (2002).
66. Gessain, A. & Duprez, R. Spindle cells and their role in Kaposi's sarcoma. *Int. J. Biochem. Cell Biol.* **37,** 2457–2465 (2005).
67. Mesri, E. A. & Cesarman, E. Kaposi's sarcoma herpesvirus oncogenesis is a notch better in 3D. *Cell Host and Microbe* **10,** 529–531 (2011).
68. Schulz, T. F. & Chang, Y. *KSHV gene expression and regulation*. *Human Herpesviruses: Biology, Therapy, and Immunoprophylaxis* (2007).
69. Wang, H.-W. W. *et al.* Kaposi sarcoma herpesvirus-induced cellular reprogramming contributes to the lymphatic endothelial gene expression in Kaposi sarcoma. *Nat Genet* **36,** 687–693 (2004).
70. Hong, Y.-K. *et al.* Lymphatic reprogramming of blood vascular endothelium by Kaposi sarcoma-associated herpesvirus. *Nat. Genet.* **36,** 683–685 (2004).
71. Carroll, P. A., Brazeau, E. & Lagunoff, M. Kaposi's sarcoma-associated herpesvirus infection of blood endothelial cells induces lymphatic differentiation. *Virology* **328,** 7–18 (2004).
72. Morris, V. A., Punjabi, A. S. & Lagunoff, M. Activation of Akt through gp130 receptor signaling is required for Kaposi's sarcoma-associated herpesvirus-induced lymphatic reprogramming of endothelial cells. *J. Virol.* **82,** 8771–9 (2008).
73. Morris, V. A. *et al.* The KSHV viral IL-6 homolog is sufficient to induce blood to lymphatic endothelial cell differentiation. *Virology* **428,** 112–120 (2012).
74. McCormick, C. & Ganem, D. The Kaposin B Protein of KSHV Activates the p38/MK2 Pathway and Stabilizes Cytokine mRNAs. *Science (80-.).* **307,** 739–741 (2005).
75. Yoo, J. *et al.* Kaposin-B Enhances the PROX1 mRNA Stability during Lymphatic Reprogramming of Vascular Endothelial Cells by Kaposi's Sarcoma Herpes Virus. *PLOS Pathog.* **6,** e1001046 (2010).
76. Yoo, J. *et al.* Opposing Regulation of PROX1 by Interleukin-3 Receptor and NOTCH Directs Differential Host Cell Fate Reprogramming by Kaposi Sarcoma Herpes Virus. *PLoS Pathog.* **8,** e1002770 (2012).
77. Hansen, A. *et al.* KSHV-encoded miRNAs target MAF to induce endothelial cell reprogramming. *Genes Dev.* **24,** 195–205 (2010).
78. Icardo, J. M. & Manasek, F. J. An indirect immunofluorescence study of the distribution of

fibronectin during the formation of the cushion tissue mesenchyme in the embryonic heart. *Dev. Biol.* **101,** 336–345 (1984).

79. Nakajima, Y., Yamagishi, T., Hokari, S. & Nakamura, H. Mechanisms involved in valvuloseptal endocardial cushion formation in early cardiogenesis: roles of transforming growth factor (TGF)-beta and bone morphogenetic protein (BMP). *Anat. Rec.* **258,** 119–127 (2000).
80. Ranchoux, B. *et al.* Endothelial-to-mesenchymal transition in pulmonary hypertension. *Circulation* **131,** 1006–1018 (2015).
81. Maddaluno, L. *et al.* EndMT contributes to the onset and progression of cerebral cavernous malformations. *Nature* **498,** 492–496 (2013).
82. Aisagbonhi, O. *et al.* Experimental myocardial infarction triggers canonical Wnt signaling and endothelial-to-mesenchymal transition. *Dis. Model. Mech.* **4,** 469–483 (2011).
83. Zeisberg, E. M., Potenta, S., Xie, L., Zeisberg, M. & Kalluri, R. Discovery of endothelial to mesenchymal transition as a source for carcinoma-associated fibroblasts. *Cancer Res.* **67,** 10123–10128 (2007).
84. Gasperini, P. *et al.* Kaposi sarcoma herpesvirus promotes endothelial-to-mesenchymal transition through notch-dependent signaling. *Cancer Res.* **72,** 1157–1169 (2012).
85. Moses, A. V *et al.* Long-term infection and transformation of dermal microvascular endothelial cells by human herpesvirus 8. *J. Virol.* **73,** 6892–902 (1999).
86. Cheng, F. *et al.* KSHV-initiated notch activation leads to membrane-type-1 matrix metalloproteinase-dependent lymphatic endothelial-to-mesenchymal transition. *Cell Host Microbe* **10,** 577–590 (2011).
87. Hanahan, D. & Weinberg, R. A. Hallmarks of cancer: the next generation. *Cell* **144,** 646–674 (2011).
88. Dupre, A., Boyer-Chatenet, L. & Gautier, J. Two-step activation of ATM by DNA and the Mre11-Rad50-Nbs1 complex. *Nat. Struct. Mol. Biol.* **13,** 451–457 (2006).
89. Petrini, J. H. J. & Stracker, T. H. The cellular response to DNA double-strand breaks: defining the sensors and mediators. *Trends Cell Biol.* **13,** 458–462 (2003).
90. Lou, Z. *et al.* MDC1 maintains genomic stability by participating in the amplification of ATM-dependent DNA damage signals. *Mol. Cell* **21,** 187–200 (2006).
91. Zou, L. & Elledge, S. J. Sensing DNA damage through ATRIP recognition of RPA-ssDNA complexes. *Science* **300,** 1542–1548 (2003).
92. Xiao, A. *et al.* WSTF regulates the H2A . X DNA damage response via a novel tyrosine kinase activity. *Nature* **457,** 57–64 (2008).
93. Cook, P. J. *et al.* Tyrosine dephosphorylation of H2AX modulates apoptosis and survival decisions. *Nature* **458,** 591–596 (2009).
94. Cruz-Garcia, A., Lopez-Saavedra, A. & Huertas, P. BRCA1 accelerates CtIP-mediated DNA-end resection. *Cell Rep.* **9,** 451–459 (2014).
95. Nicolette, M. L. *et al.* Mre11-Rad50-Xrs2 and Sae2 promote 5’ strand resection of DNA double-

strand breaks. *Nat. Struct. Mol. Biol.* **17,** 1478–1485 (2010).

96. Sung, P. Catalysis of ATP-dependent homologous DNA pairing and strand exchange by yeast RAD51 protein. *Science* **265,** 1241–1243 (1994).
97. Kim, T. *et al.* Activation of interferon regulatory factor 3 in response to DNA-damaging agents. *J. Biol. Chem.* **274,** 30686–30689 (1999).
98. Brzostek-Racine, S., Gordon, C., Van Scoy, S. & Reich, N. C. The DNA damage response induces IFN. *J. Immunol.* **187,** 5336–5345 (2011).
99. Wu, Z.-H., Shi, Y., Tibbetts, R. S. & Miyamoto, S. Molecular linkage between the kinase ATM and NF-kappaB signaling in response to genotoxic stimuli. *Science* **311,** 1141–1146 (2006).
100. Kondo, T. *et al.* DNA damage sensor MRE11 recognizes cytosolic double-stranded DNA and induces type I interferon by regulating STING trafficking. *Proc. Natl. Acad. Sci. U. S. A.* **110,** 2969–2974 (2013).
101. Peters, N. E. *et al.* A mechanism for the inhibition of DNA-PK-mediated DNA sensing by a virus. *PLoS Pathog.* **9,** e1003649 (2013).
102. Roth, S. *et al.* Rad50-CARD9 interactions link cytosolic DNA sensing to IL-1beta production. *Nat. Immunol.* **15,** 538–545 (2014).
103. Ansari, M. A. *et al.* Herpesvirus Genome Recognition Induced Acetylation of Nuclear IFI16 Is Essential for Its Cytoplasmic Translocation, Inflammasome and IFN-beta Responses. *PLoS Pathog.* **11,** e1005019 (2015).
104. Luftig, M. A. Viruses and the DNA Damage Response: Activation and Antagonism. *Annu. Rev. Virol.* **1,** 605–625 (2014).
105. Hollingworth, R. & Grand, R. J. Modulation of DNA damage and repair pathways by human tumour viruses. *Viruses* **7,** 2542–2591 (2015).
106. Lilley, C. E., Schwartz, R. A. & Weitzman, M. D. Using or abusing: viruses and the cellular DNA damage response. *Trends Microbiol.* **15,** 119–126 (2007).
107. Weitzman, M. D., Carson, C. T., Schwartz, R. A. & Lilley, C. E. Interactions of viruses with the cellular DNA repair machinery. *DNA Repair (Amst).* **3,** 1165–1173 (2004).
108. Singh, V. V., Dutta, D., Ansari, M. A., Dutta, S. & Chandran, B. Kaposi's sarcoma-associated herpesvirus induces the ATM and H2AX DNA damage response early during de novo infection of primary endothelial cells, which play roles in latency establishment. *J. Virol.* **88,** 2821–34 (2014).
109. Mariggio, G. *et al.* Kaposi Sarcoma Herpesvirus (KSHV) Latency-Associated Nuclear Antigen (LANA) recruits components of the MRN (Mre11-Rad50-NBS1) repair complex to modulate an innate immune signaling pathway and viral latency. *PLoS Pathog.* **13,** e1006335 (2017).
110. Döme, B., Hendrix, M. J. C., Paku, S., Tóvári, J. & Tímár, J. Alternative Vascularization Mechanisms in Cancer: Pathology and Therapeutic Implications. *Am. J. Pathol.* **170,** 1–15 (2007).
111. Kirschmann, D. A., Seftor, E. A., Hardy, K. M., Seftor, R. E. B. & Hendrix, M. J. C. Molecular pathways: vasculogenic mimicry in tumor cells: diagnostic and therapeutic implications. *Clin. Cancer Res.* **18,** 2726–32 (2012).

112. Orenstein, J. M. Ultrastructure of Kaposi Sarcoma. *Ultrastruct. Pathol.* **32,** 211–220 (2008).
113. Cornali, E. *et al.* Vascular endothelial growth factor regulates angiogenesis and vascular permeability in Kaposi's sarcoma. *Am. J. Pathol.* **149,** 1851–69 (1996).
114. Samaniego, F. *et al.* Vascular endothelial growth factor and Kaposi's sarcoma cells in human skin grafts. *Cell Growth Differ.* **13,** 387–95 (2002).
115. Bais, C. *et al.* G-protein-coupled receptor of Kaposi's sarcoma-associated herpesvirus is a viral oncogene and angiogenesis activator. *Nature* **391,** 86–9 (1998).
116. Wang, L., Dittmer, D. P., Tomlinson, C. C., Fakhari, F. D. & Damania, B. Immortalization of primary endothelial cells by the K1 protein of Kaposi's sarcoma-associated herpesvirus. *Cancer Res.* **66,** 3658–66 (2006).
117. Bais, C. *et al.* Kaposi's sarcoma associated herpesvirus G protein-coupled receptor immortalizes human endothelial cells by activation of the VEGF receptor-2/ KDR. *Cancer Cell* **3,** 131–43 (2003).
118. Jham, B. C. *et al.* Amplification of the Angiogenic Signal through the Activation of the TSC/mTOR/HIF Axis by the KSHV vGPCR in Kaposi's Sarcoma. *PLoS One* **6,** e19103 (2011).
119. Sodhi, A. *et al.* The Kaposi's sarcoma-associated herpes virus G protein-coupled receptor up-regulates vascular endothelial growth factor expression and secretion through mitogen-activated protein kinase and p38 pathways acting on hypoxia-inducible factor 1alpha. *Cancer Res.* **60,** 4873–80 (2000).
120. Vart, R. J. *et al.* Kaposi's sarcoma-associated herpesvirus-encoded interleukin-6 and G-protein-coupled receptor regulate angiopoietin-2 expression in lymphatic endothelial cells. *Cancer Res.* **67,** 4042–51 (2007).
121. Bala, K. *et al.* Kaposi's Sarcoma Herpesvirus K15 Protein Contributes to Virus-Induced Angiogenesis by Recruiting PLCγ1 and Activating NFAT1-dependent RCAN1 Expression. *PLoS Pathog.* **8,** (2012).
122. He, M. *et al.* Cancer angiogenesis induced by Kaposi sarcoma-associated herpesvirus is mediated by EZH2. **72,** (2012).
123. Fatahzadeh, M. Kaposi sarcoma: review and medical management update. *Oral Surg. Oral Med. Oral Pathol. Oral Radiol.* **113,** 2–16 (2012).
124. Coen, N., Duraffour, S., Snoeck, R. & Andrei, G. KSHV targeted therapy: An update on inhibitors of viral lytic replication. *Viruses* **6,** 4731–4759 (2014).
125. Szajerka, T. & Jablecki, J. Kaposi's sarcoma revisited. *AIDS Rev.* **9,** 230–6 (2007).
126. Bourboulia, D. *et al.* Short- and long-term effects of highly active antiretroviral therapy on Kaposi sarcoma-associated herpesvirus immune responses and viraemia. *AIDS* **18,** 485–93 (2004).
127. Monini, P., Sgadari, C., Toschi, E., Barillari, G. & Ensoli, B. Antitumour effects of antiretroviral therapy. *Nat. Rev. Cancer* **4,** 861–875 (2004).
128. Sgadari, C., Monini, P., Barillari, G. & Ensoli, B. Use of HIV protease inhibitors to block Kaposi's sarcoma and tumour growth. *Lancet. Oncol.* **4,** 537–47 (2003).

129. Lock, M. J., Thorley, N., Teo, J. & Emery, V. C. Azidodeoxythymidine and didehydrodeoxythymidine as inhibitors and substrates of the human herpesvirus 8 thymidine kinase. *J. Antimicrob. Chemother.* **49,** 359–66 (2002).

130. Krown, S. E., Lee, J. Y. & Dittmer, D. P. More on HIV-Associated Kaposi's Sarcoma. *N. Engl. J. Med.* **358,** 535–536 (2008).

131. Maurer, T., Ponte, M. & Leslie, K. HIV-Associated Kaposi's Sarcoma with a High CD4 Count and a Low Viral Load. *N. Engl. J. Med.* **357,** 1352–1353 (2007).

132. Nguyen, H. Q. *et al.* Persistent Kaposi sarcoma in the era of highly active antiretroviral therapy: characterizing the predictors of clinical response. *AIDS* **22,** 937–45 (2008).

133. Martellotta, F. *et al.* AIDS-related Kaposi's sarcoma: state of the art and therapeutic strategies. *Curr. HIV Res.* **7,** 634–8 (2009).

134. Vanni, T. *et al.* Systemic treatment of AIDS-related Kaposi sarcoma: Current status and perspectives. *Cancer Treat. Rev.* **32,** 445–455 (2006).

135. Von Roenn, J. H. Clinical presentations and standard therapy of AIDS-associated Kaposi's sarcoma. *Hematol. Oncol. Clin. North Am.* **17,** 747–762 (2003).

136. Kedes, D. H. & Ganem, D. Sensitivity of Kaposi's sarcoma-associated herpesvirus replication to antiviral drugs. Implications for potential therapy. *J. Clin. Invest.* **99,** 2082–2086 (1997).

137. Glesby, M. J. *et al.* Use of antiherpes drugs and the risk of Kaposi's sarcoma: data from the Multicenter AIDS Cohort Study. *J. Infect. Dis.* **173,** 1477–80 (1996).

138. Mocroft, A. *et al.* Anti-herpesvirus treatment and risk of Kaposi's sarcoma in HIV infection. Royal Free/Chelsea and Westminster Hospitals Collaborative Group. *AIDS* **10,** 1101–5 (1996).

139. Guba, M. *et al.* Rapamycin inhibits primary and metastatic tumor growth by antiangiogenesis: involvement of vascular endothelial growth factor. *Nat. Med.* **8,** 128–135 (2002).

140. Sodhi, A. *et al.* The TSC2/mTOR pathway drives endothelial cell transformation induced by the Kaposi's sarcoma-associated herpesvirus G protein-coupled receptor. *Cancer Cell* **10,** 133–143 (2006).

141. Wang, L. & Damania, B. Kaposi's sarcoma-associated herpesvirus confers a survival advantage to endothelial cells. *Cancer Res.* **68,** 4640–4648 (2008).

142. Stallone, G. *et al.* Sirolimus for Kaposi's sarcoma in renal-transplant recipients. *N. Engl. J. Med.* **352,** 1317–1323 (2005).

143. Little, R. F. *et al.* Activity of thalidomide in AIDS-related Kaposi's sarcoma. *J. Clin. Oncol.* **18,** 2593–602 (2000).

144. Heckman, C. A. *et al.* The tyrosine kinase inhibitor cediranib blocks ligand-induced vascular endothelial growth factor receptor-3 activity and lymphangiogenesis. *Cancer Res.* **68,** 4754–4762 (2008).

145. Ardavanis, A., Doufexis, D., Kountourakis, P. & Rigatos, G. A Kaposi's sarcoma complete clinical response after sorafenib administration. *Ann. Oncol.* **19,** 1658–1659 (2008).

146. Levine, A. M. *et al.* Phase I Study of Antisense Oligonucleotide Against Vascular Endothelial

Growth Factor: Decrease in Plasma Vascular Endothelial Growth Factor With Potential Clinical Efficacy. *J. Clin. Oncol.* **24,** 1712–1719 (2006).

147. Basciani, S. *et al.* Imatinib interferes with survival of multi drug resistant Kaposi's sarcoma cells. *FEBS Lett.* **581,** 5897–903 (2007).
148. Cianfrocca, M. *et al.* Matrix Metalloproteinase Inhibitor COL-3 in the Treatment of AIDS-Related Kaposi's Sarcoma: A Phase I AIDS Malignancy Consortium Study. *J. Clin. Oncol.* **20,** 153–159 (2002).
149. Beauchemin, C., Moerke, N. J., Faloon, P. & Kaye, K. M. ASSAY DEVELOPMENT AND HIGH THROUGHPUT SCREENING FOR INHIBITORS OF KAPOSI â€™ S SARCOMA-ASSOCIATED. **19,** 947–958 (2015).
150. Thompson, S., Messick, T., Schultz, D. C., Reichman, M. & Paul, M. Development of a High-Throughput Screen for Inhibitors of Epstein-Barr Virus EBNA1. **15,** 1107–1115 (2012).
151. Dorjsuren, D. *et al.* Chemical library screen for novel inhibitors of Kaposi's sarcoma-associated herpesvirus processive DNA synthesis. *Antiviral Res.* **69,** 9–23 (2006).
152. Bronstein, J. C. & Weber, P. C. A Colorimetric Assay for High-Throughput Screening of Inhibitors of Herpes Simplex Virus Type 1 Alkaline Nuclease. **245,** 239–245 (2001).
153. Lebbe, C. *et al.* Characterization of in vitro culture of HIV-negative Kaposi's sarcoma-derived cells. In vitro responses to alfa interferon. *Arch. Dermatol. Res.* **289,** 421–428 (1997).
154. Dictor, M., Rambech, E., Way, D., Witte, M. & Bendsoe, N. Human herpesvirus 8 (Kaposi's sarcoma-associated herpesvirus) DNA in Kaposi's sarcoma lesions, AIDS Kaposi's sarcoma cell lines, endothelial Kaposi's sarcoma simulators, and the skin of immunosuppressed patients. *Am. J. Pathol.* **148,** 2009–2016 (1996).
155. Aluigi, M. G. *et al.* KSHV sequences in biopsies and cultured spindle cells of epidemic, iatrogenic and Mediterranean forms of Kaposi's sarcoma. *Res. Virol.* **147,** 267–275 (1996).
156. Grundhoff, A. & Ganem, D. Inefficient establishment of KSHV latency suggests an additional role for continued lytic replication in Kaposi sarcoma pathogenesis. *J. Clin. Invest.* **113,** 124–136 (2004).
157. Nun, T. K. *et al.* Development of a fluorescence-based assay to screen antiviral drugs against Kaposi's sarcoma associated herpesvirus. *Mol. Cancer Ther.* **6,** 2360–2370 (2007).
158. Dzeng, R. K. *et al.* Small molecule growth inhibitors of human oncogenic gammaherpesvirus infected B-cells. *Mol. Oncol.* **9,** 365–376 (2015).
159. Bechtel, J. T., Liang, Y., Hvidding, J. & Ganem, D. Host Range of Kaposi's Sarcoma-Associated Herpesvirus in Cultured Cells. *Journal of Virology* **77,** 6474–6481 (2003).
160. Myoung, J. & Ganem, D. Generation of a doxycycline-inducible KSHV producer cell line of endothelial origin: Maintenance of tight latency with efficient reactivation upon induction. *J. Virol. Methods* **174,** 12–21 (2011).
161. An, F. *et al.* Long-Term-Infected Telomerase-Immortalized Endothelial Cells: a Model for Kaposi's Sarcoma-Associated Herpesvirus Latency In Vitro and In Vivo. *J. Virol.* **80,** 4833–4846

(2006).

162. Sivakumar, R. *et al.* Kaposi's sarcoma-associated herpesvirus induces sustained levels of vascular endothelial growth factors A and C early during in vitro infection of human microvascular dermal endothelial cells: biological implications. *J. Virol.* **82,** 1759–76 (2008).
163. Poole, L. J. *et al.* Altered patterns of cellular gene expression in dermal microvascular endothelial cells infected with Kaposi's sarcoma-associated herpesvirus. *J. Virol.* **76,** 3395–420 (2002).
164. Stürzl, M., Gaus, D., Dirks, W. G., Ganem, D. & Jochmann, R. Kaposi's sarcoma-derived cell line SLK is not of endothelial origin, but is a contaminant from a known renal carcinoma cell line. *Int. J. Cancer* **132,** 1954–1958 (2013).
165. Hirschhaeuser, F. *et al.* Multicellular tumor spheroids: An underestimated tool is catching up again. *J. Biotechnol.* **148,** 3–15 (2010).
166. Lipps, C. *et al.* Expansion of functional personalized cells with specific transgene combinations. *Nat. Commun.* **9,** 994 (2018).
167. Desoize, B. & Jardillier, J. Multicellular resistance: a paradigm for clinical resistance? *Crit. Rev. Oncol. Hematol.* **36,** 193–207 (2000).
168. Nakatsu, M. N. & Hughes, C. C. W. An optimized three-dimensional in vitro model for the analysis of angiogenesis. *Methods Enzymol.* **443,** 65–82 (2008).
169. Cun, X. *et al.* Gene profile of soluble growth factors involved in angiogenesis, in an adipose-derived stromal cell/endothelial cell co-culture, 3D gel model. *Cell Prolif.* **48,** 405–412 (2015).
170. Ng, C. T., Yip, W. K., Mohtarrudin, N. & Seow, H. F. Comparison of invasion by human microvascular endothelial cell lines in response to vascular endothelial growth factor (VEGF) and basic fibroblast growth factor (bFGF) in a threedimensional (3D) cell culture system. *Malays. J. Pathol.* **37,** 219–225 (2015).
171. Shao, Z. *et al.* Choroid sprouting assay: an ex vivo model of microvascular angiogenesis. *PLoS One* **8,** e69552 (2013).
172. El Assal, R. *et al.* 3-D Microwell Array System for Culturing Virus Infected Tumor Cells. *Sci. Rep.* **6,** 39144 (2016).
173. Jung, J. U., Choi, J.-K., Ensser, A. & Biesinger, B. Herpesvirus saimiri as a model for gammaherpesvirus oncogenesis. *Semin. Cancer Biol.* **9,** 231–239 (1999).
174. Desrosiers, R. C. *et al.* A herpesvirus of rhesus monkeys related to the human Kaposi's sarcoma-associated herpesvirus. *J. Virol.* **71,** 9764–9769 (1997).
175. Searles, R. P., Bergquam, E. P., Axthelm, M. K. & Wong, S. W. Sequence and genomic analysis of a Rhesus macaque rhadinovirus with similarity to Kaposi's sarcoma-associated herpesvirus/human herpesvirus 8. *J. Virol.* **73,** 3040–3053 (1999).
176. Virgin, H. W. 4th *et al.* Complete sequence and genomic analysis of murine gammaherpesvirus 68. *J. Virol.* **71,** 5894–5904 (1997).
177. Orzechowska, B. U. *et al.* Rhesus macaque rhadinovirus-associated non-Hodgkin lymphoma: animal model for KSHV-associated malignancies. *Blood* **112,** 4227–4234 (2008).

178. Simas, J. P. & Efstathiou, S. Murine gammaherpesvirus 68: a model for the study of gammaherpesvirus pathogenesis. *Trends Microbiol.* **6,** 276–282 (1998).
179. Barton, E., Mandal, P. & Speck, S. H. Pathogenesis and host control of gammaherpesviruses: lessons from the mouse. *Annu. Rev. Immunol.* **29,** 351–397 (2011).
180. Dong, S., Forrest, J. C. & Liang, X. Murine Gammaherpesvirus 68: A Small Animal Model for Gammaherpesvirus-Associated Diseases. *Adv. Exp. Med. Biol.* **1018,** 225–236 (2017).
181. Adang, L. A., Parsons, C. H. & Kedes, D. H. Asynchronous progression through the lytic cascade and variations in intracellular viral loads revealed by high-throughput single-cell analysis of Kaposi's sarcoma-associated herpesvirus infection. *J. Virol.* **80,** 10073–10082 (2006).
182. Dittmer, D. *et al.* Experimental transmission of Kaposi's sarcoma-associated herpesvirus (KSHV/HHV-8) to SCID-hu Thy/Liv mice. *J. Exp. Med.* **190,** 1857–1868 (1999).
183. Wang, L.-X. *et al.* Humanized-BLT mouse model of Kaposi's sarcoma-associated herpesvirus infection. *Proc. Natl. Acad. Sci. U. S. A.* **111,** 3146–3151 (2014).
184. Habison, A. C. *et al.* Cross-species conservation of episome maintenance provides a basis for in vivo investigation of Kaposi's sarcoma herpesvirus LANA. *PLoS Pathog.* **13,** e1006555 (2017).
185. Zhang, J. *et al.* Recombinant Murine Gamma Herpesvirus 68 Carrying KSHV G Protein-Coupled Receptor Induces Angiogenic Lesions in Mice. *PLoS Pathog.* **11,** (2015).
186. Mutlu, A. D. *et al.* In vivo growth-restricted and reversible malignancy induced by Human Herpesvirus-8/ KSHV: a cell and animal model of virally induced Kaposi's sarcoma. *Cancer cell* **11,** 245–258 (2007).
187. Cloutier, N. *et al.* Increased tumorigenicity of cells carrying recombinant human herpesvirus 8. *Arch. Virol.* **153,** 93–103 (2008).
188. Milyavsky, M. *et al.* Prolonged culture of telomerase-immortalized human fibroblasts leads to a premalignant phenotype. *Cancer Res.* **63,** 7147–57 (2003).
189. May, T., Hauser, H. & Wirth, D. Transcriptional control of SV40 T-antigen expression allows a complete reversion of immortalization. *Nucleic Acids Res.* **32,** 5529–5538 (2004).
190. Weber, W. & Fussenegger, M. Artificial mammalian gene regulation networks—novel approaches for gene therapy and bioengineering. *J. Biotechnol.* **98,** 161–187 (2002).
191. Gossen, M. & Bujard, H. Tight control of gene expression in mammalian cells by tetracycline-responsive promoters. *Proc. Natl. Acad. Sci. U. S. A.* **89,** 5547–51 (1992).
192. Baron, U., Freundlieb, S., Gossen, M. & Bujard, H. Co-regulation of two gene activities by tetracycline via a bidirectional promoter. *Nucleic Acids Res.* **23,** 3605–6 (1995).
193. May, T. *et al.* Synthetic gene regulation circuits for control of cell expansion. *Tissue Eng. Part A* **16,** 441–452 (2010).
194. Lipps, C. *et al.* Proliferation status defines functional properties of endothelial cells. *Cell. Mol. Life Sci.* **74,** 1319–1333 (2017).
195. Lieber, D. *et al.* A permanently growing human endothelial cell line supports productive infection with human cytomegalovirus under conditional cell growth arrest. *Biotechniques* **59,** 127–136

(2015).

196. Vieira, J. & O'Hearn, P. M. Use of the red fluorescent protein as a marker of Kaposi's sarcoma-associated herpesvirus lytic gene expression. *Virology* **325,** 225–240 (2004).
197. Ullrich, A. *et al.* Pretubulysin, a potent and chemically accessible tubulysin precursor from Angiococcus disciformis. *Angew. Chem. Int. Ed. Engl.* **48,** 4422–4425 (2009).
198. Ramirez-Solis, R. *et al.* Genomic DNA microextraction: a method to screen numerous samples. *Anal. Biochem.* **201,** 331–335 (1992).
199. Debacq-Chainiaux, F., Erusalimsky, J. D., Campisi, J. & Toussaint, O. Protocols to detect senescence-associated beta-galactosidase (SA-βgal) activity, a biomarker of senescent cells in culture and in vivo. *Nat. Protoc.* **4,** 1798–1806 (2009).
200. Ponce, M. L. in *Methods in molecular biology (Clifton, N.J.)* **467,** 183–188 (2009).
201. Islam, S. & Flaherty, P. Assay Methods Protocol: Endothelial Cell Tube Formation Assay. *Corning* (2012).
202. Carpentier, G. Angiogenesis Analyzer for ImageJ. in *ImageJ User and Developer conference* (2012).
203. Yu, G., Wang, L.-G., Han, Y. & He, Q.-Y. clusterProfiler: an R package for comparing biological themes among gene clusters. *OMICS* **16,** 284–287 (2012).
204. Merico, D., Isserlin, R., Stueker, O., Emili, A. & Bader, G. D. Enrichment map: a network-based method for gene-set enrichment visualization and interpretation. *PLoS One* **5,** e13984 (2010).
205. Andrews, S. Babraham Bioinformatics - FastQC A Quality Control tool for High Throughput Sequence Data. (2012). Available at: http://www.bioinformatics.babraham.ac.uk/projects/fastqc/. (Accessed: 28th June 2018)
206. Krueger, F. Babraham Bioinformatics - Trim Galore! (2012). Available at: http://www.bioinformatics.babraham.ac.uk/projects/trim_galore/. (Accessed: 28th June 2018)
207. Dobin, A. *et al.* STAR: ultrafast universal RNA-seq aligner. *Bioinformatics* **29,** 15–21 (2013).
208. Liao, Y., Smyth, G. K. & Shi, W. featureCounts: an efficient general purpose program for assigning sequence reads to genomic features. *Bioinformatics* **30,** 923–30 (2014).
209. Durinck, S. *et al.* BioMart and Bioconductor: a powerful link between biological databases and microarray data analysis. *Bioinformatics* **21,** 3439–40 (2005).
210. Robinson, M. D., McCarthy, D. J. & Smyth, G. K. edgeR: a Bioconductor package for differential expression analysis of digital gene expression data. *Bioinformatics* **26,** 139–140 (2010).
211. Kati, S. *et al.* Activation of the B cell antigen receptor triggers reactivation of latent Kaposi's sarcoma-associated herpesvirus in B cells. *J. Virol.* **87,** 8004–8016 (2013).
212. Kati, S. *et al.* Generation of high-titre virus stocks using BrK.219, a B-cell line infected stably with recombinant Kaposi's sarcoma-associated herpesvirus. *J. Virol. Methods* **217,** 79–86 (2015).
213. Menhofer, M. H. *et al.* In vitro and in vivo characterization of the actin polymerizing compound chondramide as an angiogenic inhibitor. *Cardiovasc. Res.* **104,** 303–314 (2014).
214. Braig, S. *et al.* Pretubulysin: a new option for the treatment of metastatic cancer. *Cell Death Dis.* **5,**

e1001 (2014).

215. Kretzschmann, V. K. *et al.* Novel tubulin antagonist pretubulysin displays antivascular properties in vitro and in vivo. *Arterioscler. Thromb. Vasc. Biol.* **34,** 294–303 (2014).

216. Oehler, C. *et al.* The microtubule stabilizer patupilone (epothilone B) is a potent radiosensitizer in medulloblastoma cells. *Neuro. Oncol.* **13,** 1000–1010 (2011).

217. O'Reilly, T. *et al.* Patupilone (epothilone B, EPO906) inhibits growth and metastasis of experimental prostate tumors in vivo. *Prostate* **65,** 231–240 (2005).

218. Schreurs, M., van Dijk, T. H., Havinga, R., Reijngoud, D.-J. & Kuipers, F. Soraphen, an inhibitor of the acetyl-CoA carboxylase system, improves peripheral insulin sensitivity in mice fed a high-fat diet. *Diabetes. Obes. Metab.* **11,** 987–991 (2009).

219. Marzorati, S. *et al.* Engraftment versus immunosuppression: cost-benefit analysis of immunosuppression after intrahepatic murine islet transplantation. *Transplantation* **97,** 1019–1026 (2014).

220. Omar, R. F. *et al.* Antiviral efficacy and toxicity of ribavirin and foscarnet each given alone or in combination in the murine AIDS model. *Toxicol. Appl. Pharmacol.* **143,** 140–151 (1997).

221. Kang, H. & Lieberman, P. M. Mechanism of glycyrrhizic acid inhibition of Kaposi's sarcoma-associated herpesvirus: disruption of CTCF-cohesin-mediated RNA polymerase II pausing and sister chromatid cohesion. *J Virol* **85,** 11159–11169 (2011).

222. Shao, R. & Guo, X. Human microvascular endothelial cells immortalized with human telomerase catalytic protein: a model for the study of in vitro angiogenesis. *Biochem. Biophys. Res. Commun.* **321,** 788–794 (2004).

223. Ribeiro, M. J. *et al.* Hemostatic properties of the SV-40 transfected human microvascular endothelial cell line (HMEC-1). A representative in vitro model for microvascular endothelium. *Thromb. Res.* **79,** 153–161 (1995).

224. Ades, E. W. *et al.* HMEC-1: establishment of an immortalized human microvascular endothelial cell line. *J. Invest. Dermatol.* **99,** 683–690 (1992).

225. Ferratge, S. *et al.* Initial clonogenic potential of human endothelial progenitor cells is predictive of their further properties and establishes a functional hierarchy related to immaturity. *Stem Cell Res.* **21,** 148–159 (2017).

226. Anada, T., Fukuda, J., Sai, Y. & Suzuki, O. An oxygen-permeable spheroid culture system for the prevention of central hypoxia and necrosis of spheroids. *Biomaterials* **33,** 8430–8441 (2012).

227. McMahon, K. M. *et al.* Characterization of Changes in the Proteome in Different Regions of 3D Multicell Tumor Spheroids. *J. Proteome Res.* **11,** 2863–2875 (2012).

228. Haque, M., Davis, D. A., Wang, V., Widmer, I. & Yarchoan, R. Kaposi's sarcoma-associated herpesvirus (human herpesvirus 8) contains hypoxia response elements: relevance to lytic induction by hypoxia. *J. Virol.* **77,** 6761–6768 (2003).

229. Dalton-Griffin, L., Wilson, S. J. & Kellam, P. X-box binding protein 1 contributes to induction of the Kaposi's sarcoma-associated herpesvirus lytic cycle under hypoxic conditions. *J. Virol.* **83,**

7202–7209 (2009).

230. Davis, D. A. *et al.* Hypoxia induces lytic replication of Kaposi sarcoma-associated herpesvirus. *Blood* **97,** 3244–3250 (2001).

231. Oze, H. *et al.* Impact of medium volume and oxygen concentration in the incubator on pericellular oxygen concentration and differentiation of murine chondrogenic cell culture. *Vitr. Cell. Dev. Biol. - Anim.* **48,** 123–130 (2012).

232. Hollingworth, R., Horniblow, R. D., Forrest, C., Stewart, G. S. & Grand, R. J. Localization of Double-Strand Break Repair Proteins to Viral Replication Compartments following Lytic Reactivation of Kaposi's Sarcoma-Associated Herpesvirus. *J. Virol.* **91,** (2017).

233. Krueger, A. B. *et al.* Identification of a selective small molecule inhibitor series targeting the Eyes Absent 2 (Eya2) phosphatase activity. *J. Biomol. Screen.* **18,** 85–96 (2013).

234. Krueger, A. B. *et al.* Allosteric Inhibitors of the Eya2 Phosphatase Are Selective and Inhibit Eya2-mediated Cell Migration *. **289,** 16349–16361 (2014).

235. Herrmann, J., Fayad, A. A. & Muller, R. Natural products from myxobacteria: novel metabolites and bioactivities. *Nat. Prod. Rep.* **34,** 135–160 (2017).

236. Global Statistics | HIV.gov. Available at: https://www.hiv.gov/hiv-basics/overview/data-and-trends/global-statistics. (Accessed: 13th June 2018)

237. Home - GODT. Available at: http://www.transplant-observatory.org/. (Accessed: 13th June 2018)

238. Cooley, L. S. *et al.* Reversible transdifferentiation of blood vascular endothelial cells to a lymphatic-like phenotype in vitro. *J. Cell Sci.* **123,** 3808–16 (2010).

239. O'Hara, A. J. *et al.* Pre-micro RNA signatures delineate stages of endothelial cell transformation in Kaposi sarcoma. *PLoS Pathog.* **5,** e1000389 (2009).

240. Dittmer, D. P. Transcription profile of Kaposi's sarcoma-associated herpesvirus in primary Kaposi's sarcoma lesions as determined by real-time PCR arrays. *Cancer Res.* **63,** 2010–2015 (2003).

241. Hosseinipour, M. C. *et al.* Viral profiling identifies multiple subtypes of Kaposi's sarcoma. *MBio* **5,** e01633-14 (2014).

242. Zhang, Y. M. *et al.* Vascular origin of Kaposi's sarcoma. Expression of leukocyte adhesion molecule-1, thrombomodulin, and tissue factor. *Am. J. Pathol.* **144,** 51–59 (1994).

243. Polson, A. G., Wang, D., DeRisi, J. & Ganem, D. Modulation of host gene expression by the constitutively active G protein-coupled receptor of Kaposi's sarcoma-associated herpesvirus. *Cancer Res.* **62,** 4525–4530 (2002).

244. Appleton, M. A., Attanoos, R. L. & Jasani, B. Thrombomodulin as a marker of vascular and lymphatic tumours. *Histopathology* **29,** 153–157 (1996).

245. Ho, M. *et al.* Identification of endothelial cell genes by combined database mining and microarray analysis. *Physiol. Genomics* **13,** 249–62 (2003).

246. Purushothaman, P., Uppal, T., Sarkar, R. & Verma, S. KSHV-Mediated Angiogenesis in Tumor Progression. *Viruses* **8,** 198 (2016).

247. Qian, L.-W., Xie, J., Ye, F. & Gao, S.-J. Kaposi's sarcoma-associated herpesvirus infection promotes invasion of primary human umbilical vein endothelial cells by inducing matrix metalloproteinases. *J. Virol.* **81,** 7001–10 (2007).

248. Francescone III, R. A., Faibish, M. & Shao, R. A Matrigel-Based Tube Formation Assay to Assess the Vasculogenic Activity of Tumor Cells. *Journal of Visualized Experiments : JoVE* (2011). doi:10.3791/3040

249. Haq, I.-U. *et al.* The clinical application of plasma Kaposi sarcoma herpesvirus viral load as a tumour biomarker: results from 704 patients. *HIV Med.* **17,** 56–61 (2016).

250. Boivin, G., Gaudreau, A. & Routy, J. P. Evaluation of the human herpesvirus 8 DNA load in blood and Kaposi's sarcoma skin lesions from AIDS patients on highly active antiretroviral therapy. *AIDS* **14,** 1907–1910 (2000).

251. Sun, Z. *et al.* Kaposi's Sarcoma-Associated Herpesvirus-Encoded LANA Can Induce Chromosomal Instability through Targeted Degradation of the Mitotic Checkpoint Kinase Bub1. *J. Virol.* **88,** 7367–7378 (2014).

252. Jackson, B. R., Noerenberg, M. & Whitehouse, A. A novel mechanism inducing genome instability in Kaposi's sarcoma-associated herpesvirus infected cells. *PLoS Pathog.* **10,** e1004098 (2014).

253. Krause, C. J. *et al.* MicroRNA-34a promotes genomic instability by a broad suppression of genome maintenance mechanisms downstream of the oncogene KSHV-vGPCR. *Oncotarget* **7,** 10414–32 (2016).

254. Ellison, T. J. & Kedes, D. H. Variable episomal silencing of a recombinant herpesvirus renders its encoded GFP an unreliable marker of infection in primary cells. *PLoS One* **9,** e111502 (2014).

255. Jeffery, H. C., Wheat, R. L., Blackbourn, D. J., Nash, G. B. & Butler, L. M. Infection and transmission dynamics of rKSHV.219 in primary endothelial cells. *J. Virol. Methods* **193,** 251–259 (2013).

256. Choi, Y., Bowman, J. W. & Jung, J. U. Autophagy during viral infection — a double-edged sword. *Nat. Rev. Microbiol.* **16,** 341–354 (2018).

257. Chiramel, A. I. & Best, S. M. Role of autophagy in Zika virus infection and pathogenesis. *Virus Res.* (2017). doi:10.1016/j.virusres.2017.09.006

258. Autophagy Database. Available at: http://www.tanpaku.org/autophagy/. (Accessed: 26th June 2018)

259. HADb : Human Autophagy Database. Available at: http://autophagy.lu/. (Accessed: 26th June 2018)

260. Pringle, E. S. *et al.* mTORC1 activity is dispensable for synthesis of KSHV lytic proteins. *bioRxiv* 356162 (2018). doi:10.1101/356162

261. Koopal, S. *et al.* Viral oncogene-induced DNA damage response is activated in Kaposi sarcoma tumorigenesis. *PLoS Pathog.* **3,** 1348–1360 (2007).

262. Jha, H. C. *et al.* H2AX phosphorylation is important for LANA-mediated Kaposi's sarcoma-associated herpesvirus episome persistence. *J. Virol.* **87,** 5255–5269 (2013).

263. Hollingworth, R. *et al.* Activation of DNA Damage Response Pathways during Lytic Replication of KSHV. *Viruses* **7,** 2908–2927 (2015).

264. Piscitello, D. *et al.* AKT overactivation can suppress DNA repair via p70S6 kinase-dependent downregulation of MRE11. *Oncogene* **37,** 427–438 (2018).

265. Xie, X. *et al.* The mTOR–S6K pathway links growth signalling to DNA damage response by targeting RNF168. *Nat. Cell Biol.* **20,** 320–331 (2018).

266. Dai, L. *et al.* CD147 and downstream ADAMTSs promote the tumorigenicity of Kaposi ' s sarcoma-associated herpesvirus infected endothelial cells. **7,**

267. Qin, Z., Dai, L., Toole, B., Robertson, E. & Parsons, C. Regulation of Nm23-H1 and cell invasiveness by Kaposi's sarcoma-associated herpesvirus. *J. Virol.* **85,** 3596–3606 (2011).

268. Qin, Z., Dai, L., Slomiany, M. G., Toole, B. P. & Parsons, C. Direct activation of emmprin and associated pathogenesis by an oncogenic herpesvirus. *Cancer Res.* **70,** 3884–3889 (2010).

269. Dai, L. *et al.* Role of heme oxygenase-1 in the pathogenesis and tumorigenicity of Kaposi's sarcoma-associated herpesvirus. *Oncotarget* **7,** 10459–10471 (2016).

270. Liu, R. *et al.* Induction, regulation, and biologic function of Axl receptor tyrosine kinase in Kaposi sarcoma. *Blood* **116,** 297–305 (2010).

271. Jones, T. *et al.* Viral cyclin promotes KSHV-induced cellular transformation and tumorigenesis by overriding contact inhibition. *Cell Cycle* **13,** 845–858 (2014).

272. Aoki, Y., Jones, K. D. & Tosato, G. Kaposi's sarcoma-associated herpesvirus-encoded interleukin-6. *J. Hematother. Stem Cell Res.* **9,** 137–145 (2000).

273. Aoki, Y. *et al.* Angiogenesis and hematopoiesis induced by Kaposi's sarcoma-associated herpesvirus-encoded interleukin-6. *Blood* **93,** 4034–4043 (1999).

274. Jensen, K. K. *et al.* The Human Herpes Virus 8-Encoded Chemokine Receptor Is Required for Angioproliferation in a Murine Model of Kaposi's Sarcoma. *J. Immunol.* **174,** 3686 LP-3694 (2005).

275. Montaner, S. *et al.* Endothelial infection with KSHV genes in vivo reveals that vGPCR initiates Kaposi's sarcomagenesis and can promote the tumorigenic potential of viral latent genes. *Cancer Cell* **3,** 23–36 (2003).

276. Prakash, O. *et al.* Tumorigenesis and aberrant signaling in transgenic mice expressing the human herpesvirus-8 K1 gene. *J. Natl. Cancer Inst.* **94,** 926–935 (2002).

277. Gramolelli, S. *et al.* Inhibiting the Recruitment of PLCγ1 to Kaposi's Sarcoma Herpesvirus K15 Protein Reduces the Invasiveness and Angiogenesis of Infected Endothelial Cells. *PLoS Pathog.* **11,** (2015).

278. Bollag, D. M. *et al.* Epothilones, a new class of microtubule-stabilizing agents with a taxol-like mechanism of action. *Cancer Res.* **55,** 2325–2333 (1995).

279. O'Reilly, T. *et al.* Patupilone (epothilone B, EPO906) and imatinib (STI571, Glivec) in combination display enhanced antitumour activity in vivo against experimental rat C6 glioma. *Cancer Chemother. Pharmacol.* **55,** 307–317 (2005).

List of figures

List of tables

Abbreviations

2D	Two-dimensional
3D	Three-dimensional
AcLDL	Acetylated low-density lipoproteins
ACTB	Actin beta
AIDS	Acquired immune deficiency syndrome
AIDS-KS	AIDS-associated Kaposi's sarcoma
Ang2	Angiopoetin
ANOVA	Analysis of variance
ATM	Ataxia-telangiectasia mutated kinase
ATR	ataxia telangiectasia and Rad-3-related kinase
BCL	B cell lymphoma
BEC	Blood endothelial cells
BSA	Albumin from bovine serum
C_{12}FDG	5-dodecanoylaminofluorescein di-beta-D-galactopyranoside
C1ORF43	Chromosome 1 Open Reading Frame 43
D2-40	Podoplanin
DC-SIGN	Dendritic Cell-Specific Intercellular adhesion molecule-3-Grabbing Non-integrin
DDR	DNA damage responce
DMSO	Dimethyl sulfoxide
DNA-PK	DNA-dependent protein kinase
EDTA	Ethylenediaminetetraacetic acid
EF1α	Elongation factor-1
EGM	Endothelial growth media
EndMT	Endothelial-to-mesenchymal transition
Eph2A	Ephrin Type-A Receptor 2
EphB2/B4	Ephrin Type-B Receptor 2/4
Erk	Extracellular signal–regulated kinase
Ezh2	Enhancer of zeste homolog 2
FACS	Fluorescence-activated cell sorting
FAK	Focal adhesion kinase
FCS	Fetal Bovine Serum
FuDR	5-fluoro-2'-deoxyuridine
GA	Glycarrhizic acid

GFP	Green fluorescent protein
GPCR	G-protein coupled receptor
H2AX	Histone H2AX
HAART	Highly active antiretroviral therapy
hCMV	Human cytomegalovirus
HDAC	Histone deacetylase inhibitor
HDMEC	Human dermal microvascular endothelial cells
HEK	Human embryonic kidney
Hes1	Hairy and enhancer of split-1
Hey1	Hairy/enhancer-of-split related with YRPW motif protein 1
HIF1α	Hypoxia Inducible Factor 1 Alpha
HIV	Human immunidefficiency virus
HS	Heparan sulfate
hTert	Human telomerase reverse transcriptase
HUVEC	Human umbilical vein endothelial cells
IgG	Imminoglobulin G
IRF16	Interferon regulatory factor 16
JAG1	Jagged 1
Jak2	Janus kinase 2
K-bZIP	KSHV basic domain-leucine zipper protein
KS	Kaposi's sarcoma
KSHV	Kaposi's sarcoma associated herpesvirus
LANA	Latency-associated nuclear antigen
LEC	Lymphatic endothelial cells
LYVE	Lymphatic vessel endothelial hyaluronan receptor 1
MAPK	Mitogen-activated protein kinase
mECK36	Murine endothelial precursor cells
MFI	Mean fluorescence intensity
MHV68	Murine herpesvirus 68
MMP	Metalloproteinase
mTOR	Mammalian target of rapamycin
MTT	3-(4,5-Dimethylthiazol-2-yl)-2,5-Diphenyltetrazolium Bromide
NBS1	Nibrin
NF-κB	Nuclear factor kappa B
ORF	Open reading frame
p.i.	Post infection

PAN	Noncoding polyadenylated nuclear RNA
PBS	Phosphate-buffered saline
PCR	Plymerase chain reaction
PDGFR	Platelet-derived growth factor receptor
PhA	Phosphonoformic acid trisodium salt hexahydrate
PI3K	Phosphatidylinositol-4,5-bisphosphate 3-kinase
PIP2	Phosphorylate phosphatidylinositol-(4,5) bisphosphate
PIP3	Phosphatidylinositol (3,4,5)-trisphosphate
qPCR	Quantitative PCR
PROX1	Prospero homeobox protein 1
RFP	Red fluorescent protein
Rho-GTPase	Ras homologous guanosine triphosphatase
RT	Room temperature
RTA	Replication and Transcription activator, ORF50
RT-qPCR	Reverse transcription quantitative PCR
rtTA	Reverse tetracycline-controlled transactivator
SDS	Sodium dodecyl sulfate
STAT	Signal transducer and activator of transcription
SV40	Simian vacuolating virus 40
TetO	Tet operator
TGFβ	Transforming growth factor beta
TIME cells	Telomerase-immortaliues endothelial cells
TIVE-LTC	Telomerase-immortalized human umbilical vein endothelial long term infected cells
TPA	12-O-Tetradecanoylphorbol 13-acetate
VEGF	Vascular endothelial growth factor
VEGFR	Vascular endothelial growth factor receptor
vFLIP	Viral FLICE-inhibitory protein
vIL6	Viral interleukin 6
WST	Water-soluble tetrazolium salts
WSTF	Williams Syndrome Transcription Factor
αSMA	α smooth muscle actin
γPLC	Protein kinase C gamma

Acknowledgment

I always enjoyed reading *Acknowledgements* in other theses and I was looking forward to writing one on my own. Finishing up my thesis, I feel so overwhelmed I could write a novel. But I will stick to an abridged version.

I would like to use this opportunity to sincerely thank my supervisor, Prof. Dr. Dagmar Wirth, for the opportunity to work on this project. During her presentation of the project proposal, I immediately fall in love with the topic and it was her guidance and motivation, that allowed me to keep this passion through the whole PhD time. Her endless patience and support created a unique media for my personal and professional growth and without it, I would never be able to be where I am.

I would like to thank Prof. Dr. Reinhard Köster for mentoring and reviewing my thesis. I would like to express my gratitude to my Thesis Committee, Prof. Dr. Thomas Schulz and Prof. Dr. Marc Stadler, as well as to Hansjörg Hauser, for stimulating discussions and helpful suggestions. Your input on various aspects of the project significantly advanced its development.

I would like to sincerely thank my MSYS colleagues for an amazing working atmosphere and support. Special thanks to Dr. Tom Wahlicht for his readiness to help with anything from broken PC to stubborn Western Blot, both practically and emotionally. Additionally, I would like to thank Dr. Natascha Gödecke for her creative ideas, Dr. Christoph Lipps for introducing me to the *in vivo* techniques, and Dr. Sudeep Bhushal, who always has a cup of tea and a cookie for me.

I would like to acknowledge HZI Graduate School for many opportunities to learn and develop within the graduate program.

Many thanks to Dr. Sabine Kirchhoff, Daniela Romke, Angela Walter and Sylvia Richer who were always there to give an advice and help with confusing regulations and laborious documentations both at work and in private life. I am sure, I can speak on behalf of all international students in HZI: without you we will be lost! You should know that we don't take you for granted.

A very special thank you to my loving husband, Nikita Kozlov, for his endless support and believe in me. Your curiosity about every single detail of the viral life cycle and biological methods always made me look at my studies from the different angle and discover new ideas. Without you by my side, I would barely manage.

Curriculum Vitae

Tatyana Dubich, MD

06.03.1990

Phone	0531 6181-5065
Mobile	+ 49 176 25876844
e-mail	dubichts@gmail.com
LinkedIn	linkedin.com/in/tatyana-dubich
Xing	xing.to/Tatyana_Dubich

EDUCATION

September 2014 - June 2018	PhD student, Helmholtz Center for Infection Research, HZI
September 2007 – June 2013	Medical Department, Novosibirsk National Research State University (Novosibirsk State University), Medical Doctor degree with honors (red diploma). GPA 4,93/5,00
September 2005 – June 2007	Specialized Educational Scientific Center of Physics and Mathematics, chemical and biological profile of Novosibirsk State University, graduated with honors (silver medal)

EXPERIENCE

September 2014 - present	Helmholtz Center for Infection Research, HZI, **PhD student** Project: Analysis of mechanisms of Kaposi's sarcoma associated virus latency and intervention using novel in vitro and in vivo models.
January 2017 - January 2018	**Head of Communication team** in Helmholtz Juniors Duties: information exchange between different working groups and broadcast Helmholtz Juniors news and achievements to doctoral researchers within the Helmholtz Association. I coordinated activities of the group, as well as wrote for HeJu blog and social media (Facebook, Twitter)
November 2016 - November 2017	**Elected PhD representative** in Helmholtz Center for Infection Research (DO IT) Duties: Evaluation and communication of PhD working conditions in the institute, as well as organization of events promoting internal collaborations between Doctoral Researchers
October 2013 – August 2014	Novosibirsk Scientific and Research Institute of Traumatology and Orthopedics, PhD Student Project: Chondrogenic differentiation of Mesenchymal Stem Cells in proinflammatory conditions

PUBLICATIONS

T. Dubich, A. Dittrich, H. Hauser, M. Stadler, T. F. Schulz, D. Wirth: *PI3K/mTOR pathway governs differential KSHV maintenance in 2D and 3D cell culture.*
Manuscript in preparation

T. Dubich, D. Wirth: *Function or Expansion: How to Investigate Cells of Human Blood Vessels.* Front. Young Minds. 6:25. 2018. DOI 10.3389/frym.2018.00025

T. Dubich, A. Lieske, S. Santag, G. Beauclair, J. Rückert, J. Herrmann, J. Gorges, G. Büsche, U. Kazmaier, H. Hauser, M. Stadler, T. F. Schulz, D. Wirth: *A combined in vitro and in vivo assay system for investigation of KSHV and validation of small molecule inhibitors against Kaposi's sarcoma*
Submitted

C. Lipps, M. Badar, M. Butueva, T. Dubich, I. V. Singh, S. Rau, A.Weber, M. Kracht, M. Köster, T. May, T. F. Schulz, H. Hauser, D. Wirth. *Proliferation status defines functional properties of endothelial cells.* Cell. Mol. Life Sci. 2017 Apr;74(7):1319-1333. DOI 10.1007/s00018-016-2417-5

S. V. Cheresiz, A. A. Kononova, Yu. V. Razumova, T. S. Dubich, A. A. Chepurnov, A. A. Kushch, R. Davey, A. G. Pokrovsky. *A vesicular stomatitis pseudovirus expressing the surface glycoproteins of influenza A virus*. Archives of Virology 2014 Oct;159(10):2651-8. DOI 10.1007/s00705-014-2127-y